PolyPublie
Polytechnique Montréal

POLYTECHNIQUE MONTRÉAL
UNIVERSITÉ D'INGÉNIERIE

Titre: Title:	Passive and active ion-exchanged glass waveguides and devices
Auteur: Author:	Wei-Jian Wang
Date:	1992
Type:	Mémoire ou thèse / Dissertation or Thesis
Référence: Citation:	Wang, W.-J. (1992). Passive and active ion-exchanged glass waveguides and devices [Ph.D. thesis, Polytechnique Montréal]. PolyPublie. https://publications.polymtl.ca/57972/

Document en libre accès dans PolyPublie
Open Access document in PolyPublie

URL de PolyPublie: PolyPublie URL:	https://publications.polymtl.ca/57972/
Directeurs de recherche: Advisors:	
Programme: Program:	Unspecified

Ce fichier a été téléchargé à partir de PolyPublie, le dépôt institutionnel de Polytechnique Montréal
This file has been downloaded from PolyPublie, the institutional repository of Polytechnique Montréal

https://publications.polymtl.ca

UNIVERSITÉ DE MONTRÉAL

PASSIVE AND ACTIVE ION-EXCHANGED GLASS WAVEGUIDES AND DEVICES

par

Wei-jian Wang

DÉPARTEMENT DE GÉNIE PHYSIQUE
ÉCOLE POLYTECHNIQUE

THÉSE PRÉSENTÉE EN VUE DE L´OBTENTION
DU GRADE DE PHILOSOPHIAE DOCTOR (Ph.D.)
(GÉNIE PHYSIQUE)

DECEMBER 1992

© droits réservés de Wei-jian Wang 1992.

National Library of Canada
Acquisitions and Bibliographic Services Branch
395 Wellington Street
Ottawa, Ontario
K1A 0N4

Bibliothèque nationale du Canada
Direction des acquisitions et des services bibliographiques
395, rue Wellington
Ottawa (Ontario)
K1A 0N4

Your file Votre référence

Our file Notre référence

The author has granted an irrevocable non-exclusive licence allowing the National Library of Canada to reproduce, loan, distribute or sell copies of his/her thesis by any means and in any form or format, making this thesis available to interested persons.

L'auteur a accordé une licence irrévocable et non exclusive permettant à la Bibliothèque nationale du Canada de reproduire, prêter, distribuer ou vendre des copies de sa thèse de quelque manière et sous quelque forme que ce soit pour mettre des exemplaires de cette thèse à la disposition des personnes intéressées.

The author retains ownership of the copyright in his/her thesis. Neither the thesis nor substantial extracts from it may be printed or otherwise reproduced without his/her permission.

L'auteur conserve la propriété du droit d'auteur qui protège sa thèse. Ni la thèse ni des extraits substantiels de celle-ci ne doivent être imprimés ou autrement reproduits sans son autorisation.

ISBN 0-315-90029-6

Canada

UNIVERSITÉ DE MONTRÉAL

ECOLE POLYTECHNIQUE

Cette thèse intitulée :

PASSIVE AND ACTIVE ION-EXCHANGED GLASS WAVEGUIDES AND DEVICES

présentée par : Wei-jian Wang

en vue de l´obtention du grade de Philosophiae Doctor (Ph.D.)

a été dûment acceptée par le jury d´examen constitué de :

M. MACIEJKO, Romain, Ph.D.	Président
M. NAJAFI, S. Iraj, Ph.D.	Directeur de recherche
M. HONKANEN, Seppo, Ph.D.	Membre du jury
M. WU, Chunmeng, Ph.D.	Membre du jury

To

HUA TAN

SOMMAIRE

Cette thèse présente la fabrication et la caractérisation des guides d'onde et des composants passifs et actifs réalisés par échange ionique, ils sont employés pour les applications dans le domaine de l'optique intégrée.

Une procédure de double-échange-ionique avec potassium et argent a été développée pour fabriquer des guides d'onde et des composants passifs et actifs performants.

Trois procédures différentes pour réaliser des guides d'onde dopés aux terres rares dans les substrats passifs et actifs en verre ont été étudiées. L'échange ionique avec du nitrate d'argent nitrate dilué dans des verres en silice dopés aux terres rares, des guides d'onde passifs couverts par des couches de phosphate dopées aux terres rares réalisés par la technique de "Spin-coating", et des guides d'onde composés de guides passifs ne couverts d´ un verre dopé aux terres rares. Les éléments de terres rares utilisés dans la fabrication des guides d'onde sont le néodyme et l'erbium.

Des guides d'onde avec réseaux de Bragg, des jonctions en Y symmétriques, un nouvel interféromètre de Mach-Zehnder avec quatre entrées-sorties, et un nouveau résonnateur en anneau ont été développés. Ces structures sont importantes à cause de leurs applications potentielles à la connectique des les guides d'onde dopés aux terres rares.

Finalement, un amplificateur composé de verre dopé à l'erbium a été démontré. Un gain supérieur à 10 dB dans un guide d'onde de 4,7 mm de long avec moins de 30 mW de pompe dans le guide a été obtenu.

ABSTRACT

This thesis studies the fabrication and the characterization of passive and active ion-exchanged glass waveguides and devices that are mainly used for applications in integrated optics area.

Potassium and silver double-ion-exchange process is developed to fabricate high performance passive glass waveguides and devices.

Three different processes are investigated for the fabrication of rare-earth-doped glass waveguides on active and passive substrates. They are dilute silver ion exchange for rare-earth-doped silicate glass substrates, spin-coated rare-earth-doped phosphate overlays on passive glass waveguides and composite structures employing active cover glass on passive waveguides. The main rare-earth elements employed in the fabrication of active waveguides are neodymium and erbium.

Grating assisted glass waveguides, symmetric Y-branches, a novel four-port nonsymmetric Mach-Zehnder interferometer and a new integrated optical ring resonator are developed. They are potentially important for active applications in connection with rare-earth-doped glass waveguides.

Finally, a composite erbium-doped glass waveguide amplifier is demonstrated and more than 10 dB net gain has been achieved with a 4.7 mm long sample and less than 30 mW guided pump power in the waveguide.

RÉSUMÉ

L'optique intégrée consiste en la génération, le guidage et le contrôle des ondes électromagnétiques de fréquences élevées par des circuits optiques du type "couche mince". Le concept d'optique intégrée a été initialement proposé par S.E. Miller en 1969 [1]. Ces circuits optiques miniatures ont l'avantage d'être opérationnels dans une grande bande de fréquence et d'être insensible au perturbations de faible fréquence. Les composants de l'optique intégrée sont compacts, fiables, mécaniquement et thermiquement stables et ont une faible consommation en énergie. Finalement, comme son nom l'indique, l'optique intégrée offre la possibilité d'intégrer divers composants sur un même substrat.

Le verre est un substrat intéressant pour fabriquer des composants en optique intégrée. En effet, l'indice de réfraction du verre est très comparable à celui des fibres optiques, ce qui a pour effet de réduire considérablement les pertes par couplage. Le verre est très peu absorbant dans le visible et l'infra-rouge proche; c'est de plus un solide amorphe ce qui facilite la réalisation de composants insensibles à la polarisation [3]. Le verre est très résistant aux dommages optiques, il a une bonne rigidité mécanique et, ce qui est appréciable, il peut facilement être obtenu sous différentes formes et tailles tout en gardant une grande homogénéité. Finalement le prix du verre est plus bas que celui de ses concurrents.

Les guides d'ondes optiques peuvent être réalisés par différentes méthodes. Citons la pulvérisation radio-fréquence (RF sputtering), la déposition en phase vapeur (CVD) et la "Flame Hydrolysis Deposition" (FHD). L'échange et l'implantation ionique peuvent

aussi être utilisés.

Pour cette thèse, nous avons employé la technique de l'échange ionique afin d'obtenir des composants actifs et passifs en optique intégrée sur verre.

L'échange ionique peut permettre d'obtenir un guidage faible dans le verre car l'altération de la structure ionique du substrat entraîne une modification de son indice de réfraction. L'échange ionique est rendu possible par la présence d'ions de sodium (Na+) dans le verre. Ces ions, très mobiles, peuvent aisément être échangés contre d'autres ions monovalents tels que les ions : K+, Cs+, Ag+, Rb+ et Tl+. La substitution des ions Na+ par des ions ayant une plus grande polarisabilité et un plus grand rayon atomique est la principale cause de l'accroissement de l'indice du substrat et donc de la formation de guides. Cet échange peut être purement thermique ou assisté par un champ électrique. La source d'ions peut être un sel fondu ou une fine couche métallique.

Grâce à la simplicité de sa mise en oeuvre et à sa flexibilité dans le choix des paramètres, l'efficacité de l'échange ionique est maintenant largement reconnue. En effet, les possibilités de choix de l'ouverture numérique du guide ou de ses dimensions sont multiples. Quant à la variation d'indice, elle peut être aisément contrôlée par le choix de l'espèce ionique échangée ou par la composition du verre. Le profil d'indice peut décroître de façon monotone ou se rapprocher du profil à saut d'indice suivant que l'on utilise un champ électrique ou non. L'échange ionique permet aussi de réaliser des guides plans et des composants compatibles avec les fibres optiques. Les performances des guides obtenus sont reproductibles et les pertes de propagation sont faibles.

Récemment, les fibres amplificatrices et les fibres lasers dopées aux terres raressont été étudiées intensément [15]. Ces fibres permettent d'obtenir des densités de puissance élevées, tant pour la pompe que pour le signal, ce qui entraîne un seuil plus bas et une meilleure efficacité que les lasers solides conventionnels. De plus un rapport surface sur

volume élevé, dû à la géométrie des fibres, entraîne une bonne dissipation de la chaleur. C'est pourquoi, les fibres lasers peuvent opérer en continu avec un pompage faible alors que les lasers conventionnels opèrent habituellement en régime pulsé et requièrent un pompage plus intense.

Le développement rapide des fibres lasers a considérablement augmenté l'intéret porté aux composants faits de guide plans dopés aux terres rares. De plus, des diodes lasers puissantes et fiables offrent la possibilité d'un pompage avec une densité d'énergie élevée ce qui permet d'envisager la production de sources lasers compactes et efficaces aux longueurs d'ondes utilisées de nos jours en télécommunication, traitement du signal ou médecine.

Comparés aux fibres optiques, les guides d'onde dopés aux terres rares (RED) dans le verre ont plusieurs avantages: l'un d'eux est la forte concentration en dopant. Normalement, les fibres faites par MCVD (modified chemical vapor deposition) [19], ou VAD (vapor phase axial deposition) [20] ont une concentration en dopant de quelque dizaines à quelque centaines de ppm; par contre, les guides d'onde dopés aux terres rares peuvent avoir une concentration de quelque milliers à quelque dizaine de milliers de ppm. Grâce à de telles concentrations, les longueurs des lasers guides d'onde et des amplificateurs sont relativement courtes (typiquement de quelques millimètres à quelques centimètres) par rapport à celles à fibre optique. En plus, les méthodes de fabrication des guides d'onde RED dans le verre permettent l'intégration des sources de lumière, amplificateurs optiques, et circuits passifs sur le même substrat. Ceci conduit à une haute densité d´encombrement et à une intégration compacte des composants passifs et actifs, ce qui est très difficile ou patiquement impossible dans le cas des fibres optiques. Finalement, les guides d'onde dopés aux terres rares sont potentiellement de bas prix et leurs procédés de fabrication sont simples, comparé au procédés de fabrication

compliqués des fibres optiques dopées aux terres rares.

Le but pricipal de cette thèse est d'étudier les procédés de fabrication des guides d'onde RED dans le verre et les possibilité de réalisation de lasers, amplificateurs ou d'autres applications dans la domaine de l'optique intégrée. Les composants passifs qui sont nécessaires à la connexions avec les composants actifs sont également étudiés.

Les caractérisations optiques sont nécessaires pour relier les paramètres de fabrication tells que la température de diffusion, la durée d'échange et la largeur des fenêtres aux caractéristiques optiques des guides d'onde fabriqués. Ils comprennent la variation d'indice maximale, le profil d'indice, la longueur d'onde de coupure, la région unimodale, les pertes de propagation et le profil du mode. Les mesures des paramètres optiques et physiques des guides d'onde RED dans le verre sont aussi indispensables pour fournir les informations nécessaires et les paramètres de conception des lasers, amplificateurs et autres composants. Ces mesures comprennent le spectre d'absorption, les pertes de propagation à la longueur d'onde du laser-signal, la durée de vie de la fluorescence, le spectre de fluorescence et le gain du guide d'onde actif pompé.

Dans le Chapitre I, nous traitons des échanges ioniques en une seule étape avec les couples K+-Na+, Cs+-Na+, ou Ag+-Na+ dans des verres différents (Corning 0211 et Schott BK-7), et l'échange ionique en deux étapes (double échange) dans le potassium et l'argent. La caractérisation optique des ces guides d'onde passifs a aussi été effectuée. L'avantage principal au double échange pour la fabrication des guides d'onde réside dans les faibles pertes de propagation obtenues.

Le chapitre II porte sur certains composants optiques intégrés passifs liés à l'application active des guides d'onde RED et à leur caractérisation optique : des guides d'onde avec réseau de Bragg dont le pas est submicronique, des jonctions Y symétriques pour la division de puissance, un interféromètre de Mach-Zehnder nonsymétrique à quatre

ports et un résonateur intégré en anneau . Nous avons étudié ces composants pour les raisons suivantes: les lasers guides d'onde peuvent être fabriqués en remplaçant les miroirs de la cavité non-plannaire par des "réseaux à rétroaction distriburée" pour obtenir un fonctionnement monomode. La jonction Y peut être utilisée pour étudier des coupleurs sans pertes et des lasers à cavités multiples. L'interféromètre de Mach-Zehnder peut être utilisé comme multi/démultiplexeur dans les circuits actifs intégrés avec des guide d'onde RED, et le résonateur en anneau est essentiel pour réaliser, par exemple, un laser en nano.

Le chapitre III est centré sur la discussion des procédures de fabrication des guides d'onde RED. Jusqu'à présent, trois types de procedures ont été développés pour la fabrication des guides d'onde RED dans le verre passif et les verres RED. La première est l'échange ionique dans du nitrate d'argent dilué, cela est fiable pour la fabrication des guides d'onde dans le verre en silice dopé au Nd et à l'Er. La deuxième technique, dite du"Spin-coating" , est employée pour couvrir les guides d'onde passifs par des couches de phosphate dopées aux terres rares. La dernière technique développée pour la fabrication des guides d'onde RED est la technique dite "composite", qui est simplement de recouvrir un guide d'onde passif par un verre phosphate dopé à l'erbium, ce verre est optimisé pour les effets actifs. Les propriétés des guides d'onde RED ont été également étudié.

Dans le Chapitre IV, un amplifiacteur "composite" à l'erbium est démontré. Ses caractéristiques optiques telles que l'absorption à la longueur de la pompe, les pertes de propagation autour de la longueur d'onde laser, et la relation entre la puissance de pompe et le gain du signal ont été déterminée. un gain suppérieur à 10 dB dans un guide d'onde de 4,7 mm de long avec moins de 30 mW de pompe guidée dans le guide a été obtenu.

Finalement, dans la conclusion, le résumé de cette thèse est donnée, les travaux à suivre sont aussi proposé. Ces travaux concernent principlement les applications des

guides d'onde RED dans le verre. Ces applications sont les extensions naturelles des travaux présentés, elles sont basés sur les résultats obtenus dans cette thèse, elles sont très prometteuses.

ACKNOWLEDGMENTS

First of all, I would like to express my gratitude to Prof. S. Iraj Najafi, for his guidance and patience during my research works towards Ph.D degree.

I am grateful to Dr. Seppo Honkanen and Dr. Ming-Jun Li for many valuable suggestions and discussions during the course of this work. Special thanks are extended to Dr. Seppo Honkanen for the primary review of the manuscript and helpful comments.

Thanks are due to Dr. Jacques Albert for his generous help in my fluorescence and amplification experiments at Communication Research Center (CRC).

I appreciate the help of Dr. Jacek Chrostowski for allowing me to use the equipments in his laboratory at the National Research Council (NRC).

I owe thanks to all my colleagues, especially, Paul Lefebvre, Peng-nian Shen, Hui Zhang, Dr. Qing He and Jian-yao Chen for helpful discussions and cooperations during the course of this work.

I would also like to take this opportunity to especially thank Dr. Chun-meng Wu for his great support and assistance during the early period of my Ph.D program.

I am indebted to my parents for all that they have done to support me in all my endeavours.

Finally, but certainly not the least, I shall always remain grateful to my wife, Hua Tan, for her love, understanding and constant encouragement during these years.

TABLE OF CONTENTS

LIST OF TABLES

LIST OF FIGURES

INTRODUCTION

A. Integrated Optics and Glass Waveguides

Integrated optics is based on the generation, guiding and controlling of electromagnetic energy at optical frequencies by planar thin-film-type optical circuits. The concept of "integrated optics" was first proposed by S. E. Miller in 1969 [1]. These miniature optical circuits offer the advantages of large bandwidth and insensitivity to interference by natural or man-made electromagnetic fields of low frequencies. Integrated optical components are compact and reliable, with high mechanical and thermal stability, and low power consumption. Integrated optics offers the possibility for integration of several devices on a common substrate or chip. During the past 23 years, the development in thin film and microfabrication technology, the progress in semiconductor laser diodes used as optical source and optical fibers used as optical transmission media, and the great efforts made by the researchers in integrated optics area have made the integrated optical devices very promising, and they are expected to be in practical uses in the areas of telecommunication, signal processing and sensing in the near future [2].

The optical function of an integrated optical component mainly depends on the physical properties of substrate material on which the component is made. Usually, integrated optical components are classified into three categories: passive components, which exhibit fixed optical characteristics for guided waves; dynamic components, which perform dynamic control of guided optical waves; and active components, which generate and amplify optical waves. The typical passive components such as power dividers, polarizers and mode splitters, wavelength division multi/demultiplexers,

various static couplers and wavefront sensors are fabricated on a substrate material whose physical properties (like refractive index) can not be changed by an external signal. In the dynamic devices such as modulators and switches, the guided modes are controlled via a particular physical phenomenon such as the electrooptical or the acoustooptical effect by an externally applied signal. Therefore, dynamic devices are usually made on the substrate materials having large electrooptical or acoustooptical coefficients. Lithium niobate ($LiNbO_3$) has been the prime choice for the dynamic applications. The active components such as laser sources and amplifiers are usually fabricated on the III/V compound semiconductor substrates like GaAs and InP [2].

Glass is the most important substrate material suitable for fabrication of passive integrated optical components and devices. The refractive index of glass subtrate is very close to that of optical fibers, which makes the coupling losses between glass waveguides and optical fibers very low. Glass has excellent transparency in visible and near infrared spectral regions, and can easily be made in substantially different sizes and shapes with very high homogeneity. As an amorphous material distinct from crystals, it is easier to produce polarization insensitive integrated optical components in glass [3]. In addition, glass has high threshold to optical damage, it is mechanically very rigid and relatively inexpensive.

Integrated optical glass waveguides and passive components can be made by various deposition methods such as radio frequency (RF) sputtering, chemical vapor deposition (CVD) and flame hydrolysis deposition (FHD) processes. They are also widely fabricated by ion exchange and ion implantation processes.

In this thesis, ion exchange technique is mainly employed for fabrication of passive and active glass waveguides and devices.

Ion exchange processes can result in light waveguiding structures in glass since

any alteration in the electronic structure of glass matrix yields a refractive index change. In common glass substrate, there exist usually sodium ions, which act as matrix modifiers of glass network. These sodium ions have high mobility and therefore exchange easily with other monovalent alkali ions such as K^+, Cs^+, Ag^+, Rb^+ and Tl^+. The substitution of sodium ions by ions having higher polarizabilities and larger ionic radii results in local increase of refractive index in glass substrate, thus waveguiding structures may be formed. Usually, the ion exchange process does not affect the basic structure of network formers in glass if it is carried out at temperature well below the softening point of the glass. The ion exchange can be purely thermal diffusion process, or an electric field assisted diffusion process. Both a molten salt and a metallic film such as silver can be used as an ion source.

Ion exchange has been recognized as a powerful technique for the fabrication of passive waveguides in glass substrates because of its simplicity and flexibility in choosing various cation pairs with different ion radii and polarizabilities, and in fabrication parameters. Ion exchange offers wide possibilities in choosing the numerical aperture and dimensions of waveguides. The index change can be controlled easily by proper choice of the exchanged ions and the glass composition. The index profile can be tailored from shallow graded to a step like function with the use of electric-field assistance. Ion exchange is also an accurate fabrication technique to realize planar waveguides and devices compatible with optical fibers. The ion-exchanged glass waveguides and devices have reproducible performance and low propagation losses. The planar configuration of ion-exchanged glass waveguides and passive devices facilitates simple combination with other materials (e.g. nonlinear polymers [4], rare-earth-doped active layers [5]) and devices (e.g. semiconductor light sources [6] and semiconductor detectors [7]), in order to achieve high performance hybrid integrated optical circuits. In addition, the ion

exchange process is potentially very low-cost and highly suitable for large volume production.

Since the first ion-exchanged glass waveguide was reported in 1972 by Izawa and Nakagome [8], there has been significant progress in ion-exchanged glass waveguide and passive device area. Various different ion exchange processes have been developed and a better understanding of ion exchange processes and optimization of the processes for reproducible device performance have been achieved. Most of the developments in this area are summarized in a few review papers [9-11] and in a recent book [3].

B. Rare-Earth-Doped (RED) Glass Waveguides

Rare-earth ions are employed in optical applications due to their metastable excited states over the entire range of optical frequencies [12]. For many years, rare-earths have been used to make bulk laser and amplifier devices [13,14]. In recent years, RED fiber lasers and amplifiers have been extensively studied [15]. Waveguiding structure provided by optical fiber allows high power densities for pump and signal wavelengths in RED fiber core, which results in lower threshold and higher operation efficiency compared to conventional bulk lasers. Also, the high surface area-to-volume ratio of fiber geometry leads to good heat dissipation. These factors explain why fiber laser can readily operate in continuous wave form at low pumping power levels, whereas bulk glass lasers usually only operate to give a pulsed output and require much higher pump power to obtain lasing.

The rapid development of RED silica fiber amplifiers and lasers has considerably

increased the interest in RED planar waveguide devices. Furthermore, reliable high power cw laser diode pumps provide a possibility to miniaturize conventional solid state lasers and amplifiers [16,17]. Particularly, as laser diode pump is compatible with planar guided wave structure, higher pump densities and therefore higher gain compared to bulk devices can be achieved. Laser diode pumped integrated optical RED glass waveguide lasers and amplifiers are highly promising for producing small, compact, efficient and reliable laser sources and amplifiers at wavelengths that are important in the fields like optical communication, signal processing, medicine and sensing.

RED glass waveguides offer a possibility of constructing active components in a material system that has traditionally permitted only passive devices. They can be fabricated on rare-earth-doped and undoped substrates by similar techniques as used for making passive glass waveguides. Ion exchange and ion implantation are two major techniques to produce waveguiding structures on RED glass substrates. Flame hydrolysis deposition, RF sputtering and spin-coating techniques are mainly used to deposite RED films and to make guided-wave structures on undoped substrates [18].

Comparing with their optical fiber counterparts, RED glass waveguides have some distinguished advantages. Higher dopant concentration is one of them. Usually, RED fibers made by MCVD (modified chemical vapor deposition) [19], or VAD (vapor phase axial deposition) [20] have rare-earth dopant concentration from a few tens to several hundreds ppm (parts per million), whereas RED glass waveguides can have dopant concentration from several thousands to a few tens of thousands ppm. Higher dopant concentration makes RED glass waveguide lasers and amplifiers relatively short (typical length from a few millimeters to a few centimeters) comparing with RED fiber lasers and amplifiers (typical length from several tens of centimeters to several meters). In addition, some fabrication methods used in the manufacturing and processing of RED active

waveguides permit integration of light sources, optical amplifiers and passive optical circuits on the same substrate. This results in a high packaging density and compact integration of passive and active components which would be difficult or impossible with RED fibers. Finally, RED glass waveguides are potentially low cost and their fabrication processes are easier comparing with high cost and complex fabrication processes for RED glass fibers.

The first RED glass film waveguides were made in 1972 by RF sputtering from a neodymium-doped (Nd-doped) glass target onto an undoped glass substrate (Corning 7059 glass) [21]. The deposited active film was pumped by a Xe-flash tube, and net gain of 0.36 dB/cm was observed when 1.06 μm signal light was coupled into and out of the active film waveguides by two prisms. Two years later, a glass channel waveguide laser at 1.06 μm wavelength was demonstrated [22]. The waveguides were fabricated in Nd-doped glass substrate by ion exchange process. After dielectric mirrors with high reflectivity were coated on both polished endfaces, the glass waveguide laser was pumped by a pulsed Rhodamine 6G dye laser at $\lambda = 590$ nm. It is worth to note that the lasing threshold for the waveguide laser was about half of that for the same conventional bulk laser. In 1976, RF sputtering was again used to fabricate Nd-doped glass film waveguides on glass substrates [23]. Pyrex glass substrate gave the best results (lowest propogation losses, longest fluorescent lifetime, etc.) in this work. The highest net gain of 3.9 dB/cm was obtained when the Nd-doped glass waveguide was optically pumped by a cw Rh 6G dye laser.

Though the preliminary experimental results demonstrated the lasing as well as amplification characteristics of Nd-doped glass waveguides, there were no further publications on this subject for almost thirteen years. It was until 1989, that the idea of light amplification and lasing in RED planar glass waveguides was reintroduced [24,25].

Since then, a significant number of papers have been published on this subject. The progress in this area before May 1991, particularly in respect to Nd-doped glass waveguides, amplifiers and lasers were summarized in a review paper [18]. The main characteristics [26-32] of the Nd-doped glass waveguides and corresponding fabrication processes, waveguide characteristics, as well as laser and amplifier properties are listed in Table A.

In past two years, the performance of some Nd-doped glass waveguide lasers and amplifiers has been improved [33,34] and some new types of Nd-doped glass waveguide lasers have been demonstrated. They include extended cavity operation [35] (mode-lock, Q-switch, grating tuning and single frequency operation by bulk modulators and a bulk grating) of Nd-doped glass waveguide laser, Y-branch Nd-doped glass waveguide laser and amplifier [36], and integrated Q-switched multi-cavity Nd-doped glass waveguide laser [37]. Some of their performances are included in Table B.

Erbium-doped (Er-doped) glass waveguides have also received much more attention in recent two years, because their lasing wavelengths are attractive for optical communication applications. Waveguiding structure makes Er-doped fiber/waveguide lasers and amplifiers easy to operate in cw form at room temperature, which was traditionally considered difficult for the three level laser system in the bulk structure. After Er-doped fiber lasers and amplifiers, their counterparts in planar waveguide configuration have also been demonstrated in past two years. Most of their characteristics published until now [38-46] are summarized in Table C.

C. Scope of the present work

The main purpose of this thesis is to fabricate RED glass waveguides and study their suitability for laser, amplifier and other active applications in glass integrated optics area. Passive devices, which are ultimately needed in connection with the RED active devices, are also studied.

To reach these goals requires the development of different fabrication techniques for producing high performance passive and RED active glass waveguides for various applications. A lot of emphasis is put on developing fabrication processes and demonstrating the operation of components fabricated. These processes would facilitate the integration of passive and active devices on the same substrate, and enable the realization of highly sophisticated integrated optical circuits.

Optical characterization is needed to relate the fabrication parameters such as diffusion temperature, ion exchange time and mask widths to optical characteristics of fabricated glass waveguides, which include maximum index change Δn, index profile function, cut-off wavelength, single mode operation region, propagation losses and mode profile. Measurements of optical and physical parameters for RED glass waveguides are also required, which will provide necessary information and design parameters for lasers, amplifiers and other active devices. These parameters include absorption spectra and intensities, propagation losses at laser/signal wavelengths, fluorescent lifetime, fluorescence spectra and gain when the active waveguides are pumped. The measurements will also let us know what is the influence of fabrication processes on performance of waveguides and devices. For example, fluorescent lifetime measurement indicates that the fluorescent lifetime of silver ion-exchanged Nd-doped glass waveguides is significantly reduced by ion exchange process.

We have studied single step ion-exchanged glass waveguides made by $K^+ \leftrightarrow Na^+$, $Cs^+ \leftrightarrow Na^+$, and $Ag^+ \leftrightarrow Na^+$ ion exchange processes on different soda-lime glass substrates, and dual-core glass waveguides by potassium and silver double-ion-exchange technique. Optical characterization of these passive glass waveguides has also been performed. Chapter I mainly concerns with these issues.

Some passive integrated optical components closely related to active devices have also been made and their optical characterization has been carried out. Ion-exchanged glass waveguides with gratings of submicron periodicity, symmetric Y-branches for power splitting, four-port nonsymmetric Mach-Zehnder interferometer and an integrated optical ring resonator are examples of these passive devices. These devices and their performances are discussed in chapter II. Integrated optical waveguide lasers can be fabricated by replacing the conventional non-planar cavity mirrors with distributed feedback gratings to achieve single frequency operation. Y-branches can be utilized to study lossless power splitters and multi-cavity integrated waveguide lasers, and ring resonators are attractive for realizing, for example, ring lasers.

Three different processes have been successfully developed for fabrication of RED glass waveguides on passive and in RED glass substrates. The first one is dilute silver nitrate molten salt ion exchange process, which is suitable for waveguide fabrication in Nd- and Er-doped silicate glass substrates. Spin-coating technique, as the second process developed, is employed for coating Nd- and Er-doped phosphate glass overlays on passive glass waveguides, which are fabricated by ion exchange process in soda-lime glass substrates. The last process developed for RED glass waveguide fabrication is composite technique, which is applied to combine double-ion-exchanged passive glass waveguides with Er-doped phosphate laser glass whose laser characteristics are optimized for active applications. Optical and physical properties of these RED glass waveguides

are also studied. Chapter III concentrates on the discussion of the fabrication processes and optical behavior of these waveguides.

The RED glass waveguides with suitable characteristics are selected for demonstration of some active applications. An Er-doped composite glass waveguide amplifier is demonstrated in chapter IV. Its optical characteristics such as absorption intensity at pump wavelength, propagation losses around laser wavelength, and the relations between pump power and gain are determined.

Finally, in the conclusion, the summary of the thesis is given and some future works are proposed, which mainly concern with active applications of RED glass waveguides. These interesting active applications are natural extension of the present study, and based on the results obtained in this thesis. They are very promising for successful demonstration.

This project has contributed to about 25 conference and journal publications. A list of these publications is given below.

1. "Erbium-doped composite glass waveguide amplifier," Electron. Lett., Vol.28, pp1872-1873, 1992.
2. "Composite rare-earth-doped glass waveguides and amplifiers," *SPIE Proceedings*, Vol. 1794, paper #03, 1992.
3. "A new integrated optical resonator in glass," Electron. Lett., Vol.28, pp1967-1968, 1992.
4. "Integrated optical ring resonator with a novel nonsymmetric Mach-Zehnder interferometer as input/output coupler," *SPIE Proceedings*, Vol.1794, paper #39, 1992.
5. "Four-port guided-wave nonsymmetric Mach-Zehnder interferometer," Appl. Phys. Lett., Vol.61, pp150-152, 1992.

6. "Symmetrical and nonsymmetrical Mach-Zehnder interferometers in glass," The 10th Annual Eur. Conference EFOC/LAN, Paris, June 24-26, 1992.

7. "Ion-exchanged Mach-Zehnder interferometers in glass," Appl. Opt. Vol.31, pp3381-3383, 1992.

8. "Loss characteristics of double-ion-exchanged glass waveguides," Submitted for publication.

9. "Low-loss double-ion-exchanged dual-core wabeguides," Proc. of The 10th Topical Meeting on Gradient-Index Optical Systems, paper #T.5.6, pp175-178, Spain, Oct.4-6, 1992.

10. "Composite rare-earth-doped glass waveguides," Electron. Lett., Vol.28, pp.746 -747, 1992.

11. "Silver-film ion-exchanged singlemode waveguides in Er doped phosphate glass," Electron. Lett., Vol.27, pp.2167-2168, 1991.

12. "Single-mode glass channel waveguides by ion-exchange with ionic masking," Opt. Commun. Vol. pp , 1992.

13. "Integrated optical devices in glass by ionic masking," *SPIE Proceedings*, Vol. paper # , 1992.

14. "Potassium and silver ion-exchanged dual-core glass waveguides with gratings," Appl. Phys. Lett., Vol.58, pp2607-2609, 1991.

15. "Dual-core ion-exchanged glass waveguides," *SPIE Proceedings*, Vol.1513, paper #47, 1991.

16. "Optical damage threshold of ion-exchanged glass waveguides at 1.06 μm," *SPIE Proceedings*, Vol.1538, paper #4, 1991.

17. "Glass waveguides by ion-exchange with ionic masking," *SPIE Proceedings*, Vol. 1513, pp434-440, 1991.

18. "Burried glass waveguides by ion-exchange through ionic barrier," *SPIE Proceedings*, Vol. 1506, paper #02, 1991

19. "Ion-exchanged glass waveguides with spin-coated phosphate overlays," *Proceedings of the First IEEE International Workshop on Photonic Networks, Components and Applications*, World Scientific, NJ, pp223-227, 1991.

20. "Glass waveguide with gratings," *Proceedings of the first IEEE International Workshop on Photonic networks, Components and Applications*, World Scientific, NJ, pp218-222, 1991.

21. "Ion-exchange processes for advanced glass waveguides," *Proceedings of the first IEEE International Workshop on Photonic networks, Components and Applications*, World Scientific, NJ, pp428-432, 1991.

22. "Fabrication and characterization of ion-exchanged glass channel waveguides with etched and diffused grating taps," *SPIE Proceedings*, Vol.1334, pp148-152, 1990.

23. "Rare-earth doped glass waveguides and amplifiers," *SPIE Proceedings*, Vol.1338, pp.82-87, 1990.

24. "Fabrication and characterization of neodymium-doped glass waveguides," IEEE photon. Technol. Lett., Vol.1, pp.109-110, 1989.

25. "Ion-exchanged rare-earth doped glass waveguides,"*SPIE Proceedings*, Vol.1128, paper #24, 1989.

Table A. Characteristics of neodymium-doped glass waveguide amplifiers and lasers.

Ref.	Fabrication process	Component	Nd concetration	Prop. losses dB/cm (λ,μm)	L** (mm)	Fluorescent lifetime (μs)	Pump wave-length (μm)	Laser or signal wavelength (μm)	Threshold or gain	Notes
21	Rf sputtering Nd-glass on Corning 7059	Amplifier (slab)	Target contains 3.5 wt % Nd_2O_3	0.7 (0.633) 0.45 (1.06)	30	-	Xe flash tube	1.06	Amplification of 0.36 dB/cm	Target: barium Crown Nd-doped glass
22	Tl-K-Na salt Ion-exchange	Laser (channel)	4 wt % Nd_2O_3	-	4	310 (substrate)	0.59 (pulse Rh-6G)	1.06	18 μJ	Nd-doped borosilicate glass
23	Rf sputtering Nd-glass on Pyrex 7749	Amplifier (slab)	Target contains 2 wt % Nd_2O_3	0.5 (0.633) 0.15 (1.06)	40	425 (waveguide) 573 (subatrate)	0.585 (cw Rh-6G)	1.06	3.9 dB gain	Target: barium Crown Nd-doped glass
26	FHD & RIE*	Laser (channel)	-	0.85 (1.06)	50	-	0.80	1.05 and 1.0545	150 mW (pump power)	Slope efficiency 0.12 %
27	K^+ion-exch-ange in Nd-doped glass	Laser (channel)	Schott LG-660 glass	-	10	-	0.528	1.057	7.5 mW (launch-ed pump power)	Slope efficiency 6 %
28	K^+ion-exch-ange in Nd-doped BK7	Laser (channel)	2 wt % Nd_2O_3	0.8 (0.85)	17	380	0.807	1.058	31 mW (absorbed pump power)	E-field assited diffusion
29	Ag^+ion-exch-ange in Kigre Q-246 glass	Amplifier (channel)	3.5 wt % Nd_2O_3	-	7	150 (waveguide) 300 (substrate)	0.59	1.084 (signal)	2 dB gain	Dilute silver ion-exchange
30	Rf sputtering LG-760 glass on silicon	Laser (channel)	Target contains 6 wt % Nd_2O_3	3.5 (0.6328)	4	104 (waveguide) 337 (substrate)	0.59	1.055~ 1.056	100 mW (launch-ed pump power)	Phosphate glass target
31	Ag film ion-exchange in Hoya LHG-5	Laser (channel)	3.3 wt % Nd_2O_3	-	-	-	0.802	1.054	6.9 mW (launch-ed pump power)	Phosphate glass substrate
32	Same as in ref. 31	Laser (channel)	Same as in ref. 31	-	5	-	0.802	1.325 & 1.355	33 mW (launch-ed pump power)	Low Excited State Absorption (ESA)

* FHD & RIE (Flame Hydrolysis Deposition & Reactive Ion Etching)

** L : Sample length.

Table B. Characteristics of extended Nd-doped glass waveguide lasers and amplifiers.

Ref.	Fabrication process	Component	Nd concetration	Laser or signal wavelength (μm)	Pump wave-length (μm)	Sample length (mm)	Threshold, gain or outpot power	Notes
33	FHD& RIE*	Laser	2000 ppm	1.053	0.805	40	Threshold 25 mW	Slope efficiency 1.2 %
34	Silver film ion-exchange	Amplifier	3.3 wt % Nd_2O_3	1.054	0.5145 0.808	10	3.4 dB max.gain (Ar^+laser pump)	0.027 dB/mW 0.079 dB/mW
35	E-field assisted potassiun ion-exchange	Q-switching	Bulk electro-optic modulator (peak power 1.2 W)		0.807	8	cw output power 20 mW	75 ns FWHM
		Mode-locking	Bulk acousto-optic deflctor (80 ps FWHM)			12		peak power 225 mW
		Grating tuning	Bulk grating as a feedback element (20 nm tuning width)			12		Line width 7GHz
		Single frquency	High reflectivity étalon added in cavity			12		50 MHz FWHM
36	Same as ref. 35	Y-branch laser & Amplifier	Shott LG -660 laser glass	1.057	0.807	24	26 mW absorbed pump power	0.034 dB/mW
37	Potassium ion-exchange	Y-junction Q-swich laser	1.5 wt % Nd_2O_3 in BK7	1.06	0.810	41	70 mW peak power (5 μs FWHM)	with a thermo-optical pase modulator

* FHD & RIE (Flame Hydrolysis Deposition & Reactive Ion Etching)

Table C. Characteristics of erbium-doped glass waveguides, amplifiers and lasers.

Ref.	Fabrication process	Component	Er concetration	Prop. losses dB/cm (λ,μm)	L** (mm)	Absorption dB/cm (λ,,μm)	Pump wave-length (μm)	Laser or signal wavelength (μm)	Threshold or gain	Notes
38	FHD& RIE*	Laser	8000 ppm	< 0.1	45	0.25 (0.98) 0.72 (1.54)	0.98	1.598 and 1.604	49 mW (pump power)	Slope efficiency 0.81 %
39	Potassium Ion-exchange	Waveguides	2 wt % Er_2O_3	0.8 (0.633)	-	0.4 (0.98) 2 (1.53)	-	-	-	Na-modified BK-7 glass
40	Silver film ion-exchange	Waveguides	0.25 wt % erbium	-	8	10 (0.976) 20 (1.535)	0.971	Fluorescence peak: 1.55 μm	-	Phosphate glass
41	Potassium Ion-exchange	Laser	0.5 wt % Er_2O_3	0.5	36	0.25 (0.98) 1.4 (1.54)	0.98	1.538 and 1.544	150 mW (pump power)	Slope efficiency 0.55 %
42	Composite waveguide	Waveguides	-	-	4.9	16 (0.9734)	-	-	-	QE-7 phosphate glass
43	RF sputtering	Amplifier	10000 ppm	1 (1.53)	24	8.5 (1.54)	0.975	1.53 (signal)	21 dB gain (120 mW pump power)	Lossless waveguides
44	FHD& RIE*	Amplifier	0.55 wt % erbium	< 0.16 (1.535)	194	-	0.980	1.535 (signal)	13.7 dB net gain(640 mW pump power)	0 dB gain (25 mW pump power)
45	Composite waveguide	Amplifier	-	4 (1.5231)	4.7	16 (0.9734)	0.9734	1.5231 (signal) 1.5568	10 dB 6 dB net gain	60 mW pump power

* FHD & RIE (Flame Hydrolysis Deposition & Reactive Ion Etching)

** L : Sample length.

CHAPTER I

PASSIVE GLASS WAVEGUIDES

As mentioned in introduction, ion exchange technique is a simple, flexible, accurate and powerful technique for fabrication of passive glass waveguides and devices. General principles of the technique, various monovalent ions suitable for waveguide fabrication, their advantages and drawbacks, waveguide performance resulting from various ion exchange processes, as well as present state of the art in this area are discussed in detail in references [3] and [9-11]. In this chapter, we are not going to generally discuss ion exchange processes and ion-exchanged glass waveguides, but mainly concentrate on the study of such passive ion-exchanged glass waveguides that are closely related to the development of RED glass waveguides and passive devices for various active applications. To achieve such components, an active material should be used in conjunction with passive glass waveguides. Therefore, different fabrication processes depending on the device requirements have to be developed in order to obtain efficient interaction between the guided light and active media. Active materials such as RED films employed with high quality passive glass waveguides provide a flexibility to integrate passive and active components on the same substrate, so that more sophisticated and advanced integrated optical circuits can be developed.

In the section 1.1, passive glass waveguides fabricated in glass substrates by one step ion exchange process in different molten salts are discussed. Their diffusion and optical behavior such as maximum refractive index change, index profile, and

propagation losses are studied. Some of these passive glass waveguides, for example, potassium ion-exchanged glass waveguides are employed to demonstrate active operations when they incorporate with neodymium- and erbium-doped phosphate glass overlays [5, 29]. This subject is studied in chapter III. Potassium ion exchange process is also empolyed in fabrication of some useful passive components such as Y-branches and Mach-Zehnder interferometers [47]. Silver ion-exchanged waveguides are employed in fabrication of the grating-assisted waveguides [48, 49], and they are discussed in chapter II.

Other important passive glass waveguides discussed in section 1.2 are those made by double-ion-exchange process: first potassium ion exchange, which is followed by silver ion exchange [50, 51]. Waveguides fabricated by this technique are studied. Characterization of slab and channel waveguides is also carried out and measurement results are presented. Advantages of the two-step ion-exchanged glass waveguides over their one-step ion-exchanged counterparts are pointed out. The double-ion-exchanged glass waveguides are employed to demonstrate some interesting passive devices that are potentially important for active applications of RED glass waveguides. These devices include waveguides with gratings of submicron periodicity [50], and an integrated optical ring resonator [52, 53] with a four-port nonsymmetric Mach-Zehnder interferometer [54, 55] as an input-output coupler. All of them are discussed in chapter II. In addition, the double-ion-exchanged glass waveguides are utilized in demonstration of composite RED glass waveguide structures [42], and also in demonstration of an Er-doped composite glass waveguide amplifier [45, 46]. These subjects are discussed in chapters III and IV.

1.1 Glass waveguides by one-step ion exchange process

Glass waveguides by one-step ion exchange process are fabricated in 0.5 mm thick Corning 0211 and 1 mm thick Schott BK7 glass substrates by purely thermal diffusion technique. Both slab and channel waveguides are made in order to study their diffusion and optical behavior. For channel waveguide fabrication, about 100 nm thick aluminum film is deposited in vacuum on the substrates, and mask openings are defined by conventional photolithographic technique. The mask opening widths are from 2 μm to 10 μm with 0.5 μm increment. Pure potassium nitrate, cesium nitrate and silver nitrate molten salts as ion sources are seperately ultilized to achieve glass waveguides with different optical characteristics.

After ion exchange processes, (aluminum mask is removed in the case of channel waveguides) samples are polished and following optical characterizations are performed.

1.1.1 Prism coupling measurement

First of all, the coupling angles for guided modes in slab waveguides are measured by a single-prism coupling method [56, 57]. The principle of the prism coupling measurement and the experimental set-up are schematically illustrated in Fig. 1.1 (a) and (b). The prism coupler applies the principle of distributed coupling through evanescent fields to the guided modes of slab waveguides. A prism, whose refractive index is n_p, is placed above a slab waveguide and is seperated from it by a small air-gap, which has refractive index n_a. When a plane wave with an incident angle θ enters the prism, the refracted plane wave propagates at an angle ϕ with respect to the normal of the prism

base. Total internal reflection occurs at the prism base if

$$\phi > \phi_c = \mathrm{Sin}^{-1}(n_a/n_p) \qquad (1.1.1)$$

where ϕ_c is the critical angle of total internal reflection. Under condition (1.1.1), the superposition of the incident wave and the reflected wave in the prism yields a standing wave in the vertical direction of the prism base. But in the air-gap, an evanescent field decaying exponentially is generated. The waves in the prism and in the slab waveguide are coupled through their evanescent fields in the air-gap. The field amplitudes are as indicated in Fig. 1.1 (a). The coupler permits excitation for each of guided modes by proper orientation of the direction of the incident beam. The energy interchanged through the evanescent field coupling is complete only if the components of the wave vectors parallel to the air-gap are equal for the wave in the prism and the wave in the slab waveguide. That is

$$k_p \,\mathrm{Sin}\, \phi_m = \beta_m \,. \qquad (1.1.2)$$

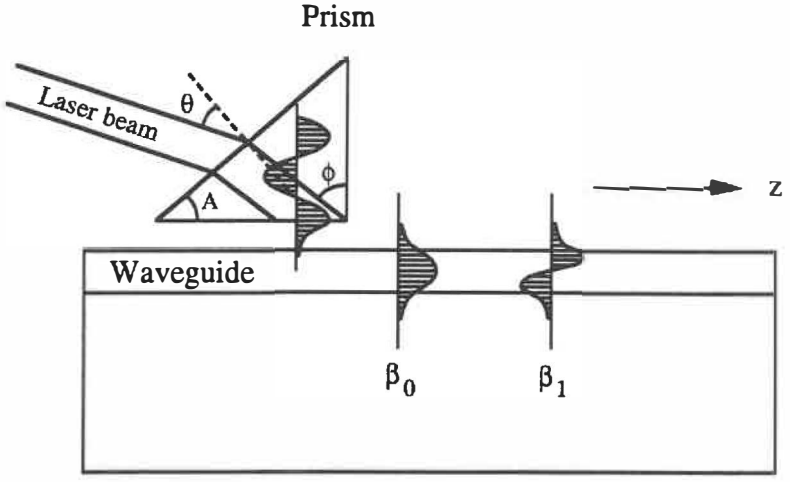

Fig. 1.1 (a) The principle of prism coupling measurement.

where $k_p = kn_p$, and k is propagation constant in vacuum, $\beta_m = kN_m$ is propagation constant for the mth guided mode (m = 0, 1, 2, ···), and N_m is the effective refractive index for the mth mode. Condition (1.1.2) is also called a phase-matched condition. It determines a set of discrete angles ϕ_m (m = 0, 1, 2, ···) corresponding to the guided modes. In addition, the maximum coupling from incident energy into a guided mode requires that the right-hand beam boundary in the prism intersects the prism corner, as shown in Fig. 1.1 (a). By some simple manipulation, it is easy to relate the angles ϕ_m in (1.1.2) to corresponding coupling angles θ_m, which are directly measurable. From measured θ_m, the effective refractive indices for guided modes can be calculated by

$$N_m = n_p \text{ Sin } [A + \text{Sin}^{-1}(\text{Sin } \theta_m / n_p)] \qquad (1.1.3)$$

where A is the base angle of the prism.

The experimental set-up for the measurement of coupling angles θ_m is schematically shown in Fig. 1.1 (b). The slab waveguide to be measured is mounted in a goniometer. The prism base is pressed against the waveguide surface by a spring-loaded clamp. A laser beam (usually, a visible He-Ne laser beam at 0.6328 μm wavelength) through a lens L_1 (with a long focal length) is coupled into the slab waveguide by the prism to excite guided modes. The guided light in each mode is end-fire coupled out of the polished endface of the waveguide by an objective L_2. By directing the output light corresponding to each guided mode through a slit and maximizing the output of the detector while ajusting the incident angle θ, we can determine the coupling angle θ_m for the mth guided mode, and calculate its effective refractive index.

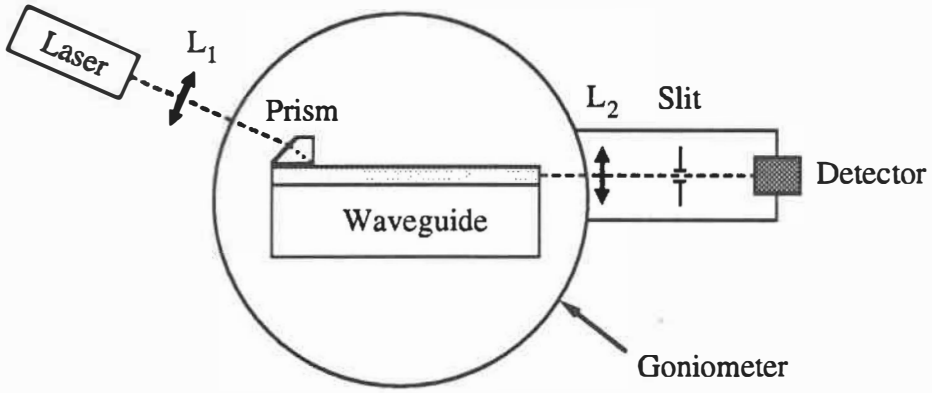

Fig. 1.1 (b) Experimental set-up for the measurement of coupling angles θ_m.

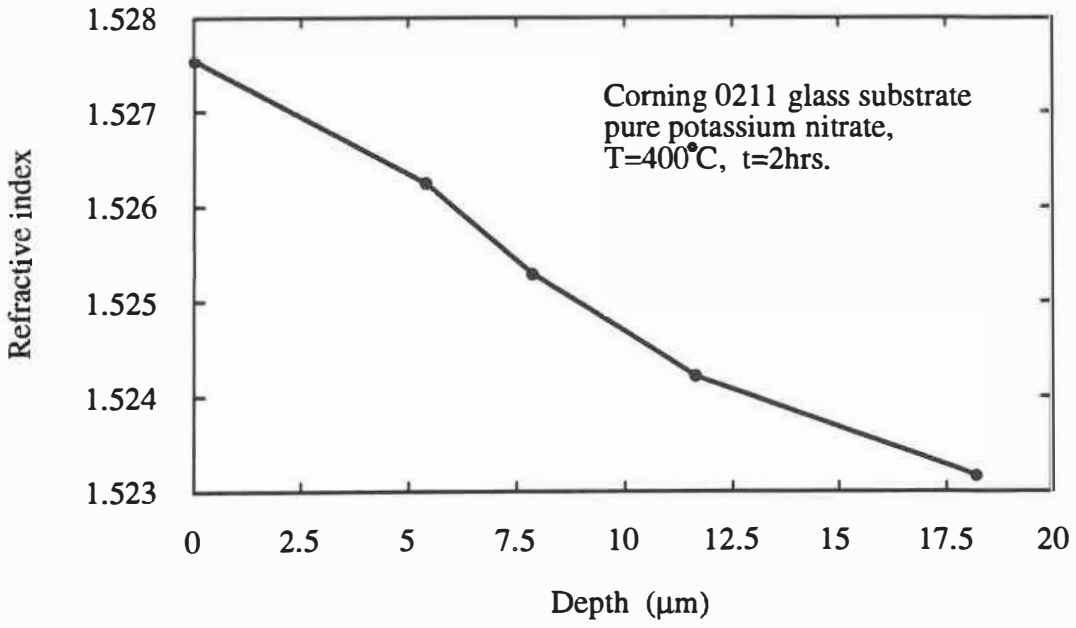

Fig. 1.2 (a) Index profile for potassium ion-exchanged slab waveguide.

1.1.2 Index profile determination

The measured effective refractive index data can be employed to determine index profile of the slab waveguide by inversed W.K.B. method [58]. Some of the index profiles for potassium, silver and cesium ion-exchanged slab waveguides are shown in Fig. 1.2 (a), (b) and (c). The fabrication conditions such as substrates, molten salts, diffusion temperature T and ion exchange time t are given in these figures.

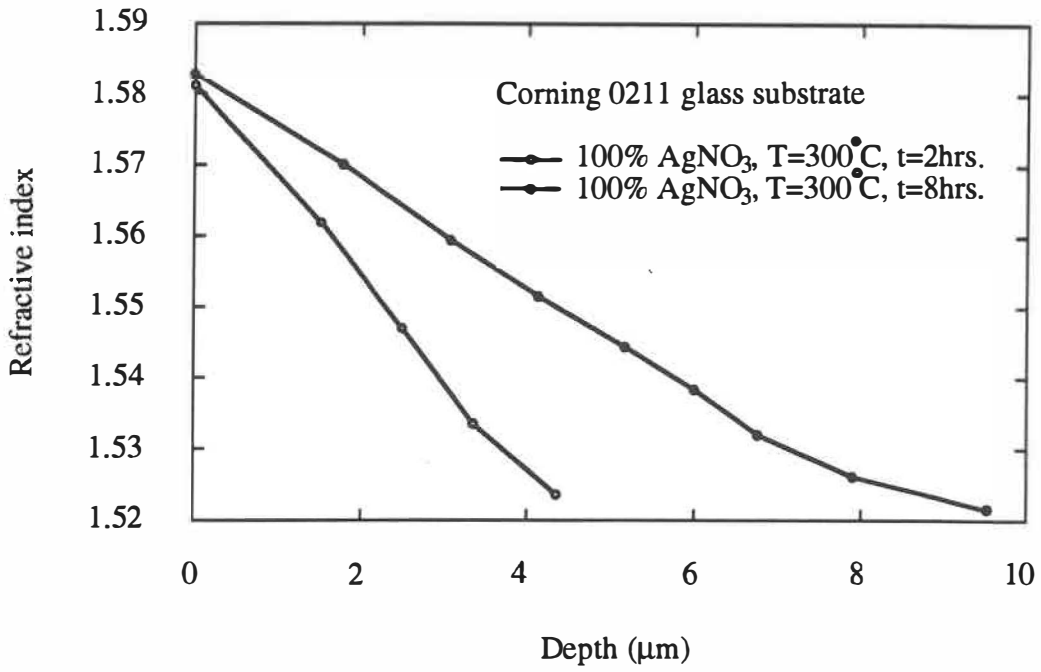

Fig. 1.2 (b) Index profiles for silver ion-exchanged slab waveguides.

The measured effective refractive indices can also be used to deduce the effective diffusion depth d (or effective diffusion coefficient D, where $D = d^2/4t$, and t is diffusion time), and maximum index change Δn and the index profile of each waveguide by fitting experimental data points to calculated W.K.B. dispersion curves of some assumed index profile function (e.g. complementary error function, Gaussian function or step index

function). Fig. 3.1 (in chapter III, page 71) shows a typical example of fitting measured data points to normalized dispersion curves (b-V curves) of W.K.B. calculation (assumed index profile function is complementary error function in this case) for silver ion-exchanged slab waveguides in neodymium-doped silicate glass substrates (Kigre Q-246). The D and Δn for the Nd-doped glass waveguides are given in section 3.1 (page 72).

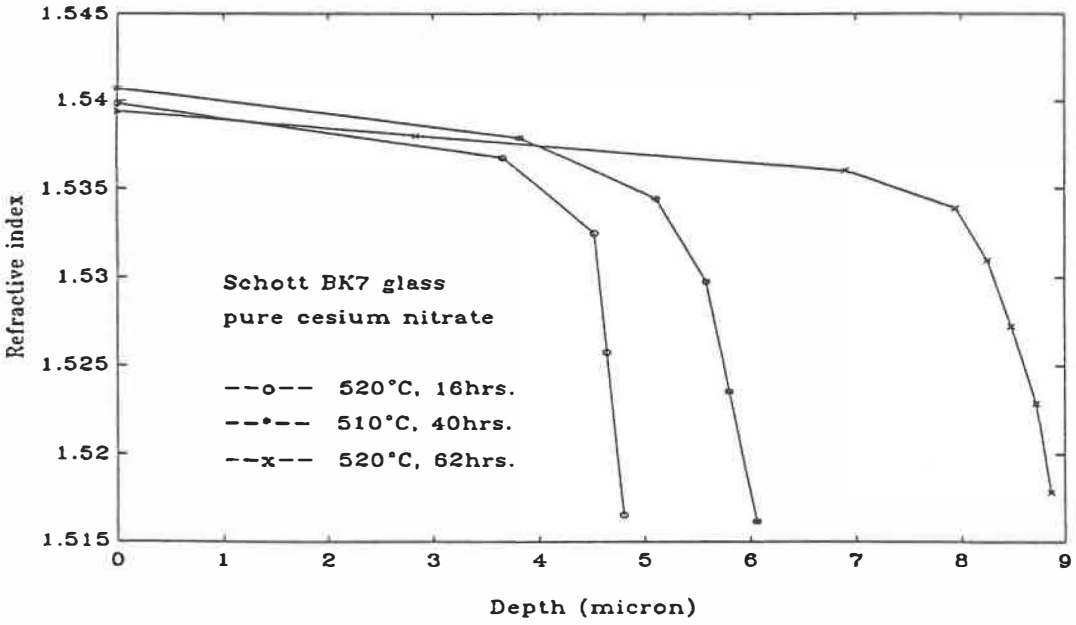

Fig. 1.2 (c) Index profiles for cesium ion-exchanged slab waveguides.

1.1.3 Propagation loss measurement of slab waveguides

Propagation losses of a slab waveguide are measured by two-prism coupling technique. The experimental set-up for the measurement is schematically shown in Fig. 1.3. The principle for the measurement is explained in the chapter 5 of the reference [3].

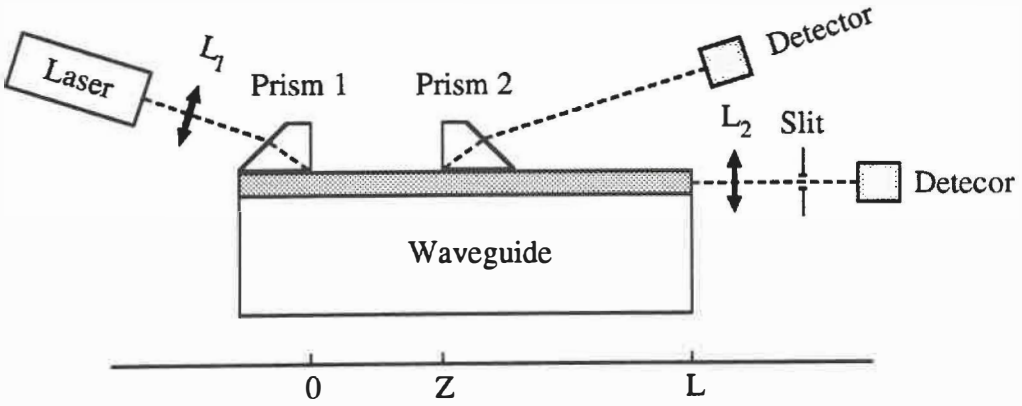

Fig. 1.3 Schematic set-up of two prism coupling method to measure propagation losses of slab waveguides.

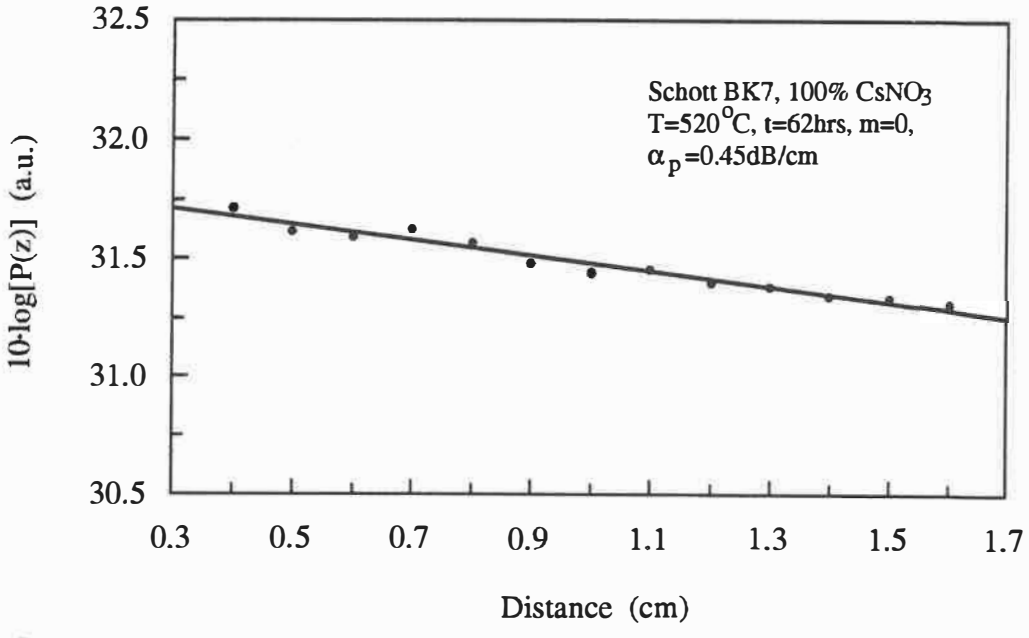

Fig. 1.4 Measured data points and linear regression, slope of the line gives losses.

Linear regression method is employed to fit measured data points to a straight line, the slope of the straight line gives the propagation losses. Fig. 1.4 gives one example for the fitting. Fabrication parameters are given in the figure, m = 0 corresponding to fundamental mode and α_p is propagation losses (dB/cm). Some of the fabrication conditions for slab waveguides by different one-step ion exchange processes and their characterization results are summarized in Table I-1.

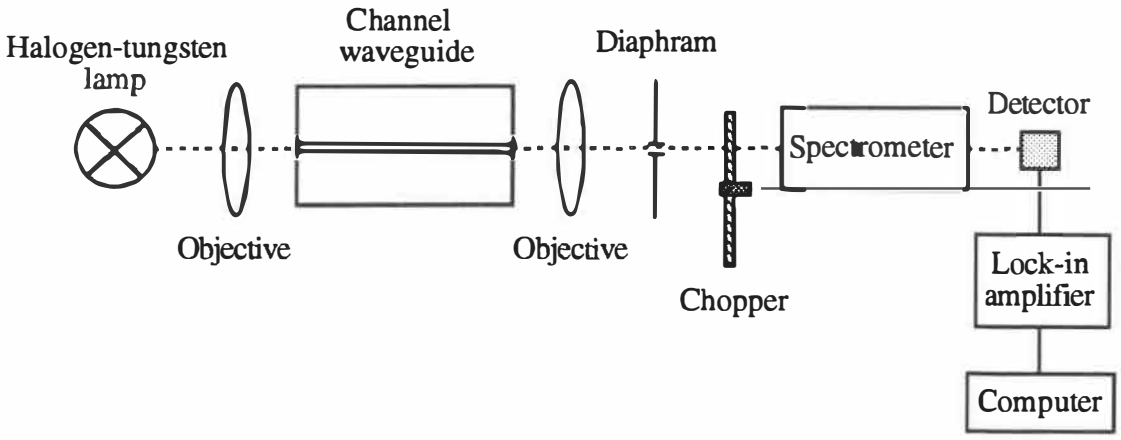

Fig. 1.5 Experimental set-up of measuring spectral transmission of channel waveguides.

1.1.4 Spectral transmission measurement

The spectral transmission measurements of channel waveguides give us important information to relate the fabrication parameters (diffusion temperature T, time t and mask opening width W, etc.) to waveguide optical behavior (such as cut-off wavelength, single mode operation region, and qualitative information about waveguide losses at

different wavelengths). Fig. 1.5 shows the schematic set-up for the measurement. Light from a halogen-tungsten lamp is coupled into a channel waveguide by an objective. Output light from the channel waveguide is collected by another objective and direct into a spectrometer after going through a diaphram, which stops stray light from the substrate. Silicon or germanium photodiode detector is employed to measure spectral signal depending on which spectral region is of interested. Output current from the detector is amplified by a lock-in amplifier and measured data is processed by a computer. Usually, the measured spectral transmission is divided by the corresponding spectral response of the system (without waveguide) to obtain normalized spectral transmission. In the following discussion, all of the spectral transmission is normalized unless otherwise

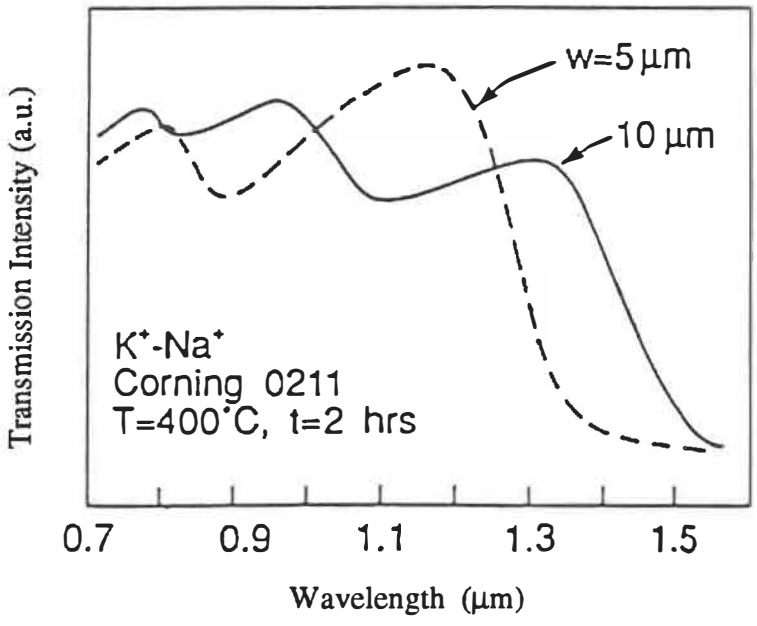

Fig. 1.6 Spectral transmission for potassium ion-exchanged channel waveguides with different mask opening widths.

explained. Typical spectral transmission for potassium ion-exchanged channel waveguides with different mask opening widths are shown in Fig. 1.6.

1.2 Glass waveguides by double-ion-exchange process

Potassium and silver ion exchange processes are very useful for fabrication of glass waveguides and simple integrated optical devices, but they are not flexible enough to satisfy different requirements in more sophisticated devices. For example, potassium ion-exchanged glass waveguides have low index change, low propagation losses, and large single mode operation region, which make the potassium ion exchange process well suitable for fabricating basic integrated optical components such as Y-branches and directional couplers [59-61]. Since the lower index change results in less tight guided mode confinement, potassium ion exchange process does not suit well for such applications that require curved waveguides with small bending radii, because radiation loss in bended waveguides increases very rapidly with reducing bending radius [47, 62, 63]. Potassium ion-exchanged glass waveguides are not suitable for fabrication of grating assisted waveguides and devices. Deep gratings are needed to achieve efficient interaction between guided light and grating structure in potassium ion-exchanged waveguides. In practice, submicron periodic gratings with their depth equal or larger than the periodicity are difficult to make. On the other hand, silver ion-exchanged glass waveguides are well suitable for these applications due to their high index change and consequently tight mode confinement. In fact, a silver ion-exchanged integrated optical ring resonator with small bending radius (less than 1 mm) [63] and an efficient grating

assisted glass waveguide [48, 49] have been successfully demonstrated. However, waveguides made by silver ion exchange process have small single mode operation region, and the waveguides are shallow and narrow. In some applications such as directional couplers, the two coupled channels must be placed very close to each other, which makes the patterning process more difficult. Furthermore, silver ion exchange through a metallic mask opening results in relatively high propagation losses due to silver metal colloids formed under the mask during ion exchange process [64].

Combining potassium and silver ion exchange processes has been demonstrated as an effective technique to fabricate channel waveguides with low propagation losses, tighter mode confinement, and more symmetric mode profile [50]. All double-ion-exchanged waveguides are fabricated in Corning 0211 glass substrates. First, potassium ion exchange is carried out in a pure potassium nitrate molten salt. Then, a silver ion exchange is performed in a pure silver nitrate molten salt. For channel waveguides, the same aluminum mask is used for the two-step ion exchange process. For comparison purposes, the waveguides with similar diffusion depth to that of the double-ion-exchanged waveguides are also made by single step ion exchange process in pure silver nitrate molten salt. The fabrication parameters are given in Table I-2. Following optical characterizations are performed.

1.2.1 Index profiles

In slab waveguides, the effective refractive indices for guided modes are measured (at 0.6328 μm waveglength) and the index profiles are determined by inversed W.K.B. method as explained in previous section. The results are shown in Fig. 1.7. In double-ion-exchanged waveguides there are two distinct refractive index regions corresponding to the two types of exchange processes. For this reason such a waveguide is also called a

dual-core waveguide. The double-ion-exchange technique can also results in a waveguide with only one guided core if fabrication parameters are properly chosen such that the diffusion depths for potassium and silver ion-exchanged regions are almost the same. The maximum index change in the silver ion-exchanged region is similar to that of single step silver ion-exchanged waveguides. However, silver ion exchange is slower in the presence of potassium ions from the first step ion exchange process. The effective diffusion coefficient of silver ions at 300 ^{0}C in the second step ion exchange process is determined as 0.008 μm/min, which is less than one third of that of silver ions in single step silver ion exchange process at the same temperature (0.028 μm/min.).

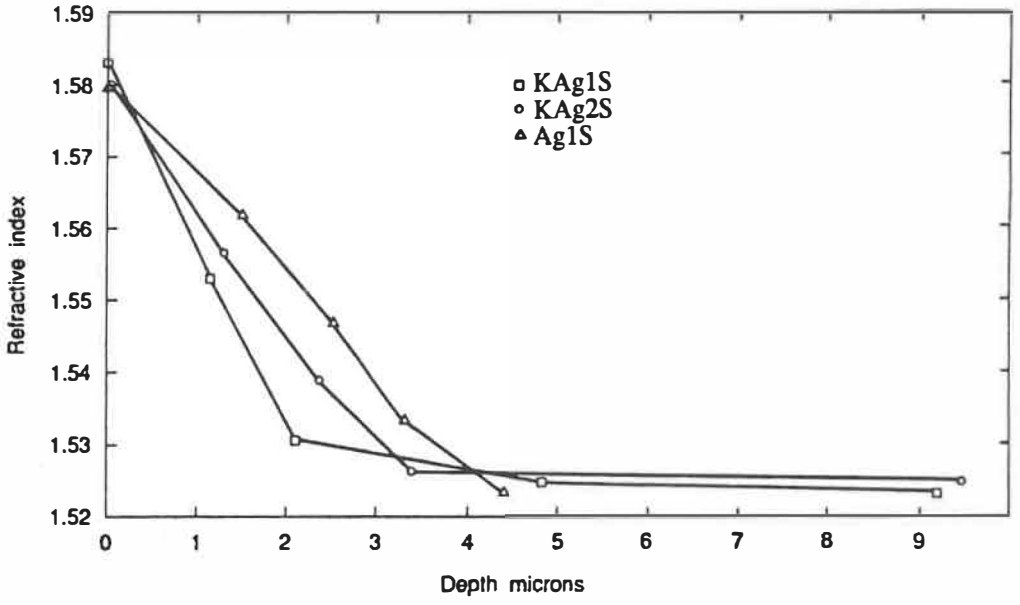

Fig. 1.7 Index profiles for one and two step ion-exchanged slab waveguides.

1.2.2 Mode profiles

In channel waveguides, the mode profiles are examined by the measurement set-up

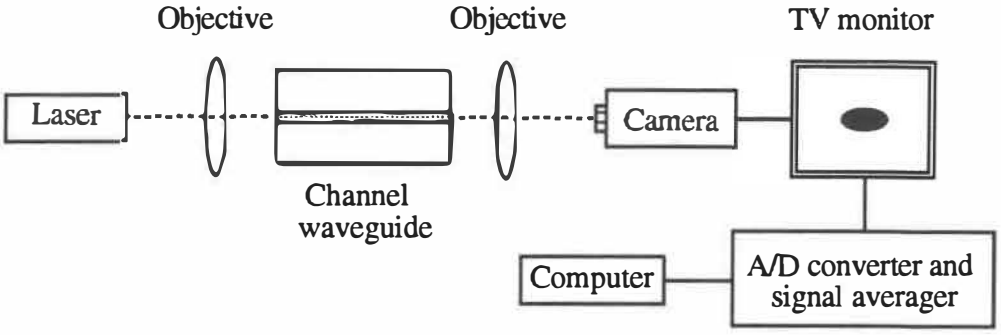

Fig. 1.8 Schematic set-up for mode profile measurement of channel waveguides.

shown in Fig. 1.8. The mode profiles are measured at 1.3 μm wavelength using an infrared video camera. The mode profiles in both lateral and transversal directions and photos for near field output from channel waveguides with 2.5 μm wide mask openings are shown in Fig. 1.9. We have observed that the transversal mode profile of the double-ion-exchanged waveguide with longer silver ion-exchange time (KAg2) is more symmetrical than that of the single step silver ion-exchanged waveguide. We believe that the maximum index change is slightly below the glass surface due to the reduced sodium ion concentration near the surface after the first step potassium ion exchange process.

1.2.3 Transmission spectra

The spectral transmission measurement is carried out by using the set-up shown in Fig. 1.5. The measurment results shown in Fig. 1.10 indicate that the single mode operation region of the double-ion-exchanged waveguides is larger than that of the pure silver ion-exchanged waveguide, and this region increases with the increase of the

second step silver ion exchange time. This indicates again that the index profiles (or mode profiles) of the double-ion-exchanged waveguides are more symmetrical.

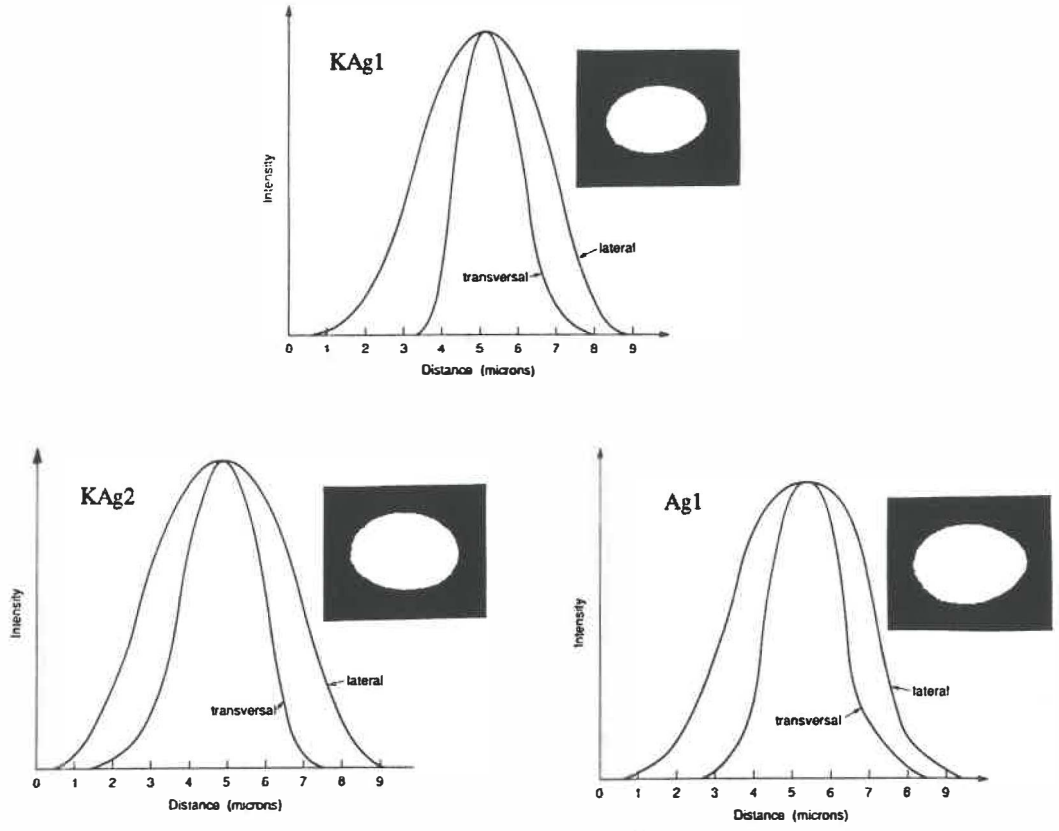

Fig. 1.9 Mode profiles and near field photos for one and two step ion-exchanged channel waveguides.

1.2.4 Propagation losses of channel waveguides

The loss measurement of channel waveguides is very important for understanding loss mechanism caused by various sources such as mask material and fabrication process itself. The measurement set-up is schematically shown in Fig. 1.11. To measure propagation losses of channel waveguides fabricated by one and two step ion exchange

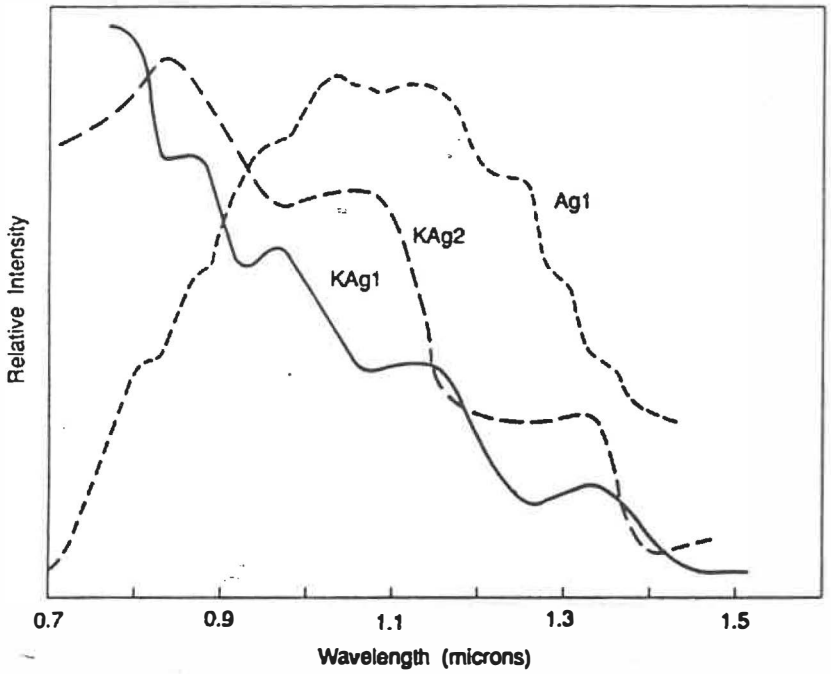

Fig. 1.10 Tansmission spectra for one and two step ion-exchanged channel waveguides.

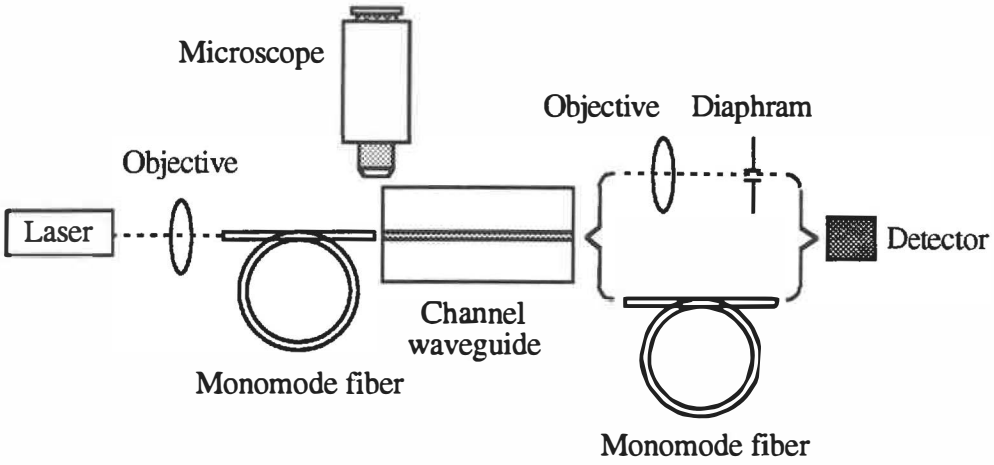

Fig. 1.11 Experimental set-up for loss measurement of channel waveguides.

processes, light from a laser diode at 1.3 μm is coupled into a monomode telecommunication fiber by a 10x objective. Output power P_0 from the fiber is butt coupled into a channel waveguide to be measured. Optical power from output port of the channel waveguide is collected by another monomode fiber or by an objective, and directed onto a germanium photodiode detector connected to a power meter. The measurement details are described as following:

Coupling losses between a fiber and a channel waveguide consist of mode mismatch loss between them, Fresnel reflective loss of endfaces, and misalignment loss caused by lateral and longitudinal displacements, and angles between axises of the fiber and the channel waveguide. When monomode fibers with very good cleaved endfaces are butt coupled to input and output ports of the channel waveguide, it is resonable to assume that the input and output coupling losses are the same provided that the fibers are carefully aligned to minimize misalignment errors and output power from the second fiber is maximized by optimizing input and output couplings. The correctness of this assumption can be confirmed by reversing input and output ports of the channel waveguide, repeating above coupling optimization procedures, and doing the measurement for several times. In our measurements, the input/output fiber position reproducibility is controlled by micro-positioners with lateral tolerances of ± 1μm and longitudinal tolerance ± 5 μm. Alignment is improved by using a microscope system to monitor the gaps between cleaved fiber endfaces and polished waveguide endfaces and to minimize angular alignment errors. Under these optimized conditions, the output power from the second fiber is given by

$$P_1 = P_0(1-\alpha_c)(1-\alpha_p)(1-\alpha_c)T_f \qquad (1.2.1)$$

where α_c and α_p correspond to coupling losses and propagation losses in the channel

waveguide, respectively. T_f corresponds to the transmission of the second fiber.

Keeping the first fiber input coupling unchanged after the measurement of P_1, a 20x microscope objective, whose transmission at the same wavelength is measured as T_0, is used instead of the second fiber to collect the power from the waveguide output port. The objective has a numerical aperture 0.5, which is much larger than that of the channel waveguides to be measured, so the objective collects all output light from the channel waveguides. After the output light going through a small diaphragm, which stops stray light from the substrate, the output power P_2 measured by the photodiode detector is given by

$$P_2 = P_0(1-\alpha_c)(1-\alpha_p)T_0 \qquad (1.2.2)$$

From the measured quantities P_0, P_1, P_2 and T_0 in eqs. (1.2.1) and (1.2.2), and estimated T_f in (1.2.1) as 0.35 dB (due to Fresnel reflections) [65], it is easy to calculate the coupling losses and propagation losses. Some measurement results are shown in the Table I-3. One of the main advantages of the double-ion-exchange process is the very low propagation losses for the channel waveguides compared with one step pure silver ion exchange process through aluminium mask openings. In addition, the two-step ion exchange process with aluminum mask for fabricating low-loss channel waveguides is much simpler than relatively difficult dielectric mask fabrication process needed for making low-loss silver ion-exchanged channel waveguides [66, 67].

Table I-1. Slab waveguide fabrication parameters and characterization results. (one-step ion exchange processes in molten salts)

Substrate	Ion	T (°C)	t (hrs)	λ (μm)	Δn	D (μm^2 /min)	Losses (dB/cm)
Corning 0211	K^+	400	2	0.6328 (TE)	0.0053	0.14	0.15 (m=0)
Corning 0211	Ag^+	300	2	0.6328 (TE)	0.062	0.028	0.54 (m=0)
Corning 0211	Cs^+	540	64	0.6328 (TE)	0.025	0.001	0.81 (m=0)
Schott BK7	Cs^+	520	62	0.6328 (TE)	0.023	0.005	0.45 (m=0)

Table I-2. Fabrication parameters for single-step and two-step ion-exchanged glass waveguides in Corning 0211 glass substrate.

Sample	Waveguide	K^+exchange		Ag^+exchange	
		T (°C)	t (min.)	T (°C)	t (min.)
KAg1S	Slab	400	140	300	150
KAg1	Channel	400	140	300	150
KAg2S	Slab	400	140	300	300
KAg2	Channel	400	140	300	300
Ag1S	Slab	–	–	300	120
Ag1	Channel	–	–	300	120

Table I-3. Loss measurement results of channel waveguides by single and two step ion exchange processes (λ = 1.3 μm).

Samples	Fabrication processes and parameters	Propogation losses	Coupling losses	Mask width
S1	Dual-core channel waveguide (Al mask) K^+: 400°C, 2.5 hrs; Ag^+: 300°C, 6 hrs.	0.3 dB/cm (±0.15dB)	3.1 dB(±0.2 dB)	4 μm
S2	Dual-core channel waveguide (Al mask) K^+: 400°C, 2.5 hrs; Ag^+: 300°C, 3.5 hrs.	0.24 dB/cm (±0.15dB)	3.6 dB(±0.2 dB)	4 μm
S3	Double-ion-exchanged channel waveguide (Al mask) K^+: 400°C, 20 min; Ag^+: 300°C, 2 hrs.	0.22 dB/cm (±0.1dB)	3 dB(±0.2 dB)	4 μm
S4	Ionic mask: K^+: 400°C, 20 min; Channel waveguide: Ag^+: 300°C, 2 hrs.	0.1 dB/cm (±0.1dB)	3.6 dB(±0.3 dB)	5 μm
S5	Slab layer: K^+: 400°C, 20 min; Channel waveguide: Ag^+: 300°C, 5 hrs.	0.6 dB/cm (±0.15dB)	4.4 dB(±0.2 dB)	4 μm
S6	Channel waveguide: (Al mask) Ag^+: 300°C, 2hrs.	1.3 dB/cm (±0.2dB)	3.3 dB(±0.2 dB)	4 μm

CHAPTER II

PASSIVE DEVICES

2.1 Gratings assisted glass waveguides

Waveguides with periodic gratings are useful components in integrated optics. These grating-assisted waveguides can be easily combined with other integrated optical elements to realize sophisticated and potentially inexpensive integrated optical circuits. Gratings are very attractive for applications in various passive and active devices. In passive applications, for instance, they can be utilized for out-of-plane interconnections, i.e. coupling guided light out of waveguides, or reversely, coupling spatial light beam into guided modes in waveguides [68]. They can be also applied to filter selected waveglengths in wavelength division multi/demultiplexing systems [69]. Whereas in active applications, the planar grating structures on waveguides can be employed to construct a resonant cavity in waveguide lasers instead of conventional non-planar type mirror cavity [70]. Grating can also be utilized to construct single longitudinal mode (or single frequency) waveguide lasers for applications in coherent optical communication.

In this section, we discuss fabrication and optical characterization of submicron periodic gratings on ion-exchanged glass channel waveguides. The gratings are fabricated by holographic interference and plasma etching techniques on the channel waveguide surfaces. Optical characterization of these grating assisted channel waveguides include grating period measurement, the determination of propagation constants of guided modes in the channel waveguides by the grating coupler, measurement of grating diffraction efficiency which characterize the interaction between

guided modes in the channel waveguides and gratings on them, and spectral transmission measurement which gives information about the reflectivity of the gratings at selected wavelength and their reflective bandwidth.

Silver and potassium ion exchange processes are employed to fabricate channel waveguides, on which submicron periodic gratings are made. Both single-step (pure potassium or silver) [48, 49] and two-step (first potassium, then following silver) [50] ion-exchanged glass channel waveguides are fabricated in order to compare the interaction between the gratings and the guided modes in different waveguides. All of the ion exchange processes are carried out through aluminum mask openings on Corning 0211 glass substrate. Fabrication parameters are given in Table II-1. After the channel

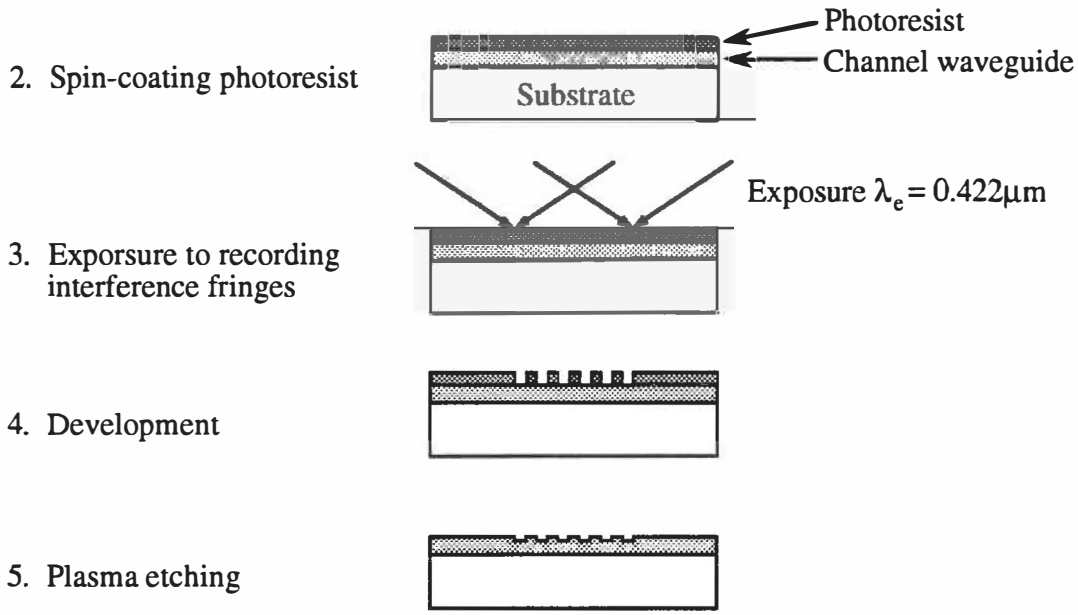

Fig. 2.1 Fabrication procedure of submicron periodic grating on ion-exchanged channel waveguides.

waveguide fabrication processes aluminum mask is removed, and grating fabrication procedure illustrated in Fig. 2.1 is followed.

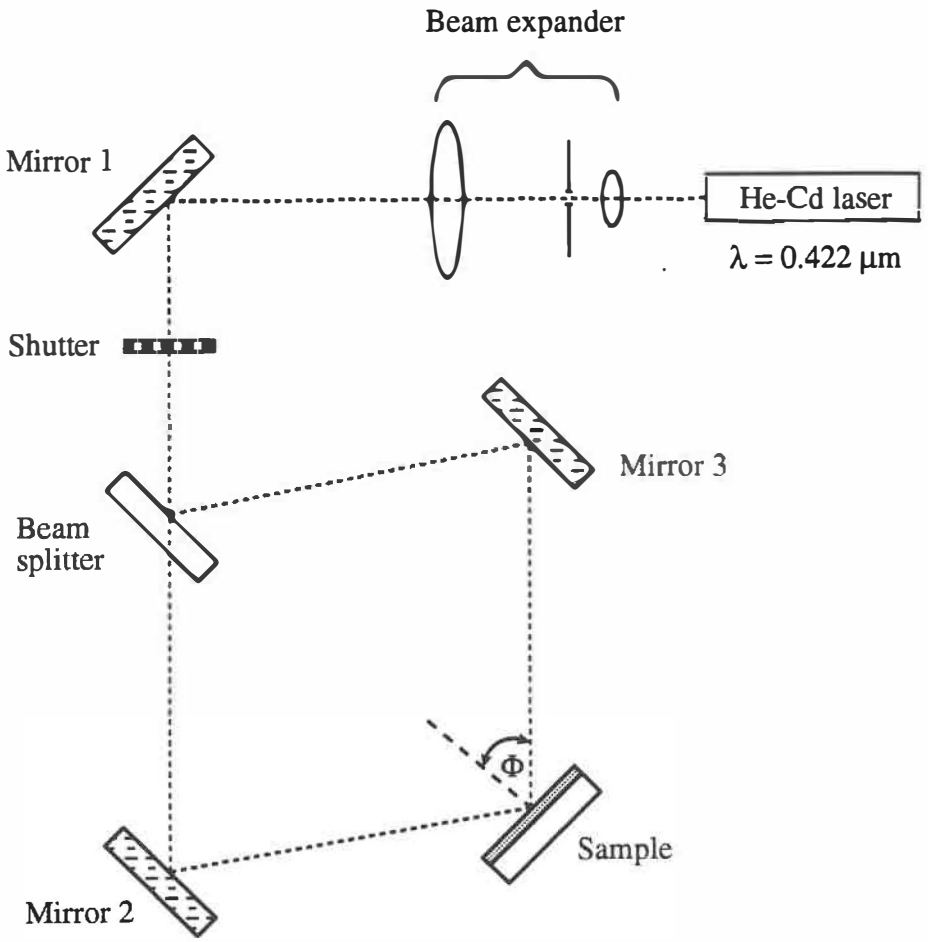

Fig. 2.2 Holographic exposure set-up for recording interference fringes.

After conventional cleaning steps, the fabricated channel waveguide surface is spin-coated with a photoresist layer. The thickness of the photoresist layer has to be carefully chosen to achieve good grating profile on the photoresist by proper exposure and development. The proper choice of the photoresist thickness is of crucial importance for

correct transfer of the grating profile on photoresist into the glass surface during the following plasma etching step, since the etching rates for the photoresist and glass substrate are different. Following baking process, the channel waveguides with photoresist layer are mounted in a holographic exposure setup shown in the Fig. 2.2 for recording interference fringes of the two coherent beams. The samples should be mounted such that the direction of interference fringes is perpendicular to the channel waveguides. Exposed samples are properly developed to achieve as high as possible contrast for the grating relief in photoresist and as thin as possible residual photoresist in the bottom of the grating relief.

The period Λ of the grating depends on the angle between the two coherent beams, and is given by

$$\Lambda = \lambda_e / 2\mathrm{Sin}\,\Phi \qquad (2.1.1)$$

where λ_e is the wavelength of the laser beam for exposure (0.422 μm in our case), and Φ is the half angle between the two beams. Holographic exposure process should be carried out under vibration-free condition to obtain high contrast interference fringes. In the plasma etching process, the gas mixture of $CF_4 : O_2 = 0.96 : 0.04$ is introduced into plasma etching chamber at vacuum around $5 \cdot 10^{-5}$ Torr. Radio frequency power for etching is about 100 W. Under these conditions, the etching rate for glass is about 13 Å / min.. The grating depth in the glass surface of about 1500 Å can be achieved. The scanning electronic microscope (SEM) is employed to observe fabricated gratings on photoresist and on glass surface before and after plasma etching process. Typical SEM photos are shown in Fig. 2.3.

When the channel waveguides with gratings are ready, the first optical characterization is the measuement of the grating period Λ, which determines the

diffraction angles of guided light for a given wavelength and reflected peak wavelength as shown as following. The measurement details are given in the chapter 5 of reference [3]. Some of the measurement results for the grating period on silver and potassium ion-exchanged glass channel waveguides are listed in Table II-1, in which a He-Ne laser (λ = 0.6328 μm) and the channel waveguide with mask width W = 10 μm are used.

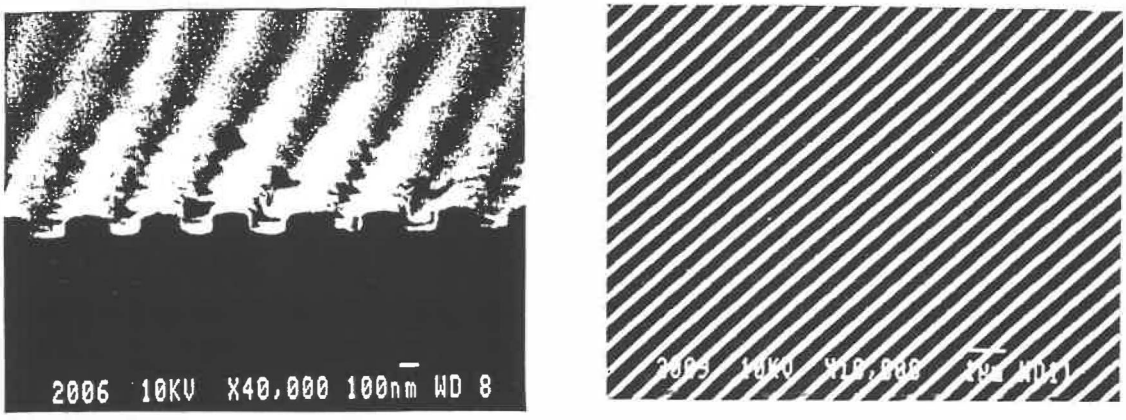

(a) (b)

Fig. 2.3 SEM photos for grating (a) on photoresist, before plasma eatching; (b) on glass surface, after plasma eatching.

In a grating-assisted waveguide, a guided mode with propagation constant β_m (at wavelength λ) will interact with the periodic refractive index perturbation, and generate scattered (or diffracted) harmonic fields with propagation constants β_h [68]. For

$|\beta_h|<2\pi/\lambda$, the grating couples guided modes into the radiation modes both in the air and in the substrate [see Fig. 2.4 (a)]. For $2\pi/\lambda< |\beta_h|<2\pi n_s/\lambda$, where n_s is the refractive index of the substrate at wavelength λ, the grating only couples guided modes into the substrate radiation modes as shown in Fig. 2.4 (b). If $|\beta_h|>2\pi n_s/\lambda$, the grating does not couple guided modes into radiation modes. In the special cases where $|\beta_h|= |\beta_m|$, the grating couples guided modes. In particular, for $\beta_h = -\beta_m$, the incident mode (forward guided mode) is coupled into reflected mode (backward guided mode) as shown in Fig. 2.4 (c). In this case, the grating acts as a distributed feedback reflector. This corresponds to the Bragg condition, at which the peak reflected wavelength (Bragg wavelength) $\lambda_B = 2N_m\Lambda$, where $N_m = \beta_m\lambda/2\pi$ is the effective refractive index for the mth guided mode.

Silmilar to the prism coupler, the gratings on the waveguide surface constitute a coupler, which can couple light into or out of the waveguide. The grating coupler has some advantages over its prism counterpart such as its pure planar structure and easier suitability for the measurement of effective refractive indices of both slab and channel waveguides. As mentioned before, the periodic perturbation of refractive index in the grating region on the channel waveguides results in mode coupling between guided modes and radiation modes. When the phase matching condition (between these modes) is satisfied, a significant power transfer occurs between them. The phase matching condition is given by

$$\beta_m = \beta_h + 2\pi\nu/\Lambda \qquad \nu = 0, \pm1, \pm2, \cdots \qquad (2.1.2)$$

where $\beta_m= 2\pi N_m/\lambda$, and $\beta_h= 2\pi \mathrm{Sin}\theta_m/\lambda$ are the propagation constants for the guided

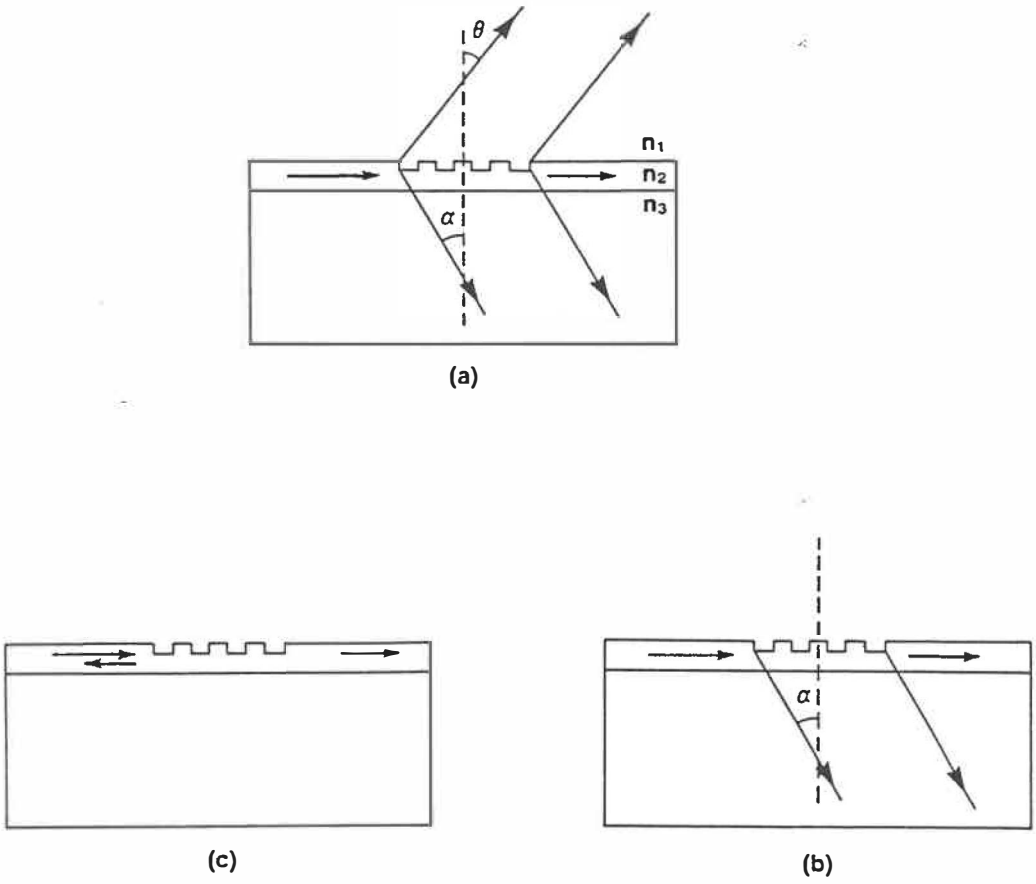

Fig. 2.4 Diffracted harmonic fields due to the interaction between guided modes at wavelength λ and grating perturbation with period Λ:

(a) harmonic field radiated into both air and substrate;

(b) harmonic field radiated into only substrate;

(c) forward guided mode is coupled into backward mode, i.e. the grating acts as a distributed feedback reflector.

modes and the radiation modes (or diffracted harmomic fields), respectively, θ_m is the angle between the diffracted wave of the mth guided mode and the normal of the grating surface, and ν is the order of the harmonic wave. Usually the first order diffracted wave is measured. In this case, the effective indices N_m can be expressed as

$$N_m = \text{Sin}\ \theta_m + \lambda/\Lambda\ . \qquad (2.1.3)$$

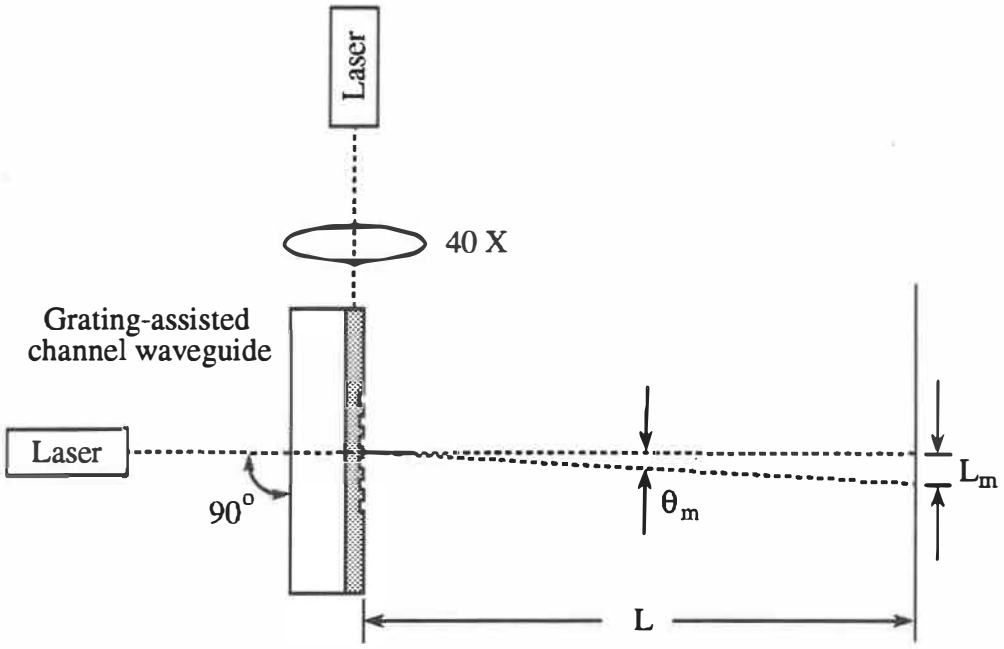

Fig. 2.5 Experimental set-up for measuring angles θ_m.

The experimental set-up for measuring angle θ_m is schematically illustrated in Fig. 2.5. Laser beam at 0.6328 μm wavelength is coupled into a channel waveguide by a 40x objective. Another laser beam determines the normal of the grating surface. Angles θ_0,

θ_1, ···, θ_n corresponding to the guided modes (m = 0, 1, ···, n) are determined by measuring distances L and L_0, L_1, ···, L_n. If L is long enough, the measurement accuracy of effective refractive indices is comparable to that of prism coupling method, about 10^{-4}. Table II-1 also gives the measured θ_m and the corresponding effective refractive indices. The channel waveguides measured are made by single-step silver and potassium ion exchange processes in pure silver nitrate at 270 ^{0}C for 4.5 hrs, and in pure potassium nitrate at 400 ^{0}C for 2hrs, respectively.

The light coupled out by the gratings (m-lines) is directed onto a camera. The far-field patterns of these m-lines are shown in the Fig. 2.6. The distance from the grating surface to the camera is 2 meters.

Fig. 2.6 Far-field patterns of m-lines coupled out by grating on a silver ion-exchanged channel waveguide. All guided modes are well excited.

The diffraction efficiency of the grating is estimated by measuring and comparing the total power in the first order diffracted waves and the total guided power from the output of the waveguide. The results of grating efficiency measurements are summarized in the Table II-2. One-step potassium ion-exchanged waveguides have a larger diffusion depth (~ 8 μm) than one-step silver ion-exchanged waveguides (~ 3 μm). Furthermore, the maximum refractive index change $\Delta n = 0.062$ for silver ion-exchanged waveguides is much larger than $\Delta n = 0.0052$ for potassium ion-exchanged waveguides. Such a big difference results in much stronger interaction between guided modes and grating in silver ion-exchanged waveguide than in potassium ion-exchanged waveguide for the same grating depth. Higher diffraction efficiency, therefore, is obtained for the former.

For the double-ion-exchanged glass waveguides with shorter silver ion-exchange time (sample KAg1), the diffraction efficiency (see Table II-3) depends on the coupling at the input of the channel waveguide, because in this waveguide light at 0.6328 μm wavelength can be guided in silver or in potassium ion-exchanged region, which results in quite different interaction between guided modes and grating. For the sample with longer silver ion-exchanged time (sample KAg2), light is only guided in silver ion-exchanged region. Therefore, its behavior is more like the single silver ion-exchanged waveguide (Ag1), but diffraction efficiency is more than two times higher.

The transmission spectrum of the grating assisted ion-exchanged channel waveguide is measured by the method explained in Chapter I (section 1.1.4). Fig. 2.7 shows the measurement result for the silver ion-exchanged channel waveguide with grating. Three distinct spectral regions (A, B, and C) corresponding to the three different propagation conditions discussed earlier (see Fig. 2.4) are clearly seen. The spectral region A corresponds to the first order harmonic fields radiation both into air and

substrate, B corresponds to radiation only into the substrate, and in the spectral region C, the grating does not couple the guided modes into radiation modes. Only at Bragg wavelength $\lambda_B = 2N_{eff}\Lambda$, the grating couples forward guided mode into backward guided mode (i.e. the incident mode is reflected, as shown by an arrow in Fig. 2.7). The relatively low reflectivity is caused by low resolution of the spectrometer.

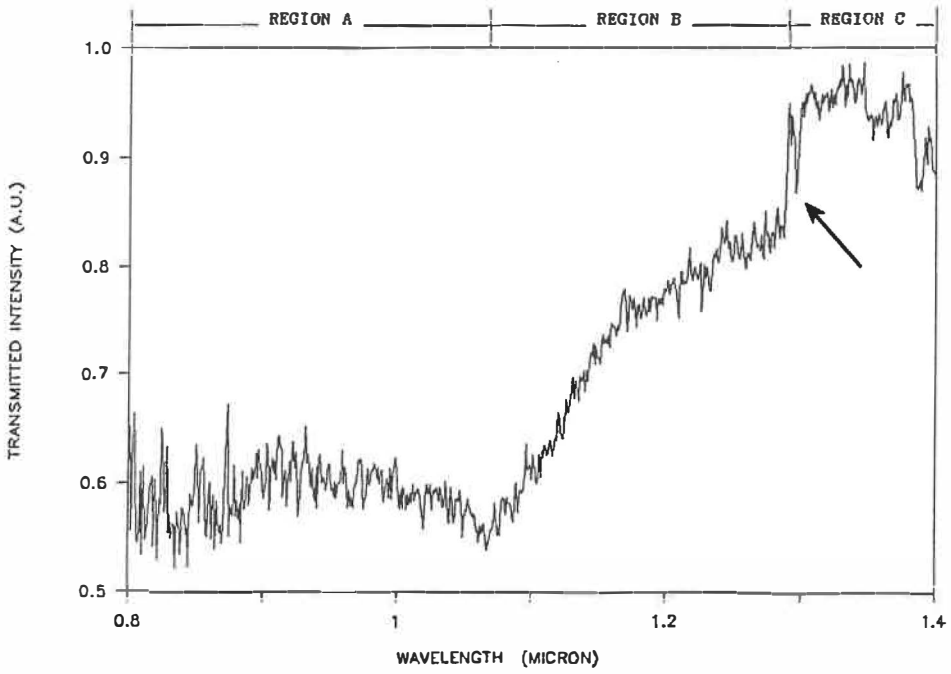

Fig. 2.7 Normalized spectral transmission of grating-assisted silver ion-exchanged channel waveguide.

To study the reflective properties of the grating in more detail, the halogen-tungsten lamp is replaced by an LED (Light Emitting Diode), whose emission spectrum covers the peak reflective wavelength of the grating. Light from the pigtailed LED is butt coupled into the grating-assisted channel waveguide and the transmitted light is measured by a high resolution spectrometer. Fig. 2.8 illustrates the spectrum of the transmitted

light of TE and TM modes of the dual core waveguide KAg1. More than 95% reflectivity at 1.261 μm wavelength is observed for the TE mode, but for TM polarization, the reflectivity is much smaller (less than 10%). The difference can be explained by the difference in coupling coefficients for TE and TM polarizations [71]. At the wavelength of reflection, the waveguide is single mode and light is guided in the silver ion-exchanged region. One-step silver ion-exchanged waveguide with grating on it has similar behavior.

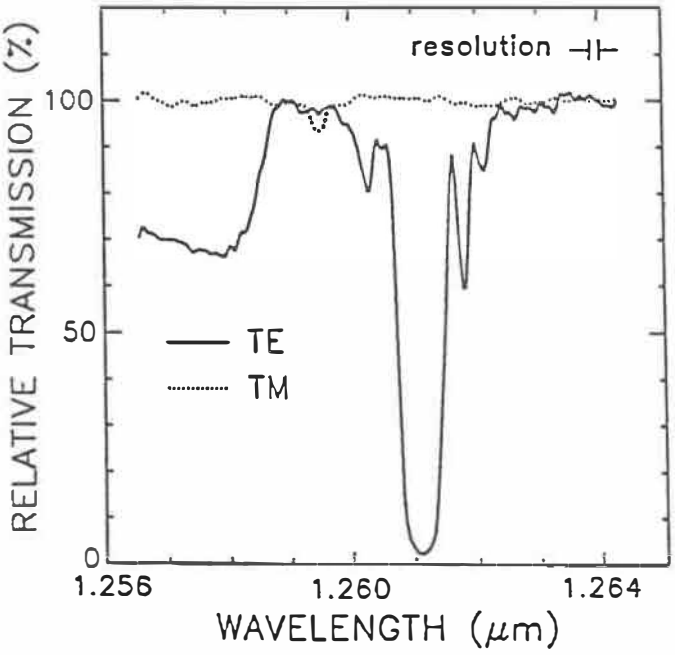

Fig. 2.8 Transmission spectrum of grating-assisted double-ion-exchanged channel waveguide excited by an LED.

2.2 Symmetrical Y-branches

Optical waveguide Y-branches are important elements for performing splitting and recombining of optical signals in guided-wave devices. Guided-wave Y-branches can be divided into two different categories according to their different application purposes. The first category is asymmetric Y-branches, which have different widths (or different propagation constants) for branching waveguides. They are mainly employed to spatially separate the guided modes in a multimode waveguide [72, 73]. Another category is symmetric Y-branches, which are widely used as power dividers in 1/N branching circuits [74, 75] and in some Mach-Zehnder interferometers [76], and in Y-junction lasers and amplifiers [36, 37].

In this section, we are mainly concerned with the discussion of symmetric Y-branches because of their potential active applications such as lossless power splitters. The Y-branch structure discussed here is schematically shown in Fig. 2.9. In a passive Y-branch structure, one of the most important problem is radiation loss in waveguide junction and taper regions, which may be quite significant when the separation angle θ between the two branching waveguides exceeds 1 degree [74]. In the Y-branch power divider, the radiation loss as a function of branching angle increases slowly for small branching angles and then rapidly for larger angles. To maintain low loss, one should therefore use small angles. However, small branching angles result in relatively long structures, which are generally undesirable due to the increase of substrate size. The branching and taper region can be specially designed to minimize the radiation loss and branching angles can be increased to several degrees, meanwhile keeping radiation loss less than a few percent [77]. However, the unavoidable radiation loss caused by

waveguide branching in the passive Y-junction can not be completely eliminated even by optimization of design for the branching structure. On the other hand, the excess radiation loss in the branching region can be compensated, in principle, by utilizing active components such as rare-earth-doped glass waveguide Y-branches. Signal amplification in such active branching circuit produced by optical pump can compensate the excess loss and even the inherent 3 dB splitting loss. Therefore, in optical pump condition, such Y-branch can act as a so-called lossless power splitter at signal wavelength.

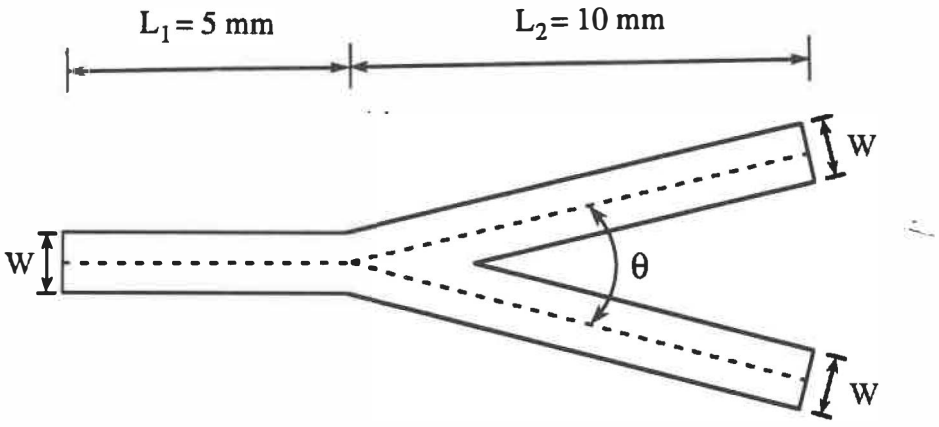

Fig. 2.9 Geometry of the symmetrical Y-branch.

The ordinary passive Y-branches discussed here are fabricated by pure potassium ion exchange process. The branching angles employed in our structure are chosen as 0.5, 1.0, 1.5, 2.0 and 2.5 degree, in order to study relations between excess radiation losses and branching angles. The potassium ion exchange is carried out in pure KNO_3 molten

salt at 400 ^{0}C for 2 hours through 5 μm wide aluminum mask openings. For comparison purpose, a straight channel waveguide with the same mask opening width is made by the same fabrication parameters. After diffusion process, aluminum mask is removed and the two endfaces of the samples are carefully polished for the following measurements.

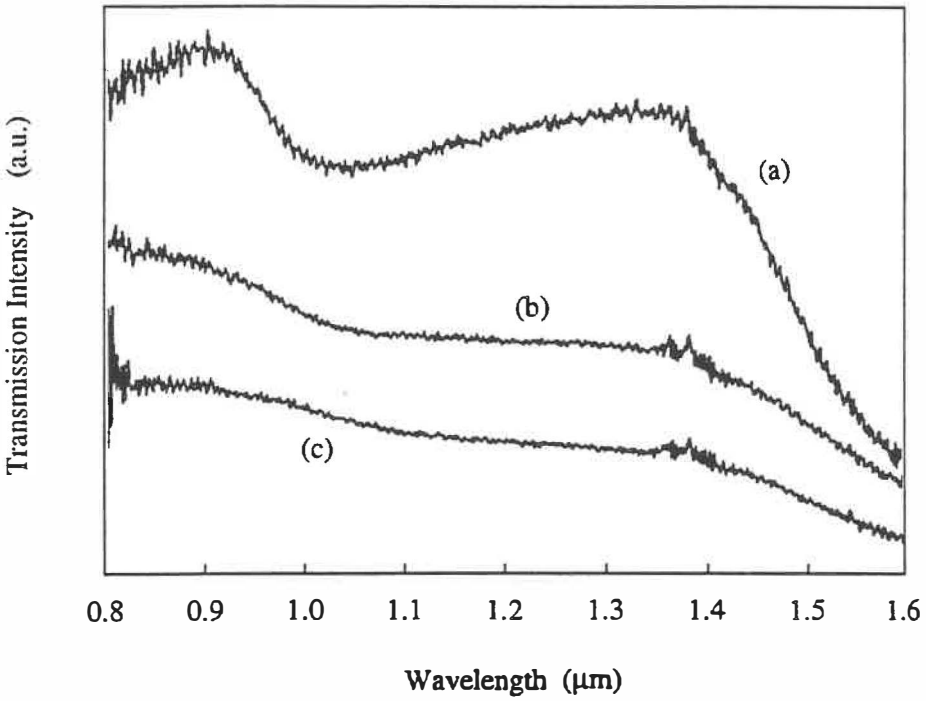

Fig. 2.10 Normalized spectral transmission from (a) a straight channel waveguide;

(b) a branching arm of the Y-branch with $\theta = 0.5^0$;

(c) a branching arm of the Y-branch with $\theta = 2.5^0$.

The normalized transmission spectrum of the straight channel waveguide is first measured by the technique explained in Chapter I (section 1.1.4), and the result is shown in the curve (a) in Fig. 2.10. The cut-off wavelength of the fundamental mode (m = 0) (defined as the wavelength at which the normalized transmission intensity of the

mode decreases down to -3dB of its maximum value) is about 1.47 μm. The cut-off wavelength for the corresponding first higher order mode (m = 1) (defined as the wavelength at which the normalized transmission intensity has a minimum value between the maxima of the fundamental mode and the first higher order mode) is about 1.02 μm. Therefore, the wavelength region for single mode operation is about 450 nm for the potassium ion-exchanged straight channel waveguide with 5 μm mask opening. For the wavelengths shorter than 1.02 μm, the straight channel waveguide is multimode. The normalized transmission spectra from one of the branching channel waveguides for the Y-branches with branching angles $\theta = 0.5^0$ and $\theta = 2.5^0$ are shown, respectively, in curves (b) and (c) in Fig. 2.10. To determine the splitting ratio of each Y-branch as a function of wavelength, the output power intensities from the two output ports of branch-

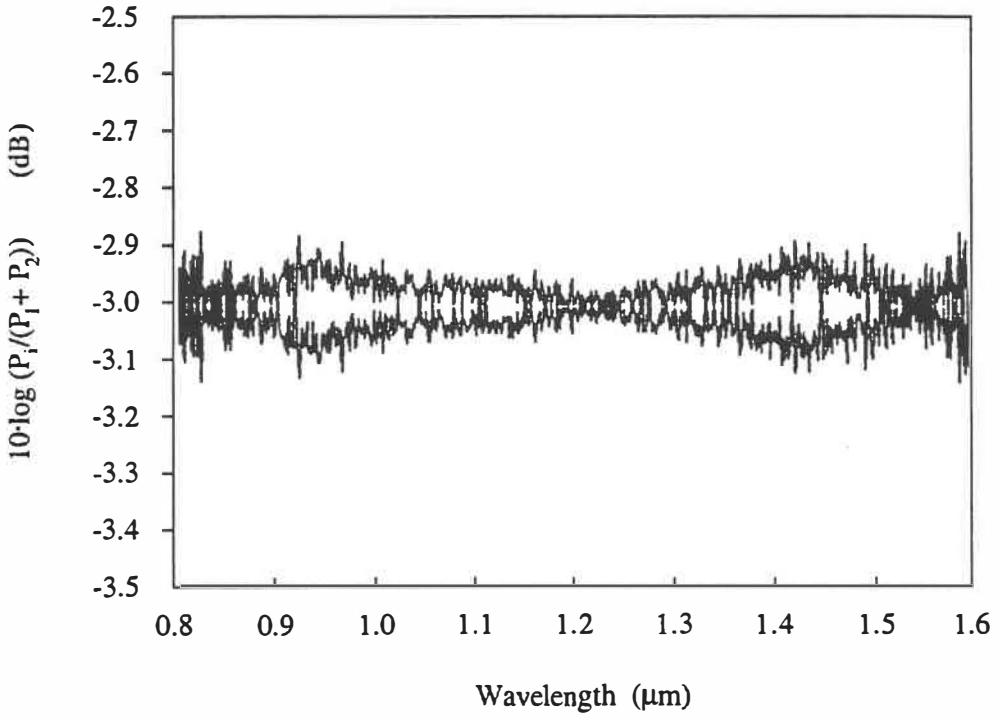

Fig. 2.11 Splitting ratio of the symmetrical Y-branch with $\theta = 0.5^0$.

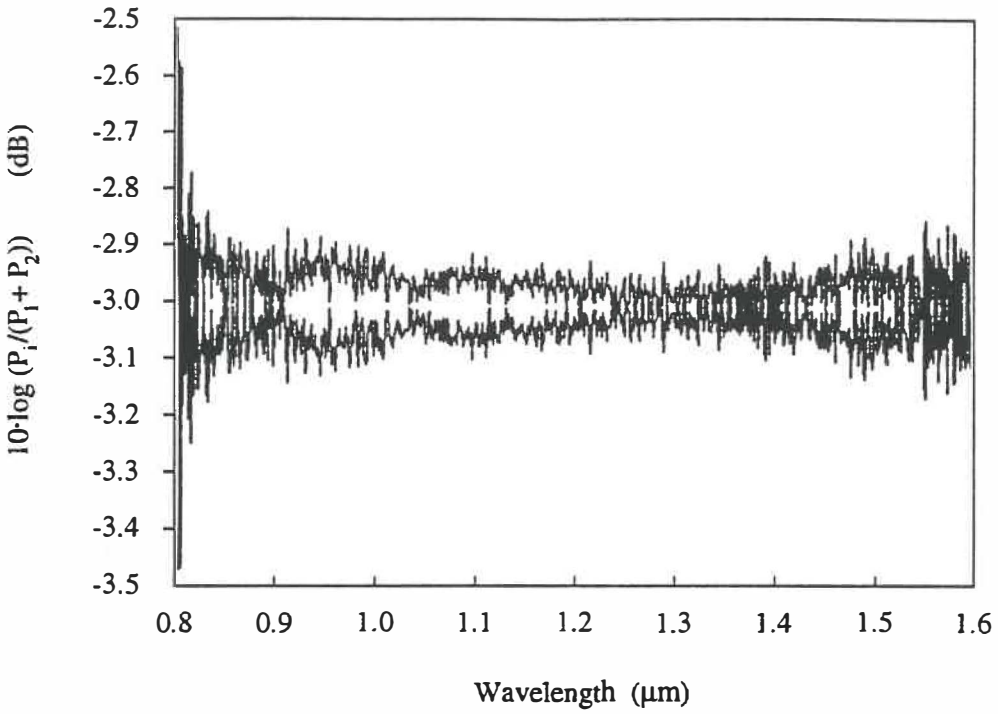

Fig. 2.12 Splitting ratio of the symmetrical Y-branch with $\theta = 2.5^0$.

ing channel waveguides are measured, and keeping input end-fire coupling unchanged during the measurement. The splitting ratio (defined in decibels as $10 \cdot \log_{10} [P_i / (P_1 + P_2)]$, where i = 1, 2; P_1 and P_2 are output powers from the two branching channel waveguides) for the Y-branches with $\theta = 0.5^0$ and $\theta = 2.5^0$ are shown in Fig. 2.11 and Fig. 2.12. Comparing these curves, we can see that in both cases the maximum deviation from 3 dB splitting ratio is less than 0.1 dB not only for the single mode operation wavelength region but also for the multimode region. The splitting ratio of the Y-branch with $\theta = 0.5^0$ at shorter wavelength region is shown in the Fig. 2.13, and it confirms the correctness of the above observation. For the Y-branch with $\theta = 2.5^0$, similar result is obtained. The measurement in shorter wavelength region is done by a silicon photodiode detector. The periodic structure in the curve is probably caused by

mode interference, because the Y-junction region can support higher order modes.

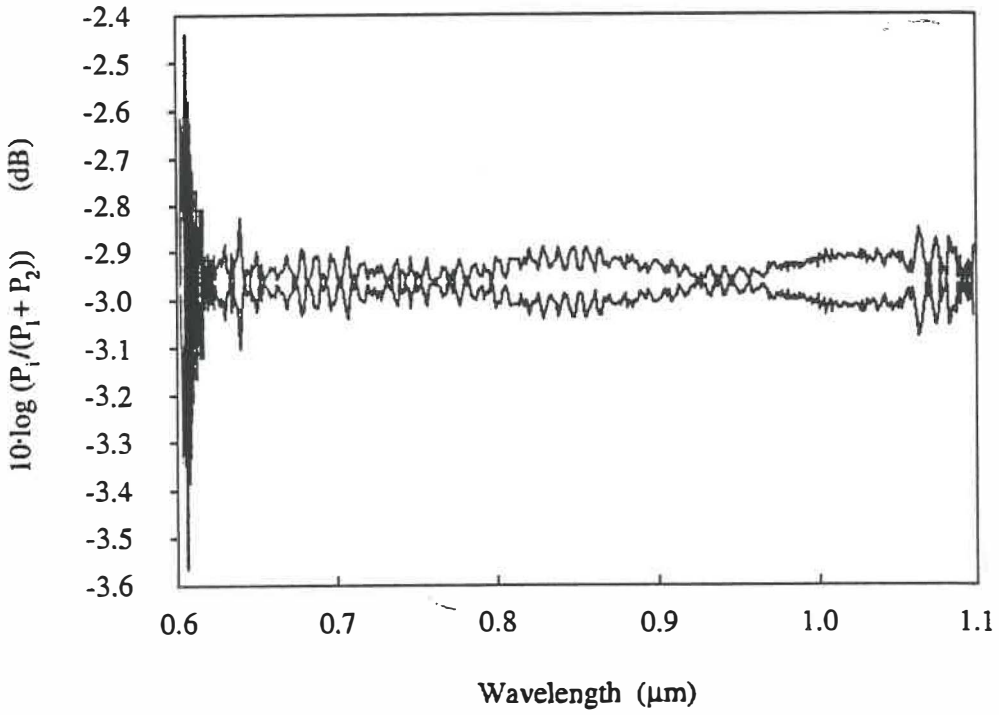

Fig. 2.13 Splitting ratio of the symmetrical Y-branch with $\theta = 0.5^0$ in multimode wavelength region.

Comparing with the results in references [47, 78], our Y-branches are nearly wavelength independent in all the measured wavelength region (from 0.7 μm to about 1.5 μm) covering both multimode and single mode operation regions. The maximum deviation from 3 dB splitting ratio is less than 0.1 dB, which indicates that the Y-branches are very well balanced for equal power dividing.

The excess losses, which are caused by radiation in the branching regions in the Y-branches, as a function of the branching angles need to be determined further in order to demonstrate the lossless power splitters when active elements are incorporated.

2.3 Four-port nonsymmetric Mach-Zehnder interferometer

Mach-Zehnder interferometer is a very important component in integrated optics. In this component, the guided light beam is divided into two portions by a beam-splitter (e.g. Y-branch, directional coupler). These two portions of the guided light beam recombine and interfere with each other in another beam splitter/combiner after going through different optical path lengths. Guided-wave Mach-Zehnder interferometers with simple symmetrical Y-branches and directional couplers have been used in wavelength multi/demultiplexers [79, 80], switches/modulators [76, 81] and polarization splitters [82]. In recent years, an optical waveguide hybrid coupler consisting of a symmetric and a nonsymmetric branching forks at a junction [83] has attracted a lot of attention. Its operation is wavelength and polarization independent and insensitive to fabrication parameters. The hybrid coupler has been utilized in fabrication of an integrated optical displacement sensor [84], in a digital optical switch on $LiNbO_3$ [85], and in a guided-wave Mach-Zehnder interferometer for 1.3 μm/1.55 μm wavelength multi/demultiplexing [86].

In this section, we discuss about design, fabrication and optical characterization of a novel four-port guided-wave nonsymmetric Mach-Zehnder interferometer based on the use of two optical hybrid couplers [54]. The configuration of the proposed structure is shown in Fig. 2.14. The structure is designed for silver ion exchange process in glass to multi/demultiplex 0.98 μm and 1.55 μm wavelengths. The device is designed by using the effective indices of guided modes, calculated by a finite difference method (see chapter 4 in ref.[3]) at different wavelengths in silver ion-exchanged waveguides. The increase in the path length due to the curved waveguides is also taken into account by

estimating the lateral shift of the mode fields in the bends [87]. A two-step ion-exchange process [50] is employed to fabricate the device in order to reduce the propagation losses caused by the silver metal colloids reduced under a metallic mask.

One of the potential applications of the proposed four-port Mach-Zehnder interferometer is the wavelength multi/demultiplexer for Er-doped fiber amplifiers and ring lasers (at 1.55 μm wavelength region), which are optically pumped at the important absorption wavelength around 0.98 μm. It can be used for making an integrated optical ring resonator by connecting ports I and III (see Fig. 2.17). The advantage of the device in a ring resonator is the accurate control of its wavelength response, which is nearly independent on the fabrication parameters. Behaviour of directional couplers used in conventional ring resonators [63, 88] is very sensitive to the process parameters. Combined with the Er-doped phosphate glass overlays by spin-coating technique [5] or with the composite Er-doped phosphate glass waveguides by clamping method [42], integration of the multiplexer and the active devices (amplifier or ring laser) in a single substrate is possible.

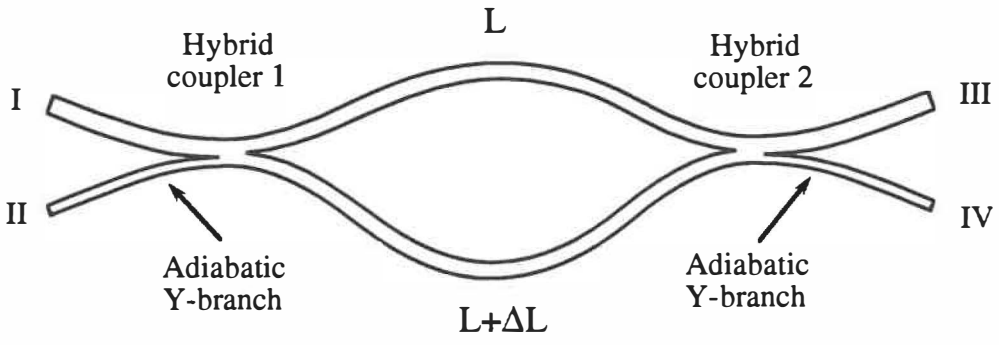

Fig. 2.14 Schematic diagram of four-port nonsymmetric Mach-Zehnder interferometer.

The proposed four-port nonsymmetric Mach-Zehnder interferometer consists of two arms with different path lengths and two hybrid couplers used as input splitter and output combiner. The two hybrid couplers have the same configuration, and each one consists of a symmetric Y-branch and a nonsymmetric adiabatic Y-branch. The mask width for the narrower arm of the nonsymmetric Y-branch is 2.5 μm, and for the wider arm it is 5.5 μm. The branching angles of the asymmetric Y-branches are chosen as 3 milliradian to satisfy an adiabatic performance. The two arms for the Mach-Zehnder interferometer have the same mask width 4 μm. The bend radius for one arm of the Mach-Zehnder interferometer is 17.5 mm, 0.75 μm lateral offsets are employed when straight and bend waveguides are connected to minimize the connection loss caused by the mode shift in curved waveguide. Tapers are used in connecting the 2.5 μm narrower arms to 4 μm waveguides of input and output ports. The input into the narrower arm (port II) excites the first higher order local antisymmetric mode in the first hybrid coupler. The path length difference between the two arms of the Mach-Zehnder interferometer is chosen as $\Delta L = 0.981$ μm. The local antisymmetric mode around $\lambda = 1$ μm is divided by the symmetric Y-branch of the first coupler into two parts, and they undergo an additional phase difference π between them after propagating through the different path lengths. They recombine in the second symmetric Y-branch with a total phase difference 2π, and excite the local fundamental mode in the second hybrid coupler which in turn is cross coupled to the wider output arm (port III) by the second nonsymmetric Y-branch. On the other hand, The two parts of the local antisymmetric mode for the wavelength around $\lambda = 1.5$ μm undergo an additional 2π phase difference between them after traveling through the two arms of the interferometer. They reach the second symmetric Y-

branch with a total phase difference 3π, and recombine to the first higher order local antisymmetric mode in the second hybrid coupler, which is coupled into the narrower output arm (port IV). Fig. 2.15 shows the theoretrical prediction. It depicts the ratio of the output power P_{IV} (from port IV) to the sum of output powers P_{III} and P_{IV} (from the ports III and IV) as a function of wavelength, when port II is the input.

A conventional photolithography technique is used to make openings in an aluminium mask on the Corning 0211 glass substrate of 0.5 mm thickness. The first step ion-exchange process is carried out by immersing the substrate in a pure potassium nitrate melt salt at 400 °C for 165 min. Then, a pure silver nitrate molten salt at 300 °C is used in the second step ion-exchange process for 210 min. Finally, aluminium mask is removed and the sample is polished to a 14.5 mm long device.

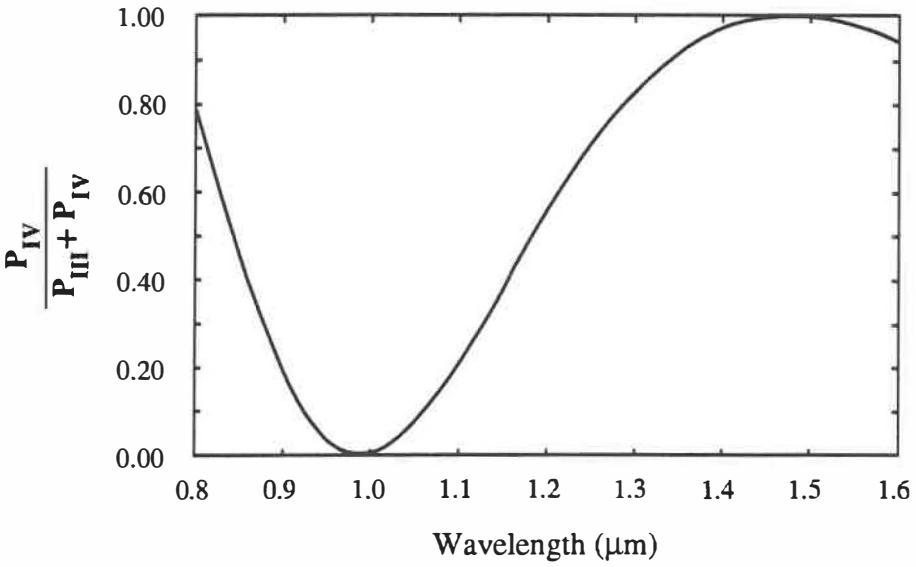

Fig. 2.15 Theoretical prediction of the four-port nonsymmetric Mach-Zehnder interferometer.

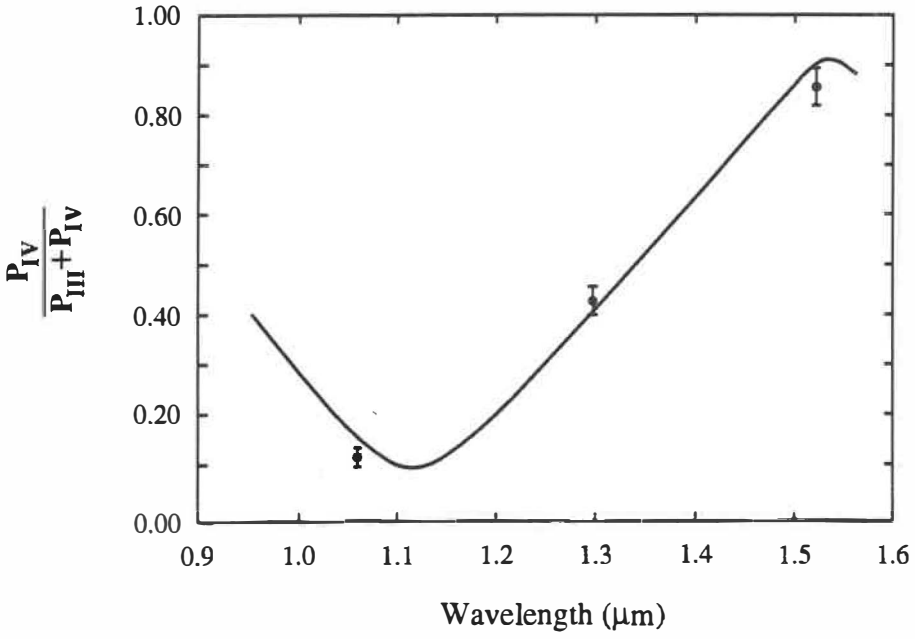

Fig. 2.16 Measured spectral transmission ratio (solid line) from the two output ports. Points are transmission ratio at discrete laser wavelengths.

Optical characterization is performed by using a single mode telecommunication fiber to couple the white light from a halogen-tungsten lamp into the narrower arm (port II) of the interferometer. Output power P_{III} and P_{IV} are collected by a 20X objective and they are directed into a scanning spectrometer after going through a mechanical chopper. A Ge photodiode detector and a lock-in amplifier are employed to detect and amplify the spectral signals. The measured data is processed by a computer connected to the lock-in amplifier. The measured spectral scanning curves are shown in Fig. 2.16. To further confirm the performance of the device, laser light from a CW Nd:YAG laser (λ = 1.06

μm), a semiconductor laser diode (λ = 1.296 μm) and a He-Ne gas laser (λ = 1.523 μm) is seperately coupled into the same arm of the device by a single mode telecommunication fiber. The transmitted light from the interferometer is focused onto a Ge photodiode detector with a 40X objective. A small aperture is placed before the detector to reduce stray light from the substrate. The measured power ratio $P_{IV}/(P_{III}+P_{IV})$ at the three wavelengths are also shown in Fig. 2.16. These measurement results are in an excellent agreement with the spectral scanning curves. Although the device is not single moded at λ=1.06 μm and λ=1.3 μm, fiber butt coupling (mainly fundamental mode excited) and the small bend radius used in the device (higher order modes filtered) ensure a proper operation. The reversed measurements by input from port IV give the same results as explained above. It confirms that the characteristics of the device is symmetric. To measure excess losses in the structure, a straight channel waveguide with 4 μm mask openning is made under identical fabrication conditions. The excess losses are determined as the difference of the transmitted light between the straight channel waveguide and the interferometer. The measured excess losses are 2.2 dB, 1.6 dB and 1.3 dB at λ = 1.06 μm, λ = 1.3 μm and λ = 1.5231 μm, respectively.

Comparing Fig. 2.15 with Fig. 2.16, there exists some disagreement between the theoretical predictions and the experimental mesurement results. This is most probably because the design is made by using the parameters for silver ion-exchanged waveguides, whereas the device is made by a two-step potassium and silver ion-exchange process. This two-step process is not yet fully understood and it is not possible to design the device for this process at present time.

As a summary of this section, a novel four-port nonsymmetric Mach-Zehnder interferometer based on two optical hybrid couplers is proposed. The interferometer is

fabricated in glass substrate by a two-step ion-exchange process. The operation of the device is tested by using continuous as well as discrete sources. The component demonstrates great capability for use in complex integrated optical devices such as ring lasers in glass to mutiplex or demultiplex different wavelengths.

2.4 Integrated optical ring resonator

Integrated optical ring resonators can be used as tunable wavelength selective filters (or optical frequency filters) and in various sensors, such as inertial rotation and temperature sensors. It can also be used to accurately measure propagation losses of low loss waveguides. Several integrated optical ring resonators have been fabricated by using different fabrication processes on different substrates, for instance, photopolimerization of PMMA on quartz substrate [89], polymer spin coating on Si substrate [90], ion-exchange process in glass substrate [63, 88, 91], proton exchange in lithium niobate [92], and CVD (chemical vapor deposition)/FHD (flame hydrolysis deposition) on silicate/silicon substrate [93-96]. All of these demonstrated ring resonators use directional coupler as an input/output coupler for the closed loop (ring) waveguide. The conventional directional couplers used in ring resonators are sensitive to fabrication parameters, and they are inherently narrow-band because low-loss small bending radius ring resonators require tight mode confinement in waveguides.

Instead of using a directional coupler, in this section, we present an integrated optical ring resonator [52] using a novel nonsymmetric Mach-Zehnder interferometer discussed in previous section as an input/output coupler [54]. The structure of the ring

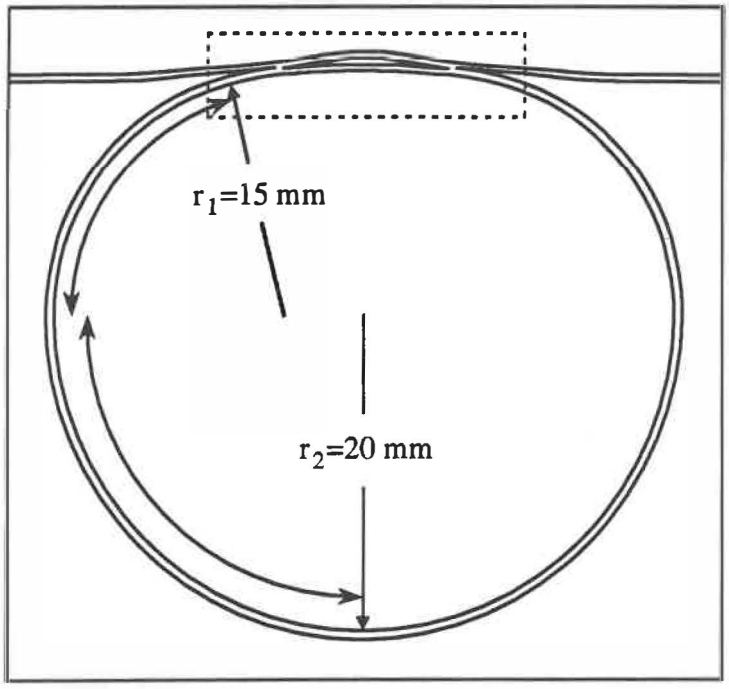

(a)

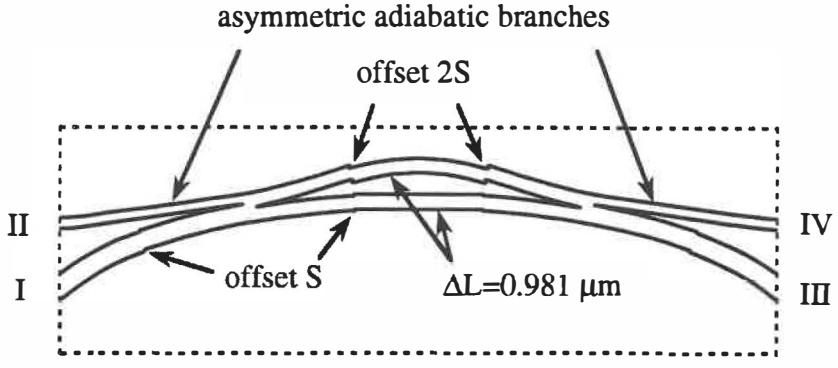

(b)

Fig. 2.17 Schematics of ring resonator (a) and nonsymmetric Mach-Zehnder interferometer (b) as an input/output coupler.

resonator and its coupler are shown in Fig. 2.17. The nonsymmetric Mach-Zehnder interferometer as the input/output coupler is essentially a 0.98 μm/1.55 μm wavelength multi/demultiplexer, which couples most of the power around 0.98 μm wavelength and a small portion of signal power around 1.55 μm into the closed loop circuit.

As shown in Fig. 2.17, the ring resonator is composed of curved channel waveguides with bending radii r_1 = 15 mm and r_2 = 20 mm, and a four-port nonsymmetric Mach-Zehnder interferomter as input/output coupler. Tapers are employed in connecting 2.5 μm narrower arms of the input/output coupler to 4 μm straight channel waveguides as input and output ports of the ring resonator. The total path length for the ring is about 12 cm.

The ring resonator is fabricated by potassium and silver double-ion-exchange process. A conventional photolithography technique is used to define mask openings in an aluminium film of about 1000 Å thick on a 0.5 mm thick Corning 0211 glass substrate. The sample is immersed in a pure potassium nitrate molten salt at 400 ^{0}C for 140 minutes. Then , the second ion-exchange step is carried out in a pure silver nitrate salt melt at 300 ^{0}C for 300 minutes. After these two ion-exchange steps, the aluminium film is removed, and the sample is carefully polished for measurement.

Laser beams from a He-Ne laser at λ = 1.5231 μm and from a laser diode at λ=1.296 μm are separately end-fire coupled into the input port of the ring resonator by a 20X microscope objective. The output power is collected by a 10X microscope objective and is passed through a small diaphram stopping the stray light from the substrate. The signal is measured by a Ge photodiode detector, whose output is recorded by a chart recorder. In order to change the optical path length of the ring resonator and to measure its resonance characteristics, it is locally heated. When the heater is removed, the sample

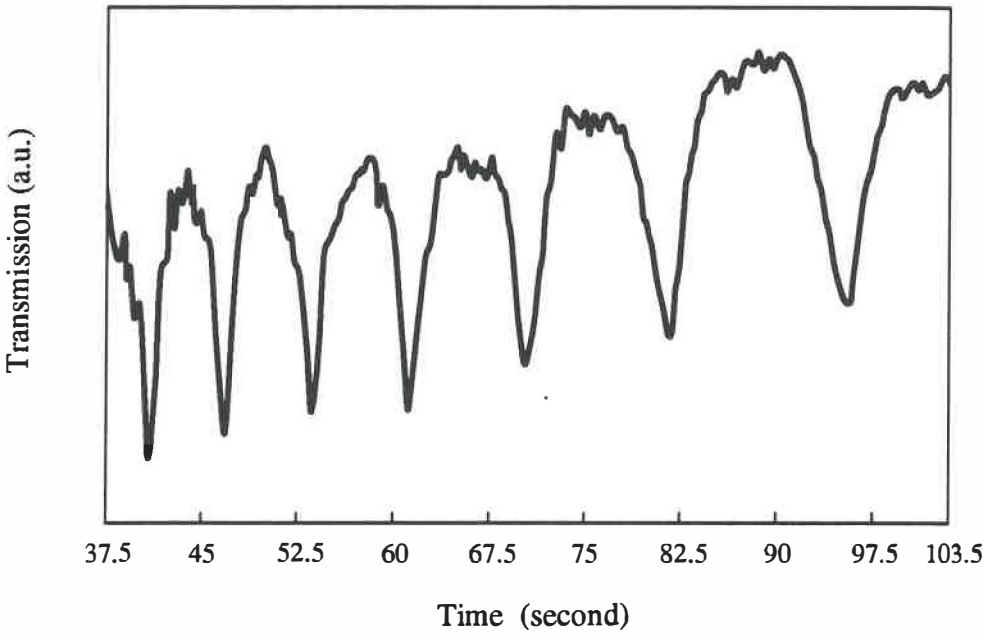

Fig. 2.18 Resonance curve for $\lambda = 1.523$ μm.

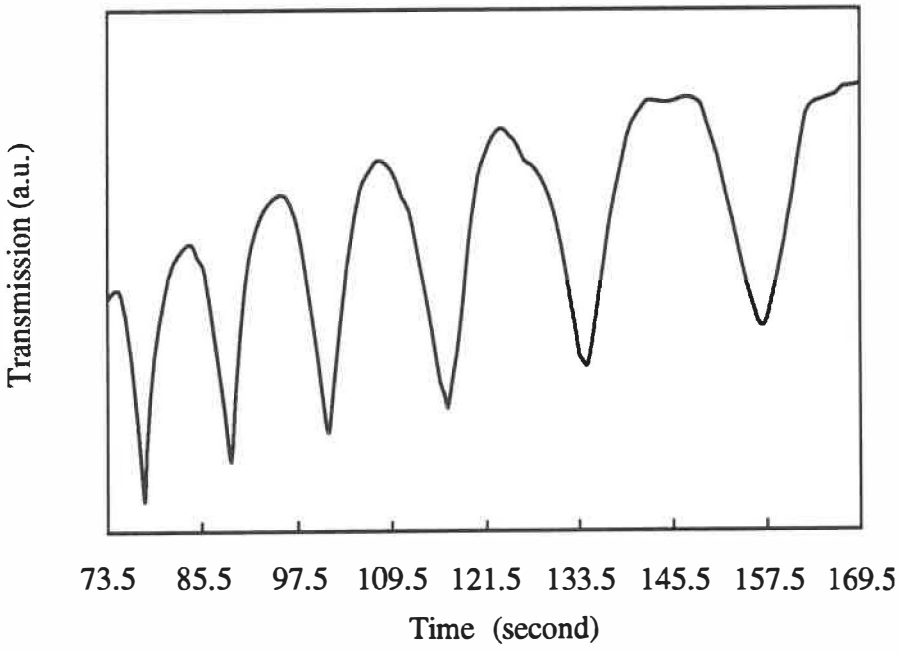

Fig. 2.19 Resonance curve for $\lambda = 1.296$ μm.

sample gradually cools down, and the resonant peaks with minimum output signal are periodically (but nonuniformly) scanned through. The measured curves shown in Fig. 2.18 and Fig. 2.19 demonstrate the resonance of the ring resonator. The finesse of 5 at $\lambda = 1.5231$ μm and the finesse of 3.2 at $\lambda = 1.296$ μm are obtained from the measurements [the definition of finesse is given in (2.4.6)].

Similar to the deduction of transmission for the ring resonator with directional coupler [88,91], the transmission for our ring resonator is given by

$$T = (1-\gamma_0)\frac{(\sqrt{1-\kappa} - \sqrt{1-\gamma_0}\, e^{-\alpha L})^2 + 4R\sin^2\left(\frac{\delta}{2}\right)}{(1-R)^2 + 4R\sin^2\left(\frac{\delta}{2}\right)} \qquad (2.4.1)$$

where $(1-\gamma_0)$ is related to the excess intensity loss for the input/output coupler, κ is cross power coupling coefficient, α is amplitude attenuation coefficient and L is total path length of the ring resonator, δ is phase shift ($\delta = \beta L$) after a round trip in the ring, and $R = \sqrt{(1-\kappa)(1-\gamma_0)}\, e^{-\alpha L}$ is effective reflectivity. When $\delta = 2m\pi$ (m=0,1,2, ···), the ring is in resonance and (2.4.1) gives the minimum transmission

$$T_{min} = (1-\gamma_0)\left[\frac{(\sqrt{1-\kappa} - \sqrt{1-\gamma_0}\, e^{-\alpha L})^2}{(1-R)^2}\right], \qquad (2.4.2)$$

and when $\delta = (2m+1)\pi/2$, non-resonant transmission is given by

$$T_{max} = (1-\gamma_0)\left[\frac{(\sqrt{1-\kappa} - \sqrt{1-\gamma_0}\, e^{-\alpha L})^2 + 4R}{(1+R)^2}\right]. \qquad (2.4.3)$$

From the normalized transmission

$$T_N = \frac{T - T_{min}}{T_{max} - T_{min}} = \frac{(1+R)^2 \sin^2\left(\frac{\delta}{2}\right)}{(1-R)^2 + 4R\sin^2\left(\frac{\delta}{2}\right)}, \qquad (2.4.4)$$

the phase difference corresponding to the full width at half maximum (FWHM) of resonant peaks can be deduced as

$$\Delta\delta = 2\mathrm{Sin}^{-1}\sqrt{\frac{(1-R)^2}{2(1+R^2)}} \quad . \tag{2.4.5}$$

Therefore, the finesse of the ring resonator F is given by the ratio of the phase difference corresponding to the free spectral range (FSR) and $\Delta\delta$ as

$$F = \frac{\pi}{\Delta\delta} = \frac{\pi}{2\mathrm{Sin}^{-1}\sqrt{\frac{(1-R)^2}{2(1+R^2)}}} \quad , \tag{2.4.6}$$

where R is effective reflectivity.

The measurement of finesse F can be employed to obtain the effective reflectivity R:

$$R = \frac{1-\mathrm{Sin}\left(\frac{\pi}{F}\right)}{\mathrm{Cos}\left(\frac{\pi}{F}\right)} \quad . \tag{2.4.7}$$

By measuring cross coupling coefficient and excess losses for the nonsymmetric Mach-Zehnder interferometer, the propagation losses for the closed ring waveguide can be estimated from $R = \sqrt{(1-\kappa)(1-\gamma_0)}\, e^{-\alpha L}$. Employing the measured values, i.e. cross coupling coefficient $\kappa \cong 0.1$ and excess loss $1-\gamma_0 \cong -1.3$ dB at $\lambda = 1.5231$ μm, and $\kappa \cong 0.6$ and excess loss $1-\gamma_0 \cong -1.6$ dB at $\lambda = 1.296$ μm, the propagation losses for the ring waveguide are estimated as 0.17 dB/cm at 1.5231 μm and 0.22 dB/cm at 1.296 μm, respectively. The latter value is in good agreement with the loss measurement results for the straight double-ion-exchanged channel waveguides at 1.296 μm wavelength [66, 67].

In summary of this section, the finesse of 5 at λ =1.5231 μm and 3.2 at λ = 1.296

μm for the integrated optical ring resonator in glass employing a novel four-port nonsymmetric Mach-Zehnder interferometer as input/output coupler has been demonstrated. The finesses, as well as cross coupling coefficients and excess losses for the coupler at corresponding wavelengths are utilized to estimate the propagation losses in the ring waveguide as 0.17dB/cm at 1.5231 μm and 0.22 dB/cm at 1.296 μm. It is worth of mentioning, that the performance of the input/output coupler and the ring resonator as a passive device are optimized, because the device will be employed in studying a lossless ring resonator and a ring laser by spin-coating erbium doped phosphate glass overlay, or by clamping a piece of Er-doped phosphate glass on the ring waveguide.

Table II-1. Fabrication parameters and some characterization results of grating assisted channel waveguides (grating length L = 3mm).

Ion exchange	T (°C)	t (hrs)	Λ (μm)	m	θ (°)	N_m
Silver ion-exchange	270	4.5	0.4227	0	3.8048	1.5634
				1	2.7603	1.5452
				2	2.0148	1.5322
Potassium ion-exchange	400	2	0.4227	0	1.6594	1.5260
				1	1.5848	1.5247

Table II-2. Measurement results of grating diffraction efficiency (Fabrication parameters are the same as Table III-1).

Waveguide	Grating (depth, μm)	$\frac{\text{Diffracted power (in air)}}{\text{Transmitted power}}$ (%)
Silver ion-exchange	~ 0.15	32.3
Potassium ion-exchanged	~ 0.15	0.43

Table II-3. Diffraction efficiency of grating on single and double ion-exchanged channel waveguides (grating length L= 1 mm).

Waveguide*	Grating (depth, μm)	$\frac{\text{Diffracted power (in air)}}{\text{Transmitted power}}$ (%)
KAg1	~ 0.15	4 ~ 42
KAg2	~ 0.15	83
Ag1	~ 0.15	32

* About fabrication parameters, see table II-2.

CHAPTER III

RARE-EARTH-DOPED GLASS WAVEGUIDES

Rare-earth-doped (RED) glass waveguides are suitable candidates for active integrated optical devices such as lasers, amplifiers, switches and modulators. They are attractive because of their small size, potentially low cost, low threshold, and stability. By using different rare-earth elements, active devices in infrared and visible spectral regions can be achieved. These devices have potential applications in optical communication, signal processing systems, laser scanning microscope, optical disk and photocopier.

There have been significant progress in fabrication of RED glass waveguides during the past four years. Several different processes have been explored. Glass waveguide lasers and amplifiers have been demonstrated. Up to now, the most important rare-earth ions used in glass waveguide lasers and amplifiers are neodymium (Nd^{3+}) and erbium (Er^{3+}). As well known, Nd is a four-level laser system and Er is a three-level laser system, they have important emission wavelengths around 1.3 μm and 1.55 μm [15].

In this chapter, three different processes are developed to fabricate RED glass waveguides. The rare-earth ions concerned in our study are also Nd^{3+} and Er^{3+}. In the section 3.1, glass waveguides in Nd- and Er-doped silicate glass substrates fabricated by dilute silver ion exchange process in a molten salt bath are discussed and related optical characterizations are carried out. In the section 3.2, spin-coated Nd and Er phosphate

glass film overlays are utilized to fabricate RED glass waveguides on passive ion-exchanged glass waveguides. This technique is more suitable for applications requiring integration of passive and active components on the same substrate. In the section 3.3, the clamping technique to make composite RED glass waveguides is developed, which combines the excellent optical properties of passive glass waveguides with optimized lasing characteristics of commercial available RED glasses. It is also a flexible technique for integration with other components on the same substrate.

3.1 Rare-earth-doped glass waveguides by silver ion exchange

The Nd-doped glass substrates used in our waveguide fabrication processes are two commercially available laser glasses, i.e. Q-246 from Kigre [97] and LG-680 from Schott [98]. These laser glasses have similar compositions. They are lithium-aluminum-silicate glasses doped with 3 wt % and 3.5 wt % Nd_2O_3, respectively.

Successful waveguide fabrication is carried out by the thermal ion exchange process in dilute silver nitrate molten salt [24, 25]. It is believed that in the fabrication processes, the ion-exchange takes place between silver ions and lithium ions, since the latter are the only alkali ions suitable for ion exchange in these laser glasses. In the following discussion, only waveguide fabrication process in Q-246 substrate is concerned since fabricated waveguides have better optical behavior compared to other glass. Dilute silver nitrate (with 0.05 gm $AgNO_3$ in 100 gm $NaNo_3$) at 330 ^{0}C is used to fabricate slab waveguides. Four waveguides with one to four guided modes at λ = 0.6328 μm are made by using diffusion times of 40, 75, 160 and 300 min., respectively. The prism

coupling method explained in chapter I (section 1.1.1) are used to measure the effective refractive indices of the guided modes. The maximum index change $\Delta n = n_s - n_b$, and effective diffusion coefficient $D = d^2/4t$ [where d is the effective diffusion depth defined as the point at which erfc(1) = 0.157] due to the exchange process are then determined by

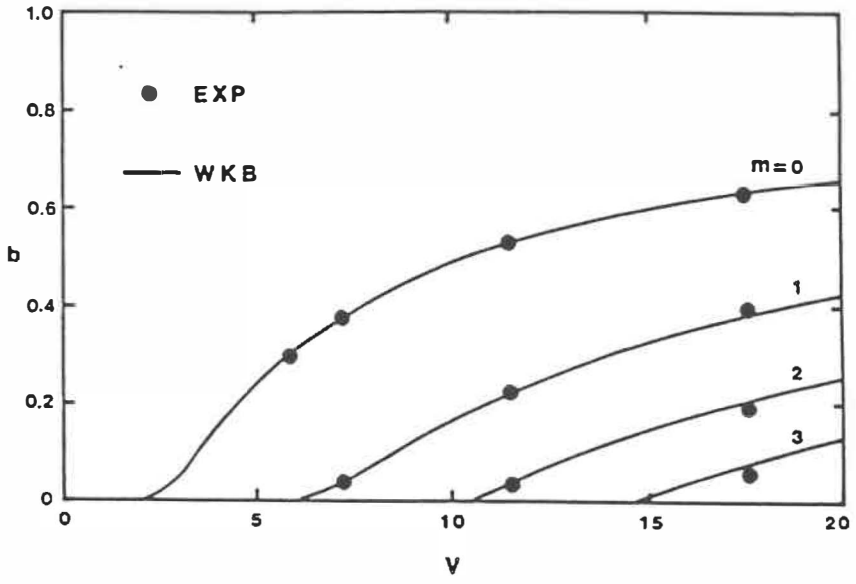

Fig. 3.1 Measured effective refractive indices fitting to the normalized dispersion curves of WKB calculation: normalized frequency $V = (2\pi/\lambda)d(n_s^2-n_b^2)^{1/2}$, and normalized refractive index $b=(N^2-n_b^2)/(n_s^2-n_b^2)$, where N is an effective refractive index.

the WKB analysis. n_b is the refractive index of bulk substrate, n_s is the refractive index on the surface of the waveguides. The measured effective refractive indices for the guided modes are employed to fit b-V curves (normalized dispersion curves) obtained

from WKB calculation with different index profile functions such as Gaussian and complimentary error function (erfc). The best fitting indicates that the erfc is a suitable function for index profile in these silver ion-exchanged waveguides. Fig. 3.1 illustrates the fitting results of the effective refractive indices obtained from prism coupling measurement with the normalized dispersion curves by WKB calculation (assuming erfc profile function). The values of $\Delta n = 0.091$ and $D = 0.0075$ μm^2/min. are deduced from this fitting.

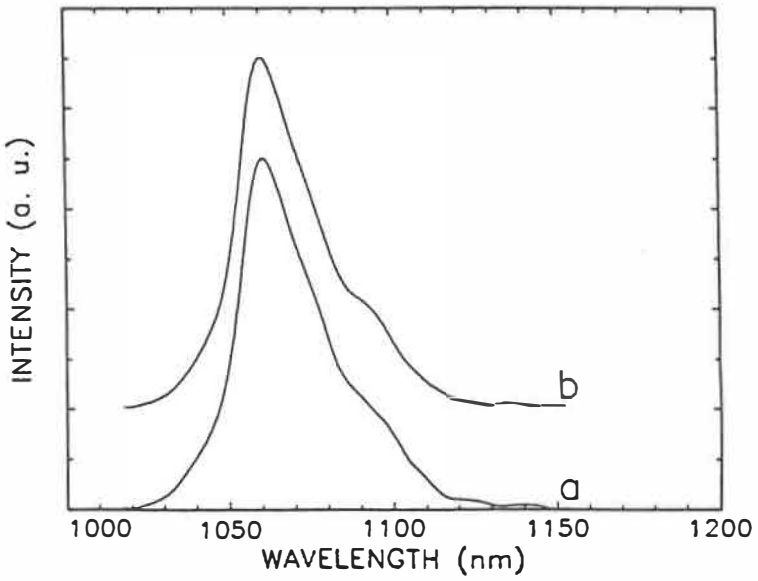

Fig. 3.2 Fluorescence spectrum of Nd-doped (a) slab waveguide and (b) bulk substrate.

The fluorescence emission spectrum measurement is performed using the slab waveguide with four modes at $\lambda = 0.6328$ μm. Both endfaces of the waveguide are polished, pump light from a dye laser ($\lambda_p = 0.590$ μm) is end-fire coupled into the waveguide and the output from the waveguide is directed into a spectrometer. The curve

(a) in Fig. 3.2 depicts the fluoresence emission spectrum from the slab waveguide. It is compared with the fluorescence spectrum (b) of the bulk substrate. No significant change is observed. Both spectra have peak emission wavelengths at 1.0606 μm with similar linewidths. This indicates that in this glass the silver ion exchange process does not significantly influence the emission spectrum.

The propagation losses of slab waveguide are measured by the technique mentioned in chapter I (section 1.1.3). The losses of a slab waveguide made in Kigre Q-246 laser glass (T = 330 ^{0}C, t = 2hrs) are 0.5 dB/cm at 1.06 μm laser wavelength, and 1.5 dB/cm at λ = 0.6328 μm. The waveguides fabricated in Schott LG-680 laser glass substrates have very high propagation losses.

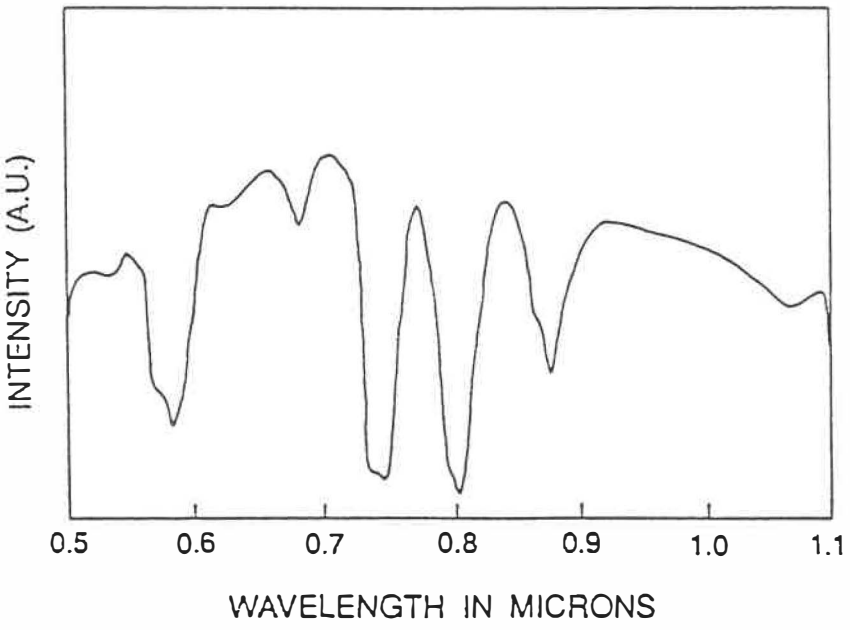

Fig. 3.3 Transmission spectrum of channel waveguide fabricated by silver ion exchange in Kigre Q-246 Nd-doped laser glass (with 10 μm mask opening).

Potassium, sodium, and cesium ion exchange processes are also employed in attempt to produce waveguides in the two commercially available Nd-doped laser glasses (Kigre Q-246 and Schott LG-680). However, silver ion exchange is the only process that results in waveguides in these glasses [29]. It seems that potassium and sodium ion exchange give a negative index change in these glasses. In cesium ion exchange, high temperatures needed for successful exchange process can not be used since these glasses do not tolerate very high temperatures (over 500 °C).

The spectral transmission measurement gives important information about the absorption wavelengths and their relative intensities in the rare-earth-doped glass waveguides. Fig. 3.3 shows the transmission spectrum from a channel waveguide produced by silver ion exchange through 10 μm mask opening in Kigre Q-246 laser glass. The absorption peaks around 0.59, 0.75, 0.8, and 0.88 μm are clearly seen.

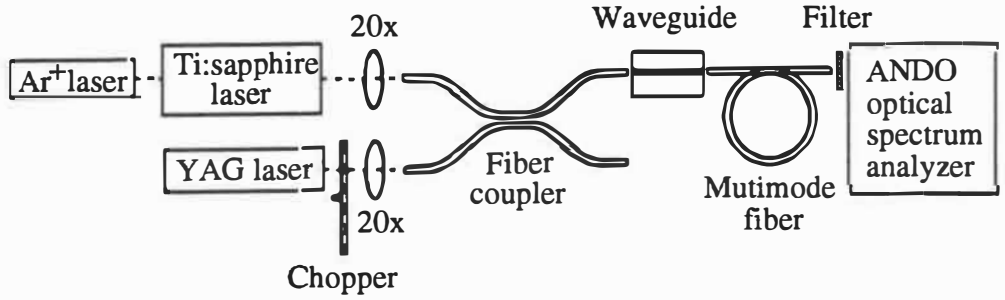

Fig. 3.4 Experimental set-up for demonstrating amplification in silver ion-exchanged glass channel waveguides.

Amplification is demonstrated by the experimental set-up shown in Fig. 3.4. A semiconductor laser pumped Nd:YAG laser at $\lambda_s = 1.063$ μm is used as signal source. The pump beam from a Ti:sapphire laser at $\lambda_p = 0.81$ μm and the chopped signal beam are seperately coupled into two input ports of an optical fiber coupler, which is used as a multiplexer to combine pump and signal power into one output port. The fiber coupler is made of single mode telecommunication fibers. The output from one port of the fiber coupler is coupled into a channel waveguide made with 9 μm mask opening width, and the waveguide output is guided into a spectrometer (ANDO optical spectrum analyser) by a multimode fiber. When both pump and signal powers are coupled into the channel waveguide, the amplified signal can be detected. Comparing chopped amplified signal with chopped unamplified signal (with pump on and off), and also considering DC fluorescence background produced by pump (no signal input), gain can be determined as the difference of amplified signal and fluorescence background. The net gain from the sample with length L ~ 5 mm is determined as ~ 3 dB when pump and signal powers from the fiber coupler are 200 mW and 500 nW, respectively.

Fluorencent lifetime τ is an important parameter needed to be measured. It is defined as the time period during which emitted fluorescence intensity decreases to 1/e of its original intensity value as the pump light is suddenly cut off. The measurement not only gives the fluorescent lifetime value of the rare-earth-doped glass waveguides, which indicates whether they are suitable for lasing and amplification applications, but also indicates the influence of the ion exchange process on the lasing properties of the rare-earth-doped glass substrate. Fig. 3.5 shows the experimental arrangement for measuring fluorescent lifetime of rare-earth-doped glass waveguide and substrate. The measurement results for the silver ion-exchanged neodymium-doped glass waveguide and the Q-246

substrate indicate that the ion exchange process decreases considerably the lifetime of the substrate (for Q-246 substrate at $\lambda = 1.06\ \mu m$ fluorescent liftime $\tau = 300\ \mu s$; but for silver ion-exchanged channel waveguides $\tau = 150\ \mu s$).

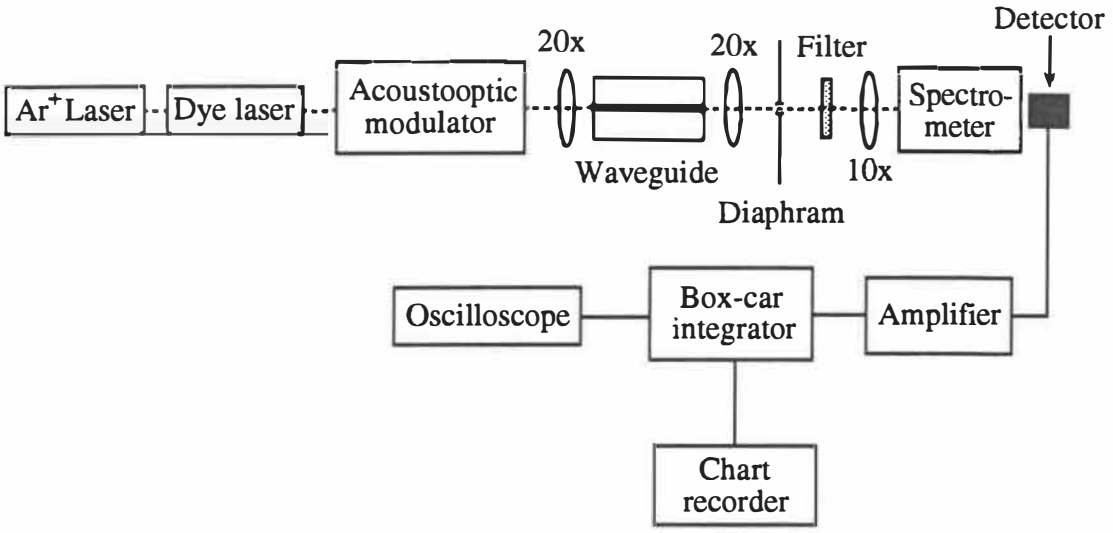

Fig. 3.5 Experimental set-up for fluorescent lifetime measurement.

Erbium-doped silicate glass waveguides are also fabricated using dilute silver ion exchange process. The waveguides are produced in a custom made glass by Kigre Inc.. It has the same composition as the neodymium-doped silicate glass (Q-246) where Nd is replaced with Er. The propagation losses of these waveguides are even lower than above mentioned silver ion-exchanged neodymium-doped glass waveguides, but their absorption intensity around 0.98 μm wavelength is so low that they are not promising for laser and amplifier applications. The main reason is that the absorption cross section of the Er^{3+} at the pumping wavelength region is very small and the erbium-doped silicate

glass substrate is not optimized for active applications.

3.2 RED phosphate glass films spin-coated on passive waveguides

Spin-coating RED active films on passive glass waveguides is another attractive technique to produre RED glass waveguides. In fact, the metal phosphate films were proposed serveral years ago [99] and iron phosphate film was employed to fabricate thin-film waveguides by spin-coating on fused silica substrate [100]. In this section, we discuss the preparation of the RED phosphate glass films, and the fabrication of RED glass waveguides by spin-coating process [5]. The structure of such a RED glass channel waveguide is schematically illustrated in Fig. 3.6. Optical characterization of the fabricated waveguides including transmission and emission spectrum measurements are carried out, which demonstrate the effectiveness of the method. The advantages and necessary improvements to the technique towards practical applications are briefly discussed.

The starting materials in our perparation process of RED phophate films are neodymium oxide (Nd_2O_3, 99.999%) and erbium oxide (Er_2O_3, 99.99%) powders. First of all, 1/1000 mole of the rare-earth oxides are dissolved in a few (3~4) millilitre hydrochloric acid (HCl, 37~38%, electronic grade) or nitric acid (HNO_3, 70~71%, electronic grade), respectively. The reaction processes are given by

$$Nd_2O_3 + 6HCl \longrightarrow 2NdCl_3 + 3H_2O \qquad (3.2.1)$$

$$Er_2O_3 + 6HNO_3 \longrightarrow 2Er(NO_3)_3 + 3H_2O \qquad (3.2.2)$$

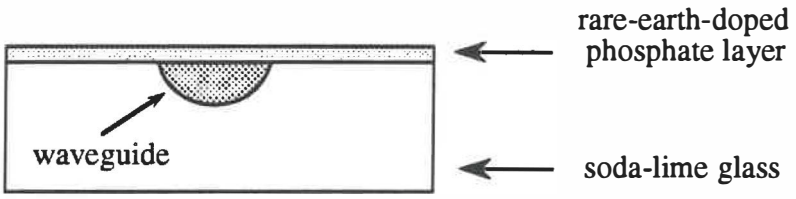

Fig. 3.6 Rare-earth phosphate film spin-coated on a passive glass channel waveguide.

During the dissolvation, the acid solution is heated up to speed the reaction, and to remove H_2O and residual acid. The heating process increases the viscosity of the solution gradually and condenses it into a jam-like state. In this state, the $NdCl_3$ or Er $(NO_3)_3$ contains very small amount of HCl or HNO_3. Before the rare-earth choloride or nitrate jams completely cool down, they are dissolved in 3~5 ml methanol solution (CH_3OH, 99.9%, electronic grade). The amount of the methanol solution to dissolve rare-earth salts relates to the thickness of spin-coated phosphate films. Orthophosphoric acid (H_3PO_4, 85~87 %, electronic grade) is heated over 200 ^{0}C for more than 1 hour to remove any residual water. Then, the equal-molar quantity of the orthophosphoric acid is added into the methanol solutions of rare-earth salts. The reaction processes are

$$NdCl_3 + H_3PO_4 \longrightarrow NdPO_4 + 3HCl \qquad (3.2.3)$$

$$Er(NO_3)_3 + H_3PO_4 \longrightarrow ErPO_4 + 3HNO_3 \qquad (3.2.4)$$

The existence of strong acids (HCl and HNO_3) is essential for preventing the rare-earth phosphate in solutions from precipitation. In addition, their volatility allows lower curing temperature after the rare-earth phosphate film is spin-coated.

The RED glass waveguides are produced by spin-coating the rare-earth phosphate solutions on potassium ion-exchanged passive channel waveguides. The passive waveguides are fabricated in corning 0211 glass substrate by conventional thermal ion exchange process in pure potassium nitrate molten salt at 400 ^{0}C for 2hrs. Aluminum mask openings of widths from 2 μm to 10 μm are defined by conventional photolithographic technique.

After the ion exchange process, two endfaces of the samples are polished, then the RED phosphate films are produced by spin-coating the rare-earth phosphate solution on the channel waveguide surfaces at 3000 to 6000 RPM (Revolutions Per Minute). The coated samples are first dried at 80 ^{0}C for about 20 min., then they are baked at 200 ^{0}C for 1 hour to obtain stable films. Usually, the thickness of a single coating layer is between 0.2 μm ~ 0.35 μm, and thicker layer can be achieved by repeating coating and drying processes. The tensile stress produced in each coating layer during the dry process will be accumulated as more layers are added and finally results in cracks in the coated films. It seems difficult to obtain RED phosphate films thicker than 0.5 μm ~ 0.6 μm at present stage.

The RED phosphate films are stable, hard and transparent. They have very good uniformity, good optical quality, and good adhesion on glass surface. The films exhibit good chemical resistance to water and organic solvents such as aceton and propanol. Aluminum phosphate films made by the same technique were analyzed by electronic microscopy and X-ray diffraction analysis [99], the film was determined as an amorphous non-porous glassy form. Optical absorbance of iron phosphate film

waveguides in visible and infrared wavelength regions (0.4 μm ~ 1.8 μm) [100] is very low. The mechanical and chemical properties exhibited by our RED phosphate films and the following optical characterization confirm that these films have similar performance as those in reference [99] and in reference [100].

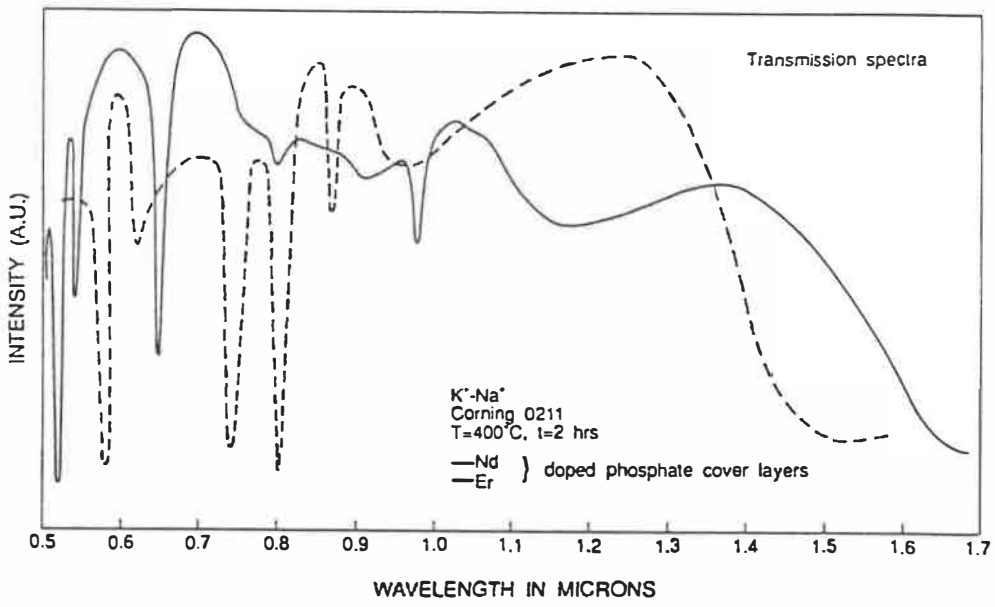

Fig. 3.7 Transmission spectra of potassium ion-exchanged channel waveguides coated with neodymium and erbium phophate overlays (mask opening width = 10 μm).

The transmission spectrum for the rare-earth-doped glass channel waveguides is measured by the technique described in chapter I (section 1.1.4). Fig. 3.7 depicts the transmission spectra of potassium ion-exchanged channel waveguides made with 10 μm wide mask opening after coating with neodymium and erbium phosphate glass overlays.

Comparaing with the transmission spectra of the same channel waveguides before the phosphate film coating in Fig. 1.6, it is observed that the single mode wavelength region is slightly shifted towards the longer wavelengths, and efficient absorptions at several important pump wavelengths are achieved. The comparison of the transmission spectra before and after rare-earth phosphate film coating also shows a very good optical quality of the films.

To observe the emission fluorescence spectra of these rare-earth-doped glass waveguides, pump light from a dye laser at $\lambda_p = 0.578$ μm and from a Ar^+ laser at $\lambda_p = 0.488$ μm are coupled into the glass channel waveguides covered by the neodymium and erbium phosphate overlays, respectively. Their emission fluorescence spectra are illustrated in Fig. 3.8.

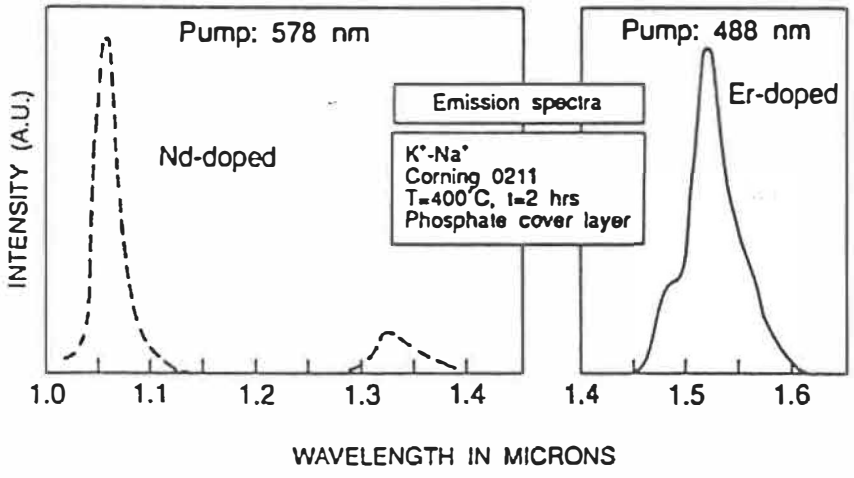

Fig. 3.8 Fluorescence spectra of glass waveguides covered by neodymium and erbium phosphate overlays.

A Leitz spectrometer is employed to determine the thicknesses and the refractive

indices of the rare-earth phosphate films and other various metal phosphate films. The measurement technique is explained in reference [101]. Some results are reported in Table III-1.

The rare-earth concentrations in the phosphate films and refractive indices of the films depend on compositions of metal phosphate coating solution, which can be easily controlled by varying the solution. Phosphate films doped with two or more active elements can be used to obtain wider and sronger absorption and/or emission spectra. For instance, adding Yb^{3+} (ytterbium) will drastically increase the absorption at ~ 0.98 μm wavelength region and sensitize the fluorescence emission of Er^{3+}. This allows fabrication of small size active components and tunable glass waveguide lasers.

In the summary of this section, RED glass waveguides are successfully fabricated by spin-coating neodymium and erbium phosphate films on passive channel waveguides. The curing temperature for the film fabrication is low, so that the process is suitable for photolithographic patterning. High optical quality, stable and hard glassy films have been achieved. Efficient absorptions at several important pump wavelengths are observed and emission fluorescence have been demonstrated. The technique is flexible in choosing the concentration of the rare-earth dopants, co-doping with other elements, ajusting refractive indices of the films, and locally patterning the films on part of a device or component. It is especially attractive for integration of RED devices with other integrated optical devices on the same substrate. For practical applications, the lasing and amplification properties of the rare-earth phosphate films (e.g. absorption/emission cross-sections, fluorescent lifetime, and rare-earth concentrations in the film) should be optimized. Also, the refractive index and the thickness of the film should be ajusted for optimal interaction of the mode field with RED layer.

3.3 Composite RED glass waveguides

As discussed before, the RED glass waveguides can be fabricated by several different processes [18]. Among these processes, ion-exchange technique is especially suited for waveguide fabrication in RED glass substrates. However, there are some limitations in practical use of the technique. The commercially available RED laser glasses usually are not well suitable for waveguide fabrication by ion exchange process, although their lasing and amplification characteristics are optimized for active applications. Potassium and silver molten salt ion exchange processes have been successfully employed to demonstrate waveguide fabrication in commercial Nd-doped silicate glass substrates [24, 27], but ion exchange processes may result in significant deterioration of the optimized lasing and amplification performance of the laser glass substrates. One of the typical evidences is the substantial decrease of fluorescent lifetime in the silver ion-exchanged waveguides comparing with that of the Nd-doped silicate substrate glass, as discussed in section 3.1. On the other hand, the best ion-exchanged RED silicate glass waveguides were obtained by mixing rare-earth oxides (Nd_2O_3) with a high optical quality passive glass (Schott BK-7) [28], in which BK-7 glass is very well suitable for waveguide fabrication by ion-exchange processes, but the mixed glass substrate is far away from the optimization from lasing and amplification performance point of view. To some degree, the hampered development of active integrated optical devices in glass can be attributed to the unavailability of commercial RED glasses optimized for both lasing characteristics and ion-exchange chemistry. The problems are especially severe with phosphate laser glasses, which are among the best glass hosts for rare-earth ions due to higher stimulated emission cross-section and lower excited state absorption (ESA). With the phosphate glasses, it is difficult to prevent surface damage when conventional ion

exchange processes with molten salt as ion sources are used. To overcome the problem of phosphate glass surface deterioration, silver films were employed as ion sources to fabricate RED phosphate glass waveguides [31, 32, 40]. In fact, this is the only method that has been successfully demonstrated to produce waveguide structures in RED phosphate laser glasses. However, in some of the best commercially available laser glasses, neither molten salt nor silver film ion exchange process results in waveguides because there are not suitable alkali ions for ion exchange in these glasses.

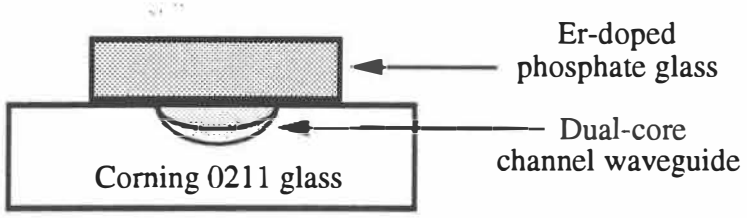

Fig. 3.9 Composite rare-earth-doped glass waveguide structure.

In this section, we propose and demonstrate a new composite RED glass waveguide configuration [42], which overcomes the above mentioned problems. In the composite structure shown in Fig. 3.9, a RED glass with excellent lasing performance is placed on the surface of an ion-exchanged waveguide, which is first fabricated into a high quality undoped passive glass substrate. This new waveguide configuration combines the excellent optical properties of ion-exchanged passive glass waveguides with the optimized lasing characteristics of commercially available laser glasses. In addition, this configuration allows the integration of other passive devices (e.g. multi/demultiplexer

for pump and signal wavelengths or for different signal wavelengths such as $\lambda \approx 1.3$ μm and $\lambda \approx 1.55$ μm, and various power dividers) in the same substrate by placing the RED glasses only on some parts of the passive waveguide devices.

Generally, the refractive index of the RED glass should be higher than the substrate index and lower than the surface index of the ion-exchanged waveguides. For proper operation of the composite RED glass waveguides, the gap between the passive waveguide glass and RED glass has to be very small. This can be easily achieved by simply pressing the two glass tightly against each other or by using advanced glass bonding techniques. Also, the refractive indices of the two glasses have to be chosen carefully to maintain waveguiding and to have a great deal of guided optical power inside the RED glass. This structure can be achieved, for instance, with a combination of a high performance Er-doped phosphate laser glass (Kigre QE-7) [102] and a high quality ion-exchanged dual-core waveguide in Corning 0211 glass [50]. The transverse refractive index profile at the lasing wavelength (~ 1.535 μm) of this kind of composite RED glass waveguide is depicted in Fig. 3.10. The refractive indices of the two glasses are from the references [102] for Kigre QE-7 and [103] for Corning 0211, respectively.

To demonstrate the operation of the composite RED glass waveguide, we first fabricated dual-core channel waveguides into Corning 0211 glass substrate by the potassium and silver double ion exchange process (see chapter I). The potassium ion exchange is performed in pure molten KNO_3 at 400 ^{0}C for 2.5 hrs, and then the silver ion exchange is carried out in pure molten $AgNO_3$ at 300 ^{0}C for 6 hrs. As a mask for the double-ion-exchange process, a 100 nm thick aluminum film is deposited and patterned by conventional photolithographic technique to have openings with widths from 2 μm to 10 μm. After the double ion exchange process, the aluminum mask is removed from the

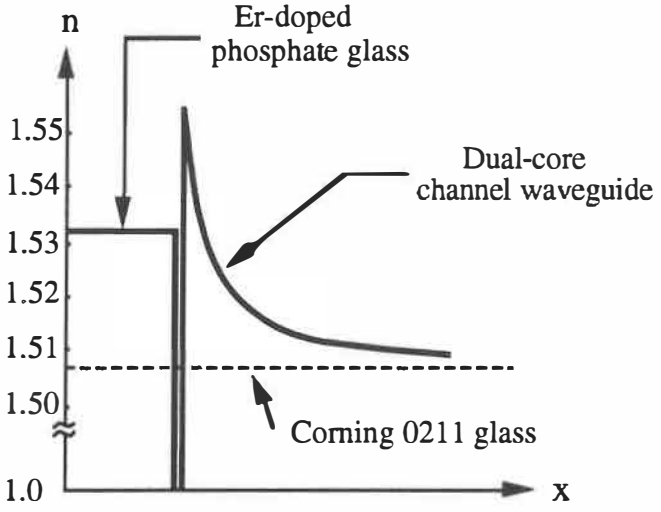

Fig. 3.10 The transverse refractive index profile for composite erbium-doped glass waveguide at $\lambda = 1.535$ μm.

surfaces of the waveguides and then an erbium doped phosphate glass piece is pressed against the waveguide chips with a small clamp made of aluminum.

In the first set of experiments, both endfaces of the two glasses clamped together are polished to study the cross-section of the composite structure and the modal behavior of the composite glass waveguide. The cross-section is examined with an optical microscope and the gap width between the two glasses is found to be less than 0.5 μm (estimated from the 400X amplification of the microscope). The modal behavior of the fabricated composite RED glass waveguides is examined by end-fire coupling light from a He-Ne laser ($\lambda = 1.5231$ μm) into the channel waveguide with a microscopic objective, and imaging the output facet onto an infra-red camera. The composite waveguides fabricated with mask openings less than 4 μm are found to be single mode at 1.5231 μm

wavelength. As an example, Fig. 3.11 shows the near field image of the composite RED waveguide, which is fabricated with a 3 μm wide mask opening.

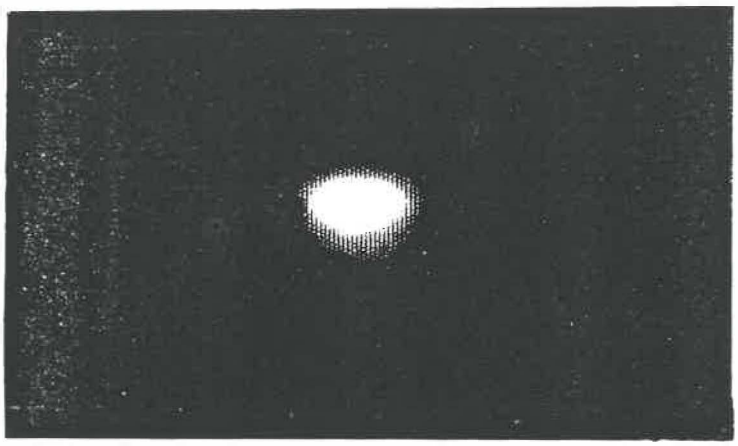

Fig. 3.11 Near-field image of a composite erbium-doped glass channel waveguide (with 3 μm mask opening).

For the spectral transmission measurements of the fabricated composite waveguides, the Kigre QE-7 glass is clamped only onto the central part of the dual-core channel waveguides, as shown in Fig. 3.12 (a). This ensures the total elimination of nonguided light propagating only in the QE-7 glass. The spectral transmission is measured with a halogen-tungsten lamp and a spectrometer, using microscope objectives for input and output coupling (see chapter I, section 1.1.2). Fig. 3.12 (b) shows the measured transmission spectrum around 0.98 μm wavelength for the composite waveguide made with 3 μm mask opening. Around 0.98 μm wavelength, which is the most important wavelength region for pumping the Er-doped composite waveguides, the absorption loss due to doped rare-earth ions is about 8 dB. Note that the composite

waveguide is only 4.9 mm long.

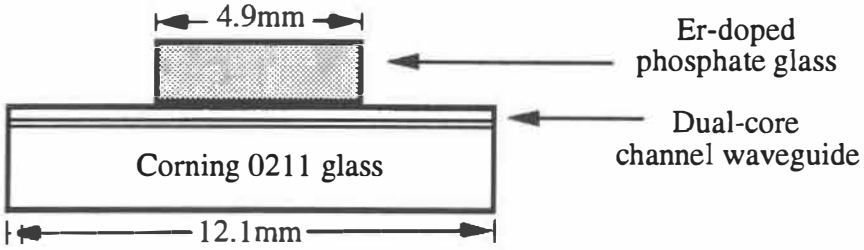

(a)

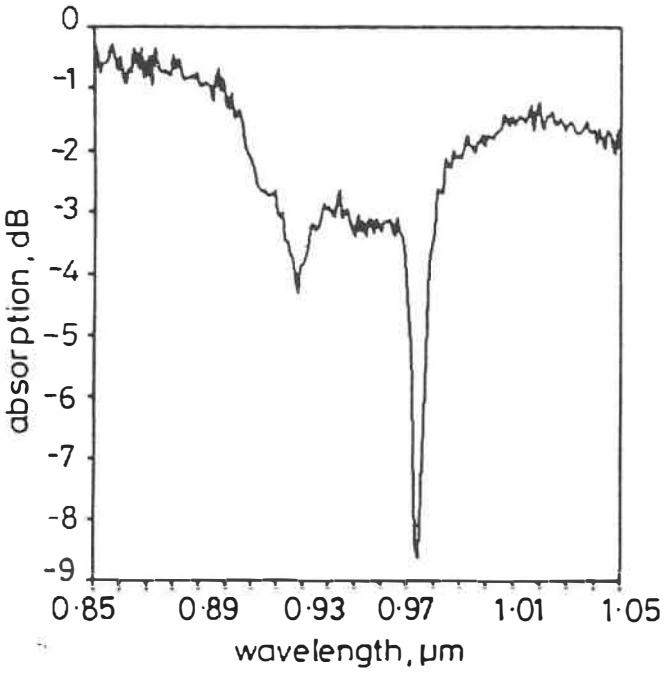

(b)

Fig. 3.12 (a) Composite erbium-doped glass waveguide structure for transmission spectral measurement. (b) Transmission spectrum of the sample with 3 μm mask opening around 0.98 μm wavelength region.

In conclusion of this section, a new composite glass waveguide structure has been proposed. Erbium-doped phosphate glass composite waveguides for light amplification and laser applications are fabricated, and their efficient operation is demonstrated. In the fabricated composite waveguide structure, the excellent waveguiding properties of passive ion-exchanged glass waveguides and the optimized lasing characteristics of the commercially available erbium-doped phosphate glass are efficiently combined. Very high absorption (~ 8 dB) at the most important pump wavelength region (~ 0.98 μm) is achieved with only 4.9 mm long composite waveguide. The absorption intensity (~ 16 dB/cm) at this wavelength region is much higher than previously reported Er-doped glass waveguides (~ 10 dB/cm in Ref. 40, 0.4 dB/cm in Ref. 39, and 0.25 dB/cm in Ref. 38). Another advantage of the QE-7 glass is that at the lasing wavlength (~ 1.535 μm) its absorption loss is only 0.001 dB/cm [102]. This shows that composite Er-doped glass waveguide has great potential in making efficient, small size ion-exchanged glass waveguide lasers and amplifiers. In addition, the approach of making composite waveguide structures can be easily extended to other types of glass waveguides, for example, semiconductor doped glass waveguides suitable for all-optical switching applications.

Table III-1. Refractive indices of phosphate thin films.

Dopant	n (λ, nm)	thickness (nm)
In	1.58 (632)	340
Ti	1.86 (440)	173
Al	1.50 (600)	717
Nd	1.53 (725)	340
Er	1.54 (620)	305

CHAPTER IV

ERBIUM-DOPED COMPOSITE GLASS WAVEGUIDE AMPLIFIER

In the previous chapter (section 3.3), a composite structure for fabrication of erbium-doped glass waveguides has been proposed and demonstrated. Considerable absorption around the important 0.98 μm pump wavelength has been achieved in the composite erbium-doped glass waveguides. In connection with the excellent optical behaviour around the lasing wavelength (~ 1.535 μm) of the erbium-doped phosphate glass (Kigre QE-7), this composite waveguide is highly promising for making very short integrated optical amplifiers and lasers. In this chapter, we report the first demonstration of optical amplification at 1.5231 μm and 1.5568 μm wavelengths in the erbium-doped composite ion-exchanged glass waveguide [45, 46]. More than 10 dB and 6 dB amplifications are respectively achieved at 1.5231 μm and 1.5568 μm wavelengths in a 4.7 mm long waveguide with only about 30 mw guided pump power at 0.9734 μm wavelength.

The composite erbium-doped glass waveguide is fabricated by pressing an erbium-doped phosphate glass piece against a dual-core ion-exchanged glass waveguide. The dual-core channel waveguide is fabricated by using potassium and silver double-ion-exchange process in a Corning 0211 glass substrate. Ion exchange is carried out through 5 μm wide opening in a 100 nm thick aluminum mask. Firstly, potassium ion exchange is performed in a pure KNO_3 molten salt at 400 ^{0}C for 2 hrs and 40 min.. Secondly,

silver ion exchange is carried out in a pure $AgNO_3$ molten salt bath at 300 ^{0}C for 3 hrs and 30 min.. Finally, the aluminum mask is chemically removed and the sample is postbaked at 300 ^{0}C for 2 hrs and 20 min.. Postbaking is employed to slightly decrease the refractive index on the waveguide surface in order to increase further the interactive between guided light and erbium-doped cover glass.

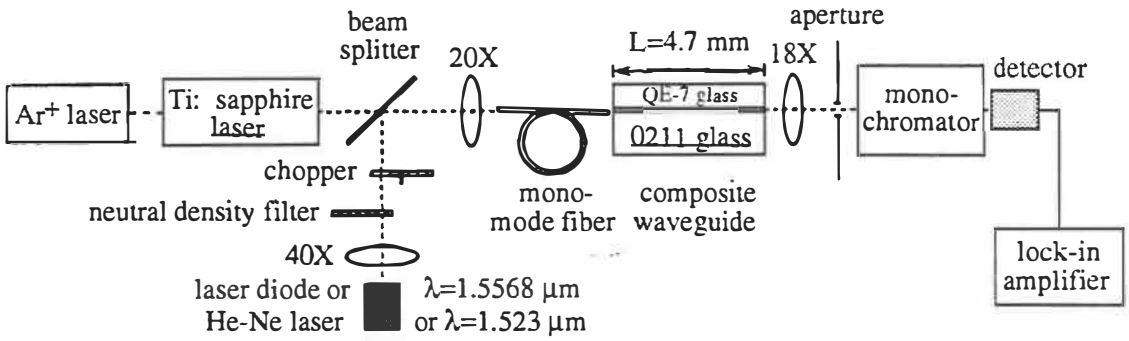

Fig. 4.1 Measurement set-up for amplification of composite waveguide amplifier.

The setup shown schematically in Fig. 4.1 is used to measure fluorescence spectrum and to perform the amplification experiment. Light from a tunable Ti: sapphire laser at 0.9734 μm waveglength [corresponding to the maximum absorption wavelength of the composite waveguide, see Fig. 3.12(b)] is used as the pump lighth, light from a He-Ne laser at 1.5231 μm wavelength or from a laser diode at 1.5568 μm wavelength is used as the signal. First of all, we measure the fluorescence spectrum of the waveguide by coupling only pump power into the composite channel waveguide. Guided fluorescence and unabsorbed pump power are collected by an objective and directed into a

spectrometer. Fig. 4.2 and Fig. 4.3 depict the fluorescence spectrum from the composite waveguide (measured in the absence of the signal light). The figures also show the output spectra of the He-Ne laser and the laser diode (signal sources), respectively, measured without pumping. The composite channel waveguide is single mode at signal wavelengths, but it supports higher order modes at pump wavelength. The pump and signal power are multiplexed into a fiber and are launched into the input port of the channel waveguide by butt coupling. To observe amplification in the composite waveguide, it is very important to obtain as large as possible overlap between pump mode and signal mode in the erbium-doped glass. To this end, the fundamental mode at the pump wavelength in the input fiber (telecommunication monomode fiber) is first excited, then the butt coupling between the fiber and the waveguide is optimized to obtain maximun amplified signal. Since the signal beam is chopped, only signal (without pumping) and amplified signal (with pumping) can be measured by the detector connected to a lock-in amplifier. The DC fluorescence has no influence in the measurement.

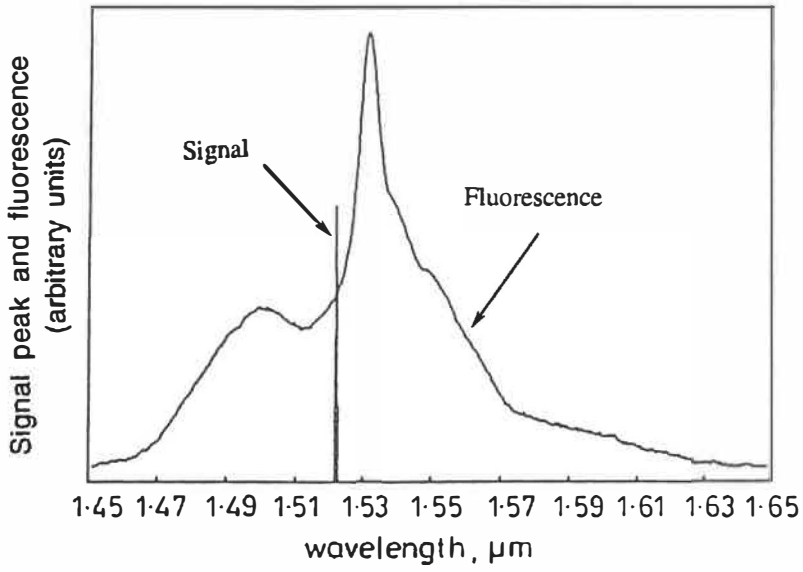

Fig. 4.2 Fluorescence spectrum and signal spectrum at 1.5231 μm wavelength.

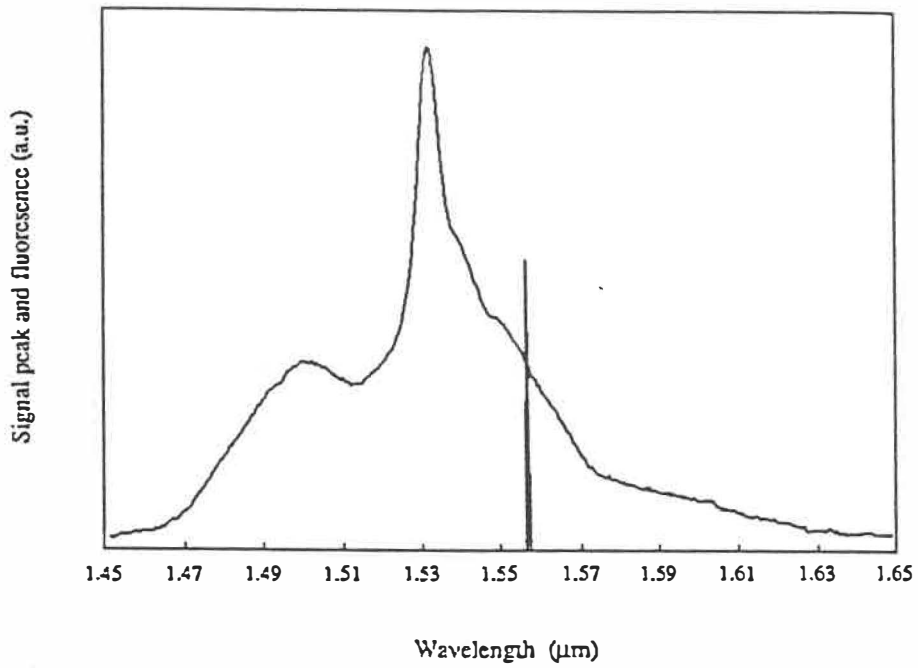

Fig. 4.3 Fluorescence spectrum and signal spectrum at 1.5568 μm wavelength.

Amplification is determined by increasing the pump power while signal power is kept constant at rather low level (small signal gain measurement), and the spectrometer is fixed to measure only signal light at the two different signal waveglengths. During the measurements, the signal power output from the monomode fiber is kept at 370 nW for λ = 1.5231 μm and at 57 nW for λ = 1.5568 μm. It is estimated that the maximum coupling efficiency from the input fiber to the composite waveguide is about 50% for both pump and signal wavelengths. The propagation losses in the composite waveguide (sample length L = 4.7 mm) are estimated to be 2 dB from a seperate measurement. These losses are mainly caused by scratches on the surface of the erbium-doped phosphate glass (because it is soft and more difficult to polish compared to the silicate glass). The total inherent loss (absorption and scattering in the ion-exchanged waveguide) at signal wavelengths is measured to be less than 0.2 dB.

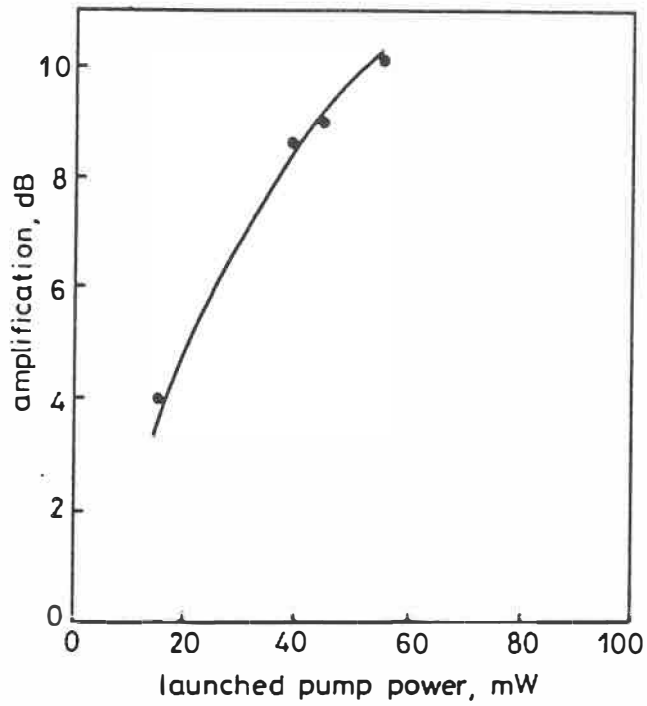

Fig. 4.4 Amplification at 1.5231 μm wavelength versus pump power from launching fiber.

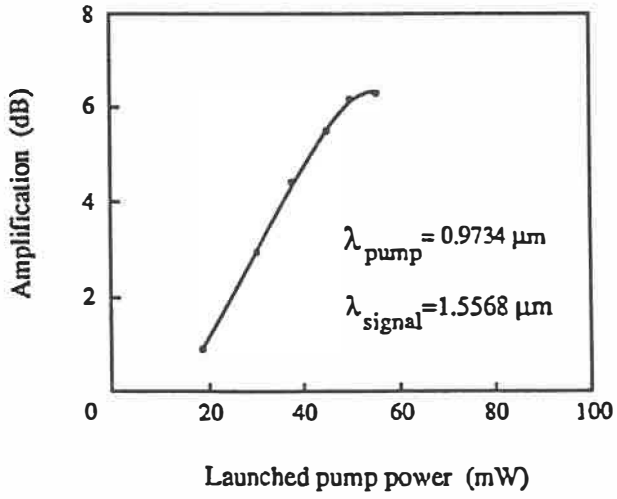

Fig. 4.5 Amplification at 1.5568 μm wavelength versus pump power from launching fiber.

Figs. 4.4 and 4.5 illustrate variation of the amplifications in the fabricated composite waveguides as a function of output pump power from the launching fiber. More than 10 dB and 6 dB amplifications are achieved with rather low pump level (less than 30 mw guided pump power in the waveguide). Laser diodes with such power levels at pump wavelength are readily available. At higher signal power level (up to 5 μW), no saturation of amplification is observed.

The actual gain should be 12 dB at 1.5231 μm wavelength and 8 dB at 1.5568 μm wavelength in the composite erbium-doped glass waveguide amplifier, because of 2 dB propagation losses. With careful polishing of the erbium-doped phosphate glass, it should be possible to reduce the propagation losses by at least 1.5 dB. By further optimization of the waveguide structure (increasing the interaction of pump mode with erbium-doped glass, and increasing the overlap between the pump mode and the signal mode), the amplification can be considerably improved. Furthermore, it is expected that the amplification will be higher if signal waveglength coincides with the peak wavelength of the fluorescence spectrum. If a longer sample and more powerful pump are used, amplification of over 20 dB seems achievable.

CONCLUSIONS

In thesis thesis, several fabrication processes have been developed to produce passive and active glass waveguides and devices. The operation of these waveguides and devices has been demonstrated successfully.

Chapter I presents one-step potassium, cesium, and silver ion-exchanged glass waveguides and (potassium and silver) double-ion-exchanged glass waveguides and their optical characterizations. The double-ion-exchange process has been demonstrated as an effective and simple fabrication technique for making low-loss waveguides and devices on general multipurpose glass substrate and with conventional metallic mask. Such waveguides have similar performance as one-step silver ion-exchanged glass waveguides, but with much lower propagation losses, more symmetric mode profile and longer single mode operation region.

In chapter II, we present fabrication and optical characterization of some passive devices that are closely related to the active applications of rare-earth-doped glass waveguides. They include grating assisted glass channel waveguides, symmetric Y-branches, a four-port nonsymmetric Mach-Zehnder interferometer and a novel integrated optical ring resonator with the four-port nonsymmetric Mach-Zehnder interferometer as an input/output coupler. They are fabricated by one-step and double-ion-exchange processes presented in chapter I. Optical characterization has been carried out for all of the passive devices. Grating assisted channel waveguides exhibit reflectivity over 95 % at its Bragg wavelength for TE polarization. The symmetric Y-branches show uniform splitting ratio

(± 0.1 dB) in single- and multi-mode wavelength regions. Spectral transmission of the four-port nonsymmetric Mach-Zehnder interferometer is similar to the theoretical prediction. The resonances of the ring resonator at different wavelengths have been demonstrated. The finesses of the ring resonator, and the coupling ratios and excess losses of the input/output coupler at 1.3 μm and 1.523 μm wavelength are used to estimate the propagation losses in the ring waveguide, the results are in good agreement with the direct loss measurements of the straight channel waveguides.

In chapter III, three fabrication processes for making rare-earth-doped glass waveguides on active and passive substrates are presented. They are dilute silver ion exchange process for RED silicate glasses, spin-coated RED phosphate glass films on passive glass waveguides and composite RED glass waveguides. In the last two processes, passive waveguides are fabricated by one-step potassium and double-ion-exchange processes, respectively. Optical characterizations are carried out for these RED glass waveguides. 3 dB amplification is demonstrated for the silver ion-exchanged Nd-doped glass waveguides. The fluorescent lifetime measurements of Kigre Q-246 glass substrate and waveguides in it show that the silver ion exchange process significantly decreases the fluorescent lifetime of the substrate glass. The efficient absorption of RED phosphate glass films spin-coated on passive waveguides has been achieved and fluorescence emission has been observed. The operation of Er-doped composite glass waveguides has been demonstrated, they have 16 dB/cm absorption around 0.98 μm wavelength.

In chapter IV, amplification at 1.5231 μm and 1.5568 μm wavelengths are demonstrated. More than 10 dB net gain at 1.523 μm wavelength has been achieved for a short (4.7 mm) erbium-doped composite glass waveguide amplifier pumped by a rather low (~ 30 mW guided) pump power.

With respect to future work, there are a number of interesting active applications based on the demonstrations of the passive devices, active waveguides and active structures developed in this thesis.

First of all, we can obtain a lossless integrated optical ring resonator (with very high finesse) and a ring laser by combining a passive ring resonator with an erbium-doped phosphate glass (Kigre QE-7) by clamping technique. Since very high gains have been achieved in a short composite erbium-doped glass waveguide, it is believed that, by gradually increasing pump power coupled into the device, the gain will be increased to such a level that it just compensates for all of the losses in the ring circuit, so the 'active ring resonator' will be resonant at signal wavelength with a very high finesse, i.e. it acts as a lossless ring resonator. When pump power is increased further, the 'active ring resonator' will oscillate even without any signal input, i.e. it will start to lase at this pump level (lasing threshold).

Another interesting application of rare-earth-doped glass waveguides relates to lossless power dividers. Active structure can be employed to completely compensate for the excess losses caused by radiation in branching region of Y-branch circuit. Since radiation losses can be significant when the Y-branches are cascaded into 1/N power dividers or when the branching angles are increased to larger than one degree, the compensation of the high excess losses is of crucial importance for practical devices. Composite structure and spin-coated rare-earth phosphate films can be possible choices for fabrication of these lossless power dividers. The neodymium-doped phosphate glass Kigre Q-98 [97] has the refrative index (~1.543) at 1.3 μm wavelength region, which is just between that of Corning 0211 glass substrate (~1.511) [103] and that of the surface of the double-ion-exchanged glass waveguides (~1.561). Therefore, composite structure is a feasible way for demonstrating the lossless power dividers both at 1.3 μm and at 1.55

μm wavelength regions. Neodymium-doped composite glass waveguide amplifiers at 1.3 μm wavelength region have to be demonstrated before they can be employed in proposed applications, and the loss characteristics of the Y-branches as a function of branching angles need to be determined experimentally.

Glass waveguide lasers with one of the cavity mirrors replaced by a grating are also attractive. It is an effective method to obtain single frequency (or single longitudinal mode) waveguide lasers. Rare-earth-doped glass waveguide laser has to be pumped externally by another laser, which is a different pump style from the internal current pump style in semiconductor laser diode. The external pump light must be coupled into distributed feedback laser cavity from outside of the active waveguide structure. For example, pump power can be coupled into the laser cavity via the four-port non-symmetric Mach-Zehnder interferometer or a directional coupler which can be designed to couple most of pump power into the laser cavity and couple very little signal out off it (to design the directional coupler as a ~ 0.98 μm/1.54 μm multi/demultiplexer) to result in laser oscillation.

It is also interesting to study the up conversion fluorescence [104] produced in erbium-doped glass waveguides because the infrared-to-visible conversion has potential importance to achieve a visible guided wave laser. The guided wave structure results in high pump power density in the waveguide and makes the up conversion fluorescence more easily observed.

REFERENCES :

[1]. MILLER, S. E., "Integrated optics: an introduction," Bell Sys. Tech. J., Vol.48, pp.2059-2068, 1969.

[2]. NISHIHARA, H., HARUNA, M., and SUHARA, T., *Optical Integrated circuits*, McGraw-Hill, New York, 1989.

[3]. NAJAFI, S. I., editor, *Introduction to Glass Integrated Optics*, Artech House, Boston, 1992.

[4]. NAJAFI, S. I., and HONKANEN, S., "Ion-exchanged glass waveguides for active integrated optical devices," Invited paper, Electrochemical Society Meeting, Toronto, Oct. 1992.

[5]. LI, M.-J., WANG, W.-J., and NAJAFI, S. I., "Ion-exchanged glass waveguides with spin-coated phosphate overlays," *Proceedings of the First IEEE International Workshop on Photonic Networks, Components and Applications*, World Scientific, NJ, pp223-227, 1991.

[6]. YI-YAN, A., CHEN,W. K., RAVI, T. S., GMITTER, T. J., BHAT, R., and YOO, K. H., "Grafted InGaAsP light emitting diodes on glass channel waveguides," Electron. Lett., Vol.28, pp341-342, 1992.

[7]. YI-YAN, A., CHEN, W. K., NGUYEN, C. K., GMITTER, T. J., BHAT, B., and JACKEL, J. L., "GaInAs/InP *pin* photodetectors integrated with glass waveguides," Electron. Lett., Vol.27, pp87-89, 1991.

[8]. IZAWA, T., and NAKAGOME, H., "Optical waveguide formed by electrically induced migration of ions in glass plates," Appl. Phys. Lett., Vol.21, pp.584-586, 1972.

[9]. FINDAKLY, T., "Glass waveguides by ion-exchange: a review," Opt. Eng.,

Vol.24, pp.244-250, 1985, and references there in.

[10]. RAMASWAMY, R. V., and SRIVASTAVA, R., "Ion-exchanged glass waveguides: a review," J. Lightwave Technol., Vol.6, pp.984-1001, 1988, and references there in.

[11]. ROSS LUDWIG, "Integrated optical components in substrate glasses," Glastech Ber., Vol.62, pp.285-297, 1989, and references there in.

[12]. REISFELD, R., and JORGENSEN, C. K., *Lasers and Excited States in Rare -earths*, Spinger-Verlag, Berlin & New York, 1977.

[13]. PATEK, K., *Glass lasers*, edited by J. G. Edwards, CRC Press, Cleveland, Ohio, 1970.

[14]. SNITZER, E., and YOUNG, C. G., "Glass lasers," in *Lasers,* Vol.2, edited by A. K. LEVINE, Marcel dekker, New York, 1968.

[15]. URQUHART PAUL, "Review of rare-earth doped fiber lasers and amplifiers," IEE Proc., Vol.135, pp.385-407, 1988, and references there in.

[16]. STREIFER, W., SCIFRES, D. R., HARNAGEL, G. L., WELCH, D. F., BERGER, J., and SAKAMOTO, M., "Advances in diode laser pumps," IEEE J. Quantum Electron., Vol.24, pp.883-893, 1988.

[17]. FAN, T. Y., and BYER, R. L., "Diode laser-pumped solid-state lasers," IEEE J. Quantum Electron., Vol.24, pp.895-912, 1988.

[18]. NAJAFI, S. I., "Rare-earth-doped glass waveguides for integrated optics," Invited paper, COST 217 Workshop on Active Fibers, Helsinki, May, 1991.

[19]. NAGEL, S. R., MACCHESNEY, and WALKER, K. L., "An overview of the modified chemical vapor deposition (MCVD) process and performance," IEEE J. Quantum Electron., Vol.18, pp.459-476, 1982.

[20]. INADA, K., "Recent progress in fiber fabrication techniques by vapor-phase

axial deposition," IEEE J. Quantum Electron., Vol.18, pp.1424-1431, 1982.

[21]. YAJIMA, H., KAWASE, S., and SEKIMOTO, Y., "Amplification at 1.06μm using Nd: glass thin-film waveguide," Appl. Phys. Lett., Vol.21, pp.407-409, 1972.

[22]. SARUWATARI, M., and IZAWA, T., "Nd-glass laser with three-dimensional optical waveguide," Appl. Phys. Lett., Vol.24, pp.603-605, 1974.

[23]. CHEN, BOR-UEI, and TANG, C. L., "Nd-glass thin-film waveguide: an active medium for Nd thin-film laser, " Appl. Phys. Lett., Vol.28, pp.435-437, 1976.

[24]. NAJAFI, S. I., WANG, W.-J., CURRIE, J. F., LEONELLI, R., and BREBNER, J. L., "Fabrication and characterization of Neodymium-doped glass waveguides," IEEE Photon. Technol. Lett., Vol.1, pp.109-110, 1989.

[25]. NAJAFI, S. I., WANG, W.-J., CURRIE, J. F., and LEONELLI, R., "Ion-exchanged rare-earth doped glass waveguides," *SPIE Proceedings*, Vol.1128, paper #24, 1989.

[26]. HIBINO, Y., KITAGAWA, T., M., SHIMIZU, M., HANAWA, F., and SUGITA, A., "Neodymium-doped silica optical waveguide laser on silicon substrate," IEEE Photon. Technol. Lett., Vol.1, pp.349-368, 1989.

[27]. SANFORD, N. A., MALONE, K. J., and LARSON, D. R., "Integrated-optic laser fabricated by field-assisted ion exchange in neodymium-doped soda-lime -silicate glass," Opt. Lett., Vol.15, pp.366-368, 1990.

[28]. MWARANIA, E. K., REEKIE, L., WANG, J. and WILKINSON, J. S., "Low-threshold monomode ion-exchanged waveguide lasers in neodymium-doped BK-7 glass," Electron. Lett., Vol.26, pp.1317-1318, 1990.

[29]. LI, M.-J., WANG, W.-J., LEONELLI, R., and NAJAFI, S. I., "Rare-earth-doped glass waveguides and amplifiers," *SPIE Proceedings*, Vol.1338, pp.82-

87, 1990.

[30]. ROBERTSON, G. R. J., and JESSOP, P. E., "Optical waveguide laser using an rf sputtered Nd: glass film," Appl. Opt., Vol.30, pp.276-278, 1991.

[31]. AOKI, H., MARUYAMA, O., and ASAHARA, Y., "Glass waveguide laser," IEEE Photon. Technol. Lett., Vol.2, pp.459-460, 1990.

[32]. AOKI, H., MARUYAMA, O., and ASAHARA, Y., "Glass waveguide laser operated around 1.3μm," Electron. Lett., Vol.26, pp.1910-1911, 1990.

[33]. HATTORI, K., KITAGAWA, T., OHMORI, Y., and KOBAYASHI, M., "Laser-diode pumping of waveguide laser based on Nd-doped silica planar lightwave circuit," IEEE Photon. Technol. Lett., Vol.3, pp.882-884, 1991.

[34]. AOKI, H., ISHIKAWA, E., and ASAHARA, Y., "Nd^{3+}-doped glass waveguide amplifier at 1.054 μm," Electron. Lett., Vol.27, pp.2351-2353, 1991.

[35]. SANFORD, N. A., MALONE, K. J., and LARSON, D. R., "Extended-cavity operation of rare-earth-doped glass waveguide lasers," Opt. Lett., Vol.16, pp.1095-1097, 1991.

[36]. SANFORD, N. A., MALONE, K. J., LARSON, D. R., and HICKEMELL, R. K., "Y-branch waveguide glass laser and amplifier," Opt. Lett., Vol.16, pp.1168-1170, 1991.

[37]. MWARANIA, E. K., MURPHY, D. M., HEMPSTEAD, M., REEKIE, L., and WILKINSON, J. S., "Integrated Q-switched multiple-cavity glass waveguide laser," IEEE Photon. Technol. Lett., Vol.4, pp.235-237, 1992.

[38]. KITAGAWA, T., HATTORI, K., SHIMIZU, M., OHMORI, Y., and KOBAYASHI, M., "Guided-wave laser based on erbium-doped silica planar lightwave circuit," Electron. Lett., Vol.27, pp.334-335, 1991.

[39]. ABOUELLEIL, M. M., BALL, G. A., NIGHAN, W. L., and OPAL, D. J.,

"Low-loss erbium-doped ion-exchanged channel waveguides," Opt. Lett., Vol.16, pp.1949-1951, 1991.

[40]. HONKANEN, S., NAJAFI, S. I., PÖYHÖNEN, P., ORECL, G., WANG, W. -J., and CHROSTOWSKI, J., "Silver-film ion-exchanged singlemode waveguides in Er doped phosphate glass," Electron. Lett., Vol.27, pp.2167-2168, 1991.

[41]. FEUCHTER, T., MWARANIA, E. K., WANG, J., REEKIE, L., and WILKINSON, J. S., "Erbium-doped ion-exchanged waveguide lasers in BK-7 Glass," IEEE Photon. Technol. Lett., Vol.4, pp.542-544, 1992.

[42]. HONKANEN, S., NAJAFI, S. I., and WANG, W.-J., "Composite rare-earth-doped glass waveguides," Electron. Lett., Vol.28, pp.746-747, 1992.

[43]. SHMULOVICH, J., WONG, A., WONG, Y. H., BECKER, P. C., BRUCE, A. J., and ADAR, R., "Er^{3+} glass waveguide amplifier at 1.5 μm on silicon," Electron. Lett., Vol.28, pp.1181-1182, 1992.

[44]. KITAGAWA, T., HATTORI, K., SHUTO, K., YASHU, M., KOBAYASHI, M., and HORIGUCHI, M., "Amplification in erbium-doped silica-based planar lightwave circuits," Electron. Lett., Vol.28, pp.1818-1819, 1992.

[45]. WANG, W.-J., NAJAFI, S. I., HONHANEN, S., HE, Q., WU, C., and GLINSKI, J., "Erbium-doped Composite glass waveguide amplifier," Electron. Lett., Vol.28, pp1872-1873, 1992.

[46]. WANG, W.-J., HONKANEN, S., NAJAFI, S. I., HE, Q., WU, C., and ROLLAND, C., "Composite Rare-earth-doped glass waveguides and amplifiers," *SPIE Proceedings*, Vol. 1794, paper #03, 1992.

[47]. NAJAFI, S. I., LEFEBVRE, P., ALBERT, J., HONKANEN, S., VAHID -SHAHIDI, A., and WANG, W.-J., "Ion-exchanged Mach-Zehnder

interferometers in glass," Appl. Opt. Vol.31, pp3381-3383, 1992.

[48]. LI, M.-J., WANG, W.-J., NAJAFI, S. I., ALBERT, J., and HILL, K. O., "Glass waveguide with gratings," *Proceedings of the first IEEE International Workshop on Photonic networks, Components and Applications*, (World Scientific, NJ), pp218-222, 1990.

[49]. LI, M.-J., NAJAFI, S. I., WANG, W.-J., SIMARD, J. R., ALBERT, J., HILL, K. O., and LEUNG, A., "Fabrication and characterization of ion-exchanged glass channel waveguides with etched and diffused grating taps," *SPIE Proceedings*, Vol.1334, pp148-152, 1990.

[50]. LI, M.-J., HONKANEN, S., WANG, W.-J., LEONELLI, R., ALBERT, J., and NAJAFI, S. I., "Potassium and silver ion-exchanged dual-core glass waveguides with gratings," Appl. Phys. Lett., Vol.58, pp2607-2609, 1991.

[51]. LI, M.-J., HONKANEN, S., WANG, W.-J., LEONELLI, R., and NAJAFI, S. I., "Dual-core ion-exchanged glass waveguides," *SPIE Proceedings*, Vol.1513, paper #47, 1991.

[52]. WANG, W.-J., HONKANEN, S., NAJAFI, S. I., and TERVONEN, A., "A new integrated optical resonator in glass," Electron. Lett., Vol.28, pp1967-1968, 1992.

[53]. WANG, W.-J., HONKANEN, S., NAJAFI, S. I., and TERVONEN, A., "Integrated optical ring resonator with a novel nonsymmetric Mach-Zehnder interferometer as input/output coupler," *SPIE Proceedings*, Vol.1794, paper #39, 1992.

[54]. WANG, W.-J., HONKANEN, S., NAJAFI, S. I., and TERVONEN, A., "Four-port guided-wave nonsymmetric Mach-Zehnder interferometer," Appl. Phys. Lett., Vol.61, pp150-152, 1992.

[55]. HONKANEN, S., NAJAFI, S. I., LEFEBVRE, P., WANG, W.-J., and TERVONEN, A., "Symmetrical and nonsymmetrical Mach-Zehnder interferometers in glass," The 10th Annual Eur. Conference EFOC/LAN, Paris, June 24-26, 1992.

[56]. ULRICH, R., and TORGE, R., "Measurement of thin film parameters with a prism coupler," Appl. Opt., Vol.12, pp2091-2098, 1973.

[57]. SELIGSON, J., "Prism couplers guided-wave optics: design considerations," Appl. Opt. Vol.26, pp2609-2617, 1987.

[58]. WHITE, J. M., and HEIDRICH, P. F., "Optical waveguide refractive index profiles from measurement of mode indices: a simple analysis," Appl. Opt., Vol.15, pp151-155, 1976.

[59]. NAJAFI, S. I., "Optical behavior of potassium ion-exchanged glass waveguides," Appl. Opt., Vol.27, pp3728-3731, 1988.

[60]. NAJAFI, S. I., and WU, C., "Potassium ion-exchanged glass waveguide directional couplers at 0.6328 and 1.3 μm," Appl. Opt., Vol.28, pp2459-2460, 1989.

[61]. BETTS, R. A., LUI, F., and DAGIAS, S., "Wavelength and polarization insensitive optical splitters fabricated in K^+/Na^+ ion-exchanged glass," IEEE Photon. Tech. Lett., Vol.2, pp481-483, 1990.

[62]. VAN DEL TOL, J. G. M., VERHOOF, J. W., DIEMEER, M. B. J., and PENNINGS, E. C. M., "S-bends using offsets in fiber-compatible K^+ - Na^+ ion-exchanged glass waveguides," Electron. Lett., Vol.27, pp379-380, 1991.

[63]. WALKER, R. G., and WILKINSON, C. D. W., "Integrated optical ring resonators made by silver ion-exchange in glass," Appl. Opt., Vol.22, pp1029-1035, 1983.

[64]. WALKER, R. G., WILKINSON, C. D. W., and WILKINSON, J. A. H., "Integrated optical waveguiding structures made by silver ion-exchage in glass: 1. the propagation characteristics of strip ion-exchanged waveguides; a theoretical and experimental investigation," Appl. Opt., Vol.22, pp1923-1928, 1983.

[65]. DERI, R. J., YASUOKA, N., MAKIUCHI, M., KURAMATA, A., and WADA, O., "Efficient fiber coupling to low-loss diluted multiple quantum well optical waveguides," Appl. Phys. Lett., Vol.55, pp1495-1497, 1989.

[66]. WANG, W.-J., HONKANEN, S., and NAJAFI, S. I., "Loss characteristics of double-ion-exchanged glass waveguides," Submitted for publication.

[67]. WANG, W.-J., HONKANEN, S., NAJAFI, S. I., and LI, M.-J., "Low-loss double-ion-exchanged dual-core waveguides," GRIN'92, Poster paper, Spain, Oct.4-6, 1992.

[68]. TAMIR, T., "Beam and waveguide coupler," in *Integrated Optics*, Ed. by T. Tamir, Spring-Verlag, New York, 1982.

[69]. TIEFENTHALER, K., and LUKOSZ, W., "Integrated optical switches and gas sensors," Opt. Lett., Vol.10, pp137-139, 1984.

[70]. YARIV, A., and NAKAMURA, M., "Periodic structures for integrated optics," IEEE J. Qantum Elecron., Vol.13, pp233-253, 1977.

[71]. LI, M.-J., and NAJAFI, S. I., "Polarization dependence of grating assisted wave-guide Bragg reflectors," Appl. Opt., submitted for publication.

[72]. KAPON, E., and THURSTON, R. N., "Multichannel waveguide junctions for guided-wave optics," Appl. Phys. Lett., Vol.50, No.24, pp1710-1712, 1987.

[73] YAJIMA, H., "Dielectric thin film optical branching waveguide," Appl. Phy. Lett., Vol.22, pp647-649, 1973.

[74]. OKUDA, E., TANAKA, I., and YAMASAKI, T., "Planar gradient-index glass

waveguide and its applications to a 4-port branched circuits and star coupler," Appl. Opt., Vol.3, pp1745-1748, 1984.

[75]. PÖYHÖNEN, P., HONKANEN, S., TERVONEN, A., TAHKOKORPI, M., and ALBERT, J., "Plannar 1/8 splitter in glass by photoresist masked silver film ion exchange," Electron. Lett., Vol.27, pp1319-1320, 1991.

[76]. TTEYZ, G. V., "Silicon Mach-Zehnder waveguide interferometer operating at 1.3 μm," Electron. Lett. Vol.27, pp118-120, 1991.

[77]. WEISSMAN, Z., MAROM, E., and HARDY, A., "Very low-loss Y-junction power divider," Opt. Lett., Vol.14, No.15, pp293-295, 1989.

[78]. BETTS, B. A., LUI, F., and DAGIAS, S., "Wavelength and polorization insensitive optical splitters fabricated in K+ / Na+ ion-exchanged glass," IEEE Photon. Tech. Lett., Vol.2, pp481-483, 1990.

[79]. VERBEEK, B. H., HENRY, C. H., OLSSON, N. A., ORLOWSKY, K. J., KAZARINOV, R. F., and JOHNSON, B. H., "Integrated four-channel Mach-Zehnder multi/demultiplexer fabricated with phosphorous doped SiO_2 waveguides on Si," J. Lightwave Technol., Vol.6, pp1011-1015, 1988.

[80]. YI-YAN, A., DERI, R. J., SETO, M., and HAWKINS, R. J., "GaAs/GaAlAs asymmetric Mach-Zehnder demultiplexer with reduced polarization dependence," IEEE Photon. Technol. Letter., Vol.1, pp 83-85, 1989.

[81]. MARTIN, W. E., "A new waveguide switch/modulator for integrated optics," Appl. Phys. Lett., Vol.26, pp562-564, 1975.

[82]. SHANI, Y., HENRY, C. H., KISTLER, R. C., and ORLOWSKY, K. J., "Four-port integrated optic polarization splitter," Appl. Opt., Vol.29, pp337-339, 1990.

[83]. IZUTSU, M., ENOKIHARA, A., and SUETA, T., "Optical-waveguide hybrid

coupler," Opt. Lett., Vol.7, pp549-551, 1982.

[84]. IZUTSU, M., ENOKIHARA, A., and SUETA, T., "Optical-waveguide micro-displacement sensor," Electron. Lett., Vol.18, pp867-868, 1982.

[85]. SILBERBERG, Y., PERLMUTTER, P., and BARAN, J. E., "Digital Optical switch," Appl. Phys. Lett., Vol.51, pp1230-1232, 1987.

[86]. TERVONEN, A., PÖYHÖNEN, P., HONKANEN, S., and TAHKOKORPI, M., "A guided wave Mach-Zehnder interferometer structure for wavelength multiplexing," IEEE Photon.Technol. Lett., Vol.3, pp516-513, 1991.

[87]. CHEN, Y., LIN, W., and FUJI, Y., "Local field analysis of bent graded-index planar waveguides," J. Lightwave Technol., Vol.8, pp1461-1469, 1990.

[88]. CONNORS, J. M., and MAHAPATRA, A., "High finesse ring resonators made by silver ion exchange in glass," J. Lightwave Technol., Vol.5, pp1686-1689, 1987.

[89]. HAAVISTO, J., and PAJER, G. A., "Resonance effects in low-loss ring waveguides," Opt. Lett., Vol.5, pp510-512, 1980.

[90]. HIDA, Y., IMAMURA, S., and IZAWA, T., "Ring resonator composed of low loss polymer waveguides at 1.3 μm," Electron. Lett., Vol.28, pp1314-1316, 1992.

[91]. HONDA, K., GARMIRE, E. M., and WILSON, K. E., "Characteristics of an integrated optics ring resonator fabricated in glass," J. Lightwave Technol., Vol.2, pp714-719, 1984.

[92]. MAHPATRA, A., and ROBINSON, W. C., "Integrated-optic ring resonators made by proton exchange in lithium niobate," Appl. Opt., Vol.24, pp2285-2286, 1985.

[93]. NAUMAN, A., and BOYD, J. T., "Ring resonator fabricated in phosphosilicate

glass films deposited by chemical vapor deposition," J. Lightwave Technol., Vol.4, pp.1294-1303, 1986.

[94]. BISMUTH, J., GIDON, P., REVOL, F., and VALETTE, S., "Low-loss ring resonators fabricated from silicon based integrated optics technologies," Electron. Lett., Vol.27, pp722-724 , 1991.

[95]. ADAR, R., SHANI, Y., HENRY, C. H., KISTLER, R. C., BLONDER, G. E., and OLSSON, N. A., "Measurement of very low-loss silica on silicon waveguides with a ring resonator," Appl. Phy. Lett., Vol.58, pp444-445, 1991.

[96]. INOUE, Y., KOMINATO, T., TACHIKAWA, Y., and ISHIDA, O., "Finesse evaluation of integrated-optic ring resonators with heterodyne detection technique," Electron. Lett., Vol.28, pp. 684-686, 1992.

[97]. PRODUCT CATALOG, Kigre Inc., 100 Marshland Poad, Hilton Head, SC 29929, U.S.A..

[98]. LASER GLASS PRODUCT CATALOG, Schott Glass Technologies Inc., 400 York Avenue, Duryea, Pennsylvania 18642, U.S.A..

[99]. ROTHON, R. N., "Solution-deposited metal phosphate catings," Thin. Solid. Films, Vol.77, pp149-153, 1981.

[100]. SLOPER, A. N., and FLANAGAN, M. T., "Novel iron phosphate optical waveguides fabricated by a low temperature process," Electron. Lett., Vol.24, pp353-355, 1988.

[101]. SHEN, P.-N., LI, M.-J., NAJAFI, S. I., and CURRIE, J. F., "Optical and mechanical characterization of spin-on deposited silicon and titanium dioxide films," *SPIE Proceedings*, Vol.1328, paper #33, 1990.

[102]. KIGRE INC., Laser Glass Data Sheets, 1991.

[103]. TERVONEN, A., PÖYHÖNEN, P., HONKANEN, S., TAHKOKORPI, M.,

and TAMMELA, S., "Examination of two-step fabrication methods for single-mode fiber compatible ion-exchanged glass waveguides," Appl. Opt., Vol.30, pp338-343, 1991.

[104]. JACKEL, J. L., YI-YAN, A., VOGEL, E. M., VON LEHMEN, A., JOHNSON, J. J., and SNITZER, E., "Guided blu and green upconversion fluorescence in an erbium-ytterbium-containing silicate glass," Appl. Opt. Vol.31, pp3390-3392, 1992.

ÉCOLE POLYTECHNIQUE DE MONTRÉAL
3 9334 00290452 0